COMPARATIVE EVALUATION OF THE MICROGAP AT THE IMPLANT-ABUTMENT INTERFACE WITH PREMACHINED AND CUSTOMIZED LASER-SINTERED COBALT-CHROMIUM ABUTMENTS - AN *IN VITRO* STUDY

Dissertation Submitted to

THE TAMILNADU Dr. M.G.R. MEDICAL UNIVERSITY

In partial fulfillment for the Degree of

MASTER OF DENTAL SURGERY

BRANCH I

PROSTHODONTICS AND CROWN & BRIDGE

MAY 2018

THE TAMILNADU Dr. M.G.R. MEDICAL UNIVERSITY
CHENNAI

DECLARATION BY THE CANDIDATE

I hereby declare that this dissertation titled "COMPARATIVE EVALUATION OF THE MICROGAP AT THE IMPLANT-ABUTMENT INTERFACE WITH PREMACHINED AND CUSTOMIZED LASER-SINTERED COBALT-CHROMIUM ABUTMENTS - AN *IN VITRO* STUDY" is a bonafide and genuine research work carried out by me under the guidance of **Dr. N. S AZHAGARASAN, M.D.S.,** Professor and Head of the Department, Department of Prosthodontics and Crown & Bridge, Ragas Dental College and Hospital, Chennai.

Date: 30. 01. 2018

Place: **Chennai**

Dr. ASHWINI SUKANYA. GU
Post Graduate Student
Department of Prosthodontics
and Crown & Bridge,
Ragas Dental College and Hospital,
Chennai

CERTIFICATE

This is to certify that the dissertation titled "**COMPARATIVE EVALUATION OF THE MICROGAP AT THE IMPLANT-ABUTMENT INTERFACE WITH PREMACHINED AND CUSTOMIZED LASER-SINTERED COBALT-CHROMIUM ABUTMENTS - AN *IN VITRO* STUDY**" is a bonafide record work done by **Dr. ASHWINI SUKANYA. GU** under our guidance and to our satisfaction during her post graduate study period between **2015 – 2018**.

This dissertation is submitted to **THE TAMILNADU Dr. M.G.R. MEDICAL UNIVERSITY**, in partial fulfillment for the Degree of **MASTER OF DENTAL SURGERY – PROSTHODONTICS AND CROWN & BRIDGE, BRANCH I.** It has not been submitted (partial or full) for the award of any other degree or diploma.

Guided by:

Dr. N.S. Azhagarasan, M.D.S.,
Principal, Professor and Head,
Department of Prosthodontics and
Crown & Bridge
Ragas Dental College & Hospital,
Chennai.　　PRINCIPAL
RAGAS DENTAL COLLEGE AND HOSPITAL
UTHANDI, CHENNAI-600 119,

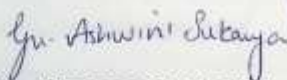# THE TAMILNADU Dr. M.G.R. MEDICAL UNIVERSITY

CHENNAI

PLAGIARISM CERTIFICATE

This is to certify the dissertation titled "COMPARATIVE EVALUATION OF THE MICROGAP AT THE IMPLANT-ABUTMENT INTERFACE WITH PREMACHINED AND CUSTOMIZED LASER-SINTERED COBALT-CHROMIUM ABUTMENTS - AN *IN VITRO* STUDY" of the candidate Dr. ASHWINI SUKANYA. GU for the award of Degree of MASTER OF DENTAL SURGERY in BRANCH I - PROSTHODONTICS AND CROWN & BRIDGE.

On verification with the urkund.com website for the purpose of plagiarism check, the uploaded thesis file contains from introduction to conclusion pages shows **2% percentage** of plagiarism, as per the report generated and it is enclosed in Annexure – IV.

Date: 30. 01. 2018   Place: Chennai.

Dr. ASHWINI SUKANYA. GU
Post Graduate Student,
Department of Prosthodontics and
Crown & Bridge,
Ragas Dental College & Hospital,
Chennai.

Dr. N.S. Azhagarasan, M.D.S., Guide,
Head of the Department of
Prosthodontics and
Crown & Bridge,
Ragas Dental College & Hospital,
Chennai.

PRINCIPAL
RAGAS DENTAL COLLEGE AND HOSPITAL
UTHANDI, CHENNAI-600 119.

RAGAS DENTAL COLLEGE & HOSPITAL

(Unit of Ragas Educational Society)
Recognized by the Dental Council of India, New Delhi
Affiliated to The Tamilnadu Dr. M.G.R. Medical University, Chennai

2/102, East Coast Road, Uthandi, Chennai - 600 119. INDIA.
Tele : (044) 24530002, 24530003-06. Principal (Dir) 24530001 Fax : (044) 24530009

TO WHOMSOEVER IT MAY CONCERN

Date: 27.01.18

Place: Chennai

From

The Institutional Review Board,

Ragas dental college,

Uthandi,

Chennai – 600119.

The dissertation topic "COMPARATIVE EVALUATION OF THE MICROGAP AT THE IMPLANT-ABUTMENT INTERFACE WITH PREMACHINED AND CUSTOMIZED LASER-SINTERED · COBALT – CHROMIUM ABUTMENTS- AN *INVITRO* STUDY"submitted by DR. ASHWINI SUKANYA. GU has been approved by the Institutional Ethics Board of Ragas Dental College and Hospital.

DR.N.S. AZHAGARASAN, MDS.,

Member Secretary,

Institutional Ethics Board,

Ragas Dental College & Hospital

Uthandi, Chennai – 600119.

ACKNOWLEDGEMENT

Completion of this dissertation was possible with the support and encouragement of several people .It is not a fair task to acknowledge all the people who made this thesis possible with a few words. However I will try to do my best to extend my appreciation to everyone who helped me scientifically and emotionally throughout this study and made it an unforgettable experience for me.

*I am extremely grateful to my **Guide, Professor Dr.N.S.Azhagarasan,M.D.S., Principal., Head of the Department,** Department of Prosthodontics and Crown & Bridge, Ragas Dental College and Hospital, Chennai, for his diligent encouragement, inspiration and constant motivation. His encouraging suggestions in innovating the methodology with recent advancements need a special mention. I am extremely grateful that he has guided me and has provided heartfelt support throughout my postgraduate programme which has always driven the best out of me. I would like to thank him for building confidence in me throughout my work. This work would not have been possible without his exceptional guidance and with his personal attention. His patience and perseverance had benefitted me in every facet of my study. The timely help and encouragement rendered by him had been enormously helpful throughout the period of my postgraduate study.I successfully overcame many difficulties. His unflinching courage and conviction will always inspire me. It is to him that I dedicate this work.*

I also thank him for permitting me to make use of the amenities in the institution.

CONTENTS

LIST OF TABLES

ANNEXURE I

METHODOLOGY- OVERVIEW

ANNEXURE II

FIGURES

Fig. No.		TITLE
Fig. 1	:	Titanium dental implant, standard platform, internal hexagon 3.75mm diameter, 10 mm length
Fig. 2	:	Premachined titanium abutment, standard platform, internal hexagon
Fig. 3	:	Cobalt -chromium powder
Fig. 4	:	Titanium dioxide spray for CAD/CAM scanning
Fig. 5	:	Spirit level indicators
Fig. 6a	:	Putty consistency Polyvinylsiloxane impression material
Fig. 6b	:	Light body consistency Polyvinylsiloxane impression material
Fig. 6c	:	Dispensing gun
Fig. 6d	:	Auto mixing spiral
Fig. 7	:	Clear autopolymerising acrylic resin
Fig. 8	:	Aluminium oxide powder -110μm
Fig. 9	:	Emery papers
Fig. 10	:	Distilled water

ANNEXURE III

List of SEM photomicrographs

ANNEXURE IV

GRAPHS

Graph No	Title
1	Basic and mean microgap at the implant-abutment interface of Ti implants and Ti premachined abutments at point IA at the platform level for Group I.
2	Basic and mean microgap at the implant-abutment interface of Ti implants and Ti premachined abutments at point IB at the platform level for Group I.
3	Basic and mean microgap at the implant-abutment interface of Ti implants and Ti premachined abutments at point IC at the platform level for Group I.
4	Basic and mean microgap at the implant-abutment interface of Ti implants and Ti premachined abutments at point ID at the internal connection level for Group I.
5	Basic and mean microgap at the implant-abutment interface of Ti implants and Ti premachined abutments at point IE at the internal connection level for Group I.

6	Basic and mean microgap at the implant-abutment interface of Ti implants and Ti premachined abutments at point IF at the internal connection level for Group I.
7	Basic and mean microgap at the implant-abutment interface of Ti implants and customized laser-sintered Co-Cr abutments at the point IIA at the platform level for Group II.
8	Basic and mean microgap at the implant-abutment interface of Ti implants and customized laser-sintered Co-Cr abutments at point IIB at the platform level for Group II.
9	Basic and mean microgap at the implant-abutment interface of Ti implants and customized laser-sintered Co-Cr abutments at point IIC at the platform level for Group II.
10	Basic and mean microgap at the implant-abutment interface of Ti implants and customized laser-sintered Co-Cr abutments at point IID at the internal connection level for Group II.
11	Basic and mean microgap at the implant-abutment interface of Ti implants and customized laser-sintered Co-Cr abutments at point IIE at the internal connection level for Group II.
12	Basic and mean microgap at the implant-abutment interface of Ti implants and customized laser-sintered Co-Cr abutments at

point IIF at the internal connection level for Group II.

| 13 | Comparative evaluation of mean microgap at the implant-abutment interface at point A at platform level for Group I & Group II (IA vs IIA). |

| 14 | Comparative evaluation of mean microgap at the implant-abutment interface at point B at platform level for Group I & Group II (IB vs IIB). |

| 15 | Comparative evaluation of mean microgap at the implant-abutment interface at point C at platform level for Group I & Group II (IC vs IIC). |

| 16 | Comparative evaluation of mean microgap at the implant-abutment interface at point D at internal connection level for Group I & Group II (ID vs IID). |

| 17 | Comparative evaluation of mean microgap at the implant-abutment interface at point E at internal connection level for Group I & Group II (IE vs IIE). |

| 18 | Comparative evaluation of mean microgap at the implant-abutment interface at point F at internal connection level for Group I & Group II (IF vs IIF). |

ANNEXURE V

- Plagiarism report

INTRODUCTION

Dental implants are being used increasingly important in the field of oral rehabilitation of partial or completely edentulous patients in both the anterior and posterior regions of the mouth with success rate > 90%.[21,22,25,26,31,38,44,50,52,66] Their performance over conventional prosthetic reconstructions is based on the high percentage of implants with a non-eventful tissue integration phase and the broad range of prosthetic options without the need to prepare adjacent teeth resulting in prostheses with improved function and esthetics.[43,66]

Dental implant system consist of two components, that is, the endosseous implant(s) that is placed during the first surgical phase and the transmucosal abutment(s), which are later secured onto the implant(s) to support single or multi-unit prosthetic restorations.[10,11,12,28,39,44,56] Despite our improved knowledge of the mechanisms of osseointegration, some failures still occur with implant restorations, which can be either mechanical or biological.[5,8,22,26,29,30] Most of these failures can be attributed to the screw-joint mechanism between the fixture and abutment.[20,29,31,36,52]

The use of screw to clamp the implant fixture and abutment should provide a stable implant- abutment joint, which can be achieved through a clamping force generated through the application of tightening torque, which is called pre-load. This pre-load should be maintained more than the unclamping forces (joint separating force) derived from the occlusal function.[23,25,31,34,37,41,44,57,61,62] Screw loosening or fracture occurs whenever there is an increase in joint separating forces than the clamping forces that hold the screw joint. Tightening torque

should be according to the manufacturer's recommended value and with the mechanical torque device to achieve and maintain the preload of the screw type connections. Although controlled torque application and altered screw designs have significantly improved performance, they have not eliminated the joint problem entirely.

Marginal integrity at the implant-abutment interface is important to reduce stress transfer to the bone, screw joint and to prevent movements at the deep implant- abutment interface.[7,8,18,48] The efficiency of the implant abutment joint depends on several factors such as, component design, connection geometry between implant – abutment, mechanical adjustment between fixture and its set surface on abutments, mechanical and physical component properties and torque application.[25,55,56] The success of this joint is directly related to attaining and maintaining a proper pre-load over time.[3,8,31]

There are at least 20 different implant abutment interfaces available. These implant-abutment interface determine the joint strength, lateral and rotational stability. Branemark's original external hex connection design and the other similar abutments that followed it were only 0.7 mm in height, and reported screw joint complications and screw loosening ranging from 6% to 48%.[12,49] These were attributed to the short, vulnerable connection design that offered lesser resistance to lateral and rotational forces. To overcome inherent limitations with the external hexagon design, alternate connections have been developed. Currently internal implant-abutment connection geometry is advocated as it could distribute intra

oral forces deeper within the implant and protects the retention screws from excess loading and provides a strong and stable interface.[42,45,51,55,56]

Prosthesis supported by multiple implants has better load distribution and hence lower stress concentration at the implant- abutment interface compared to the single tooth prosthesis. Bending moments becomes more significant in single tooth prosthesis as the load distribution effect is absent.[12,32,51,62] Prosthetic complications are more related to single tooth replacements, which include, abutment screw fracture, abutment screw loosening, and implant fracture. [8,43,51]

In regular prosthetic protocols pre-machined components are used to reduce the risk of mechanical complications.[61] Various studies have reported lower micro-gap and misfit values for pre-machined abutments than with cast-on abutments.[15,16,37,38] In routine clinical practice, the restoring prosthodontist uses one particular system of implant and its original components including abutments and screws as supplied by that manufacturer.[27,59] These components are thus from the original equipment manufacturer.[9]

A microgap at the implant-abutment interface is inevitable, though premachined components provided by the manufacturer are considered to be well-matched with the least interface gaps. Although premachined abutments are favored, however, in certain situations, customized abutments are indicated. These custom abutments allow for an individual emergence profile of the reconstruction directly by the abutment.[40,54] Implant abutments can be customized by casting, milling and laser-sintering procedures.[23] Surface irregularities due to customization process can

enhance the microgap at the implant-abutment interface.[23] The control of roughness on the mating surfaces at the implant-customized abutment interface could reduce afore mentioned complications by controlling the microgap.[23] Hence the focus of research is directed towards these objectives. There are number of studies available on milled and cast abutments [18,37,52] but new manufacturing technique, for example, laser sintering[2,23] are becoming available. On the other hand, laser sintering enables direct fabrication of prototypes for development of prostheses.[2] A number of studies have evaluated the implant-abutment interface microgap for various implant systems and connection designs using premachined abutments.[16,17,24,25,64] Published research evaluating the misfit between implant-abutment interface using customized laser-sintered abutments are sparse.[2,23] Currently studies investigating the interface microgap between implant and customized laser-sintered abutments are relatively few in the literature.

Various techniques for measurement of microgap at the implant-abutment interface have been reported, which include, probing with dental explorers,[39] use of periotest device,[39] direct observations of the implant–abutment interface performed by radiography,[33,41] scanning electron microscopy(SEM),[5,16,17,23,24,28,32,35,47,52,59,63,67] scanning laser microscopy (SLM)[6] and optical microscopy(O.M.),[17,28] 3D micro-tomographic technique,[45,53] optical coherence tomography.[39] Among the methods to analyse the implant-abutment interface, scanning electron microscopy is a well-documented method, which is reported to be an efficient method for this type of analysis.

In light of the above, the aim of the present *in vitro* study was to comparatively evaluate the microgap at the implant – abutment interface with premachined and customized laser-sintered Cr-Co abutments using scanning electron microscopy (SEM). The null hypothesis of the present study was that there would be no significant difference in microgap at the implant-abutment interface with either premachined or customized abutments.

The objectives of the present study included the following:

1. To measure the microgap at the implant-abutment interface of Ti implants and Ti premachined abutments at point A at the platform level using scanning electron microscope (Group I).

2. To measure the microgap at the implant-abutment interface of Ti implants and Ti premachined abutments at point B at the platform level using scanning electron microscope (Group I).

3. To measure the microgap at the implant-abutment interface of Ti implants and Ti premachined abutments at point C at the platform level using scanning electron microscope (Group I).

4. To measure the microgap at the implant-abutment interface of Ti implants and Ti premachined abutments at point D at the internal connection level using scanning electron microscope (Group I).

5. To measure the microgap at the implant-abutment interface of Ti implants and Ti premachined abutments at point E at the internal connection level using scanning electron microscope (Group I).

6. To measure the microgap at the implant-abutment interface of Ti implants and Ti premachined abutments at point F at the internal connection level using scanning electron microscope (Group I).

7. To measure the microgap at the implant-abutment interface of Ti implants and customized laser-sintered Co-Cr abutments at point A at the platform level using scanning electron microscope (Group II).

8. To measure the microgap at the implant-abutment interface of Ti implants and customized laser-sintered Co-Cr abutments at point B at the platform level using scanning electron microscope (Group II).

9. To measure the microgap at the implant-abutment interface of Ti implants and customized laser-sintered Co-Cr abutments at point C at the platform level using scanning electron microscope (Group II).

10. To measure the microgap at the implant-abutment interface of Ti implants and customized laser-sintered Co-Cr abutments at point D at internal connection level using scanning electron microscope (Group II).

11. To measure the microgap at the implant-abutment interface of Ti implants and customized laser-sintered Co-Cr abutments at point E at internal connection level using scanning electron microscope (Group II).

12. To measure the microgap at the implant-abutment interface of Ti implants and customized laser-sintered Co-Cr abutments at point F at internal connection level using scanning electron microscope (Group II).

13. To compare the microgap at the implant-abutment interface between Ti implants and Ti premachined abutments with that of Ti implants and customized laser-sintered Co-Cr abutments at point A at the platform level using scanning electron microscope (Group I vs. Group II).

14. To compare the microgap at the implant-abutment interface between Ti implants and Ti premachined abutments with that of Ti implants and customized laser-sintered Co-Cr abutments at point B at the platform level using scanning electron microscope (Group I vs. Group II).

15. To compare the microgap at the implant-abutment interface between Ti implants and Ti premachined abutments with that of Ti implants and customized

laser-sintered Co-Cr abutments at the most internal point C at the platform level using scanning electron microscope (Group I vs. Group II).

16. To compare the microgap at the implant-abutment interface between Ti implants and Ti premachined abutments with that of Ti implants and customized laser-sintered Co-Cr abutments at point D at internal connection level using scanning electron microscope (Group I vs. Group II).

17. To compare the microgap at the implant-abutment interface between Ti implants and Ti premachined abutments with that of Ti implants and customized laser-sintered Co-Cr abutments at point E at internal connection level using scanning electron microscope (Group I vs. Group II).

18. To compare the microgap at the implant-abutment interface between Ti implants and Ti premachined abutments with that of Ti implants and customized laser-sintered Co-Cr abutments at point F at internal connection level using scanning electron microscope (Group I vs. Group II).

REVIEW OF LITERATURE

Vidigal et al (1995)[64]analyzed implant- abutment connection interface of five different types of titanium implants: Branemark system, Screw-vent, IMZ, TF and SR-Press by using Scanning electron microscope. A gap of 50μm was exhibited by the SR-Press and TF Implant, a gap of up to 150μm, signified an important role in accumulation ofbacterial plaque in the oral cavity. Thereby, concluded that a good fit of implant-abutment interface will not only avoid bacterial growth however, helps the patient for a better oral hygiene.

Dellow et al (1997)[19]investigated scanning electron microscope analysis of the interfacial fit of interchanged components of four dental implant systems: Southern Implant system, Branemark, Swede-vent, and Steri-OSS. The analysis reported vertical and horizontal discrepancies at the outer circumference of implant – abutment interface. From the study analysis, it was established implant system abutments are compatible and the accuracy of each component connects with or exceeds the standards set by the original Swedish (Branemark) system. Small microgap measurements were comprehended between implant – abutment interface indicating good machining tolerant when various systems are interchanged.

Ormacohea et al (1999)[49]observed maximum permissible X-ray tube angulations that demonstrated the accuracy of abutment fit to the implant using Bra imnemarkplant system. A manual screwdriver was employed to tighten the abutment screws and gaps of 21, 42, 50, 100 and 150μm were appreciated between the abutment and the implant interface. The results shown that the x-ray tube angulations altered

vertically from 0º, 5º, and 10º to 15º.It was confirmed that as the implant / abutment gaps decreased, the maximum x ray tube angulations should be between 5 and 10 degree.

Guimaraes et al (2001)[31] assessed the implant- abutment marginal fittings in terms of tightening torque, bacterial micro leakage, abutment design, conical degree and occlusion. Tightening torque is an important factor to improve mechanical and biological properties of the implant and abutment interface. Scanning electron microscopy revealed a marginal gap of 5mm and 45mm, hence proving an efficient method.

Broggini et al (2003)[14]assessed the changes in abutment timing (submerged vs. non-submerged two-piece implants) connection or the presence of a microgap (two-piece, non-submerged implants vs. one-piece non-submerged implants) affect the composition of inflammatory cells adjacent to the implants. Increase in the inflammatory cell content may due to the adhesion and proliferation of bacteria on the biofilm found at the implant-abutment gap during soft tissue manipulation for prosthetic component installation.

Jung Kim et al (2005)[38] utilized the field-emission Scanning electron microscope to determine the fit of Fixture/Abutment/Screw interfaces of internal connection implant systems. Five implant systems were selected AVANA, Bioplant, Dio, Neoplant, Implantium. Two fixtures from each group of implant system were acquired at random, Two-piece type abutment and one-piece type abutment with each implant system were used. The implant fixtures were perpendicularly mounted in acrylic resin block. Each two-piece abutment and one-piece type secured to the implant

fixture by a screw. These implant – abutment assemblies were embedded in liquid unsaturated polyester and cross sectioned using grinder polishing unit. Finally, specimens were analyzed for fit between implant/ abutment/ Screw interfaces. The study concluded that implant/Abutment/Screw connection interfaces of internal connection systems made in Korea were in good condition and materials, mechanical properties, quality of milling differed depending on the manufacturing companies.

Coelho et al (2007)[17] determined the Cross-Sectional analysis of the implant abutment interface and assessed the implant- abutment gap of two piece screw connected external hexagon implant system as a function of radius. Under an optical microscope, the series of micrographs were linked through computer software and the implant-abutment gap measurements were made along the gap region. This adaptation as a function of a radius is of vital importance and precisely predicting the mechanical influence of implant-abutment gap distances in any implant system resulting in an improved connection design.

Kano et al (2007)[36] determined the classification system to measure the implant-abutment microgap based on the horizontal and vertical microgap of the implant-abutment interface in four groups of abutments using external hexagon implants. Machined titanium abutments, premachined palladium abutments cast-on with palladium alloy, plastic burnout abutments cast with nickel chromium alloy, and plastic burnout abutments cast with cobalt chromium alloy were utilized as abutments. Under the optical microscope observation, the results showed a horizontal misfit greater than vertical misfit in all groups including the machined group.

Tsuge et al (2007)[63] assessed the marginal fit and microgaps of internal &

external hex implant-abutment interface with internal anti rotation configuration. Marginal fit and the size of the microgap at the implant- abutment interface were measured by scanning laser microscope and Scanning electron microscope. There were mean vertical discrepancy ranging from 22.6 to 62.2μm, while horizontal discrepancy ranged from -27.1 to 16.0μm. Microgap values of all I-A interfaces assessed in this study ranged from 2.3 to 5.6μm. SEM images of implant-abutment interface suggested no relationship between the geometrical factors and the type of anti-rotation configuration.

Yuzugullu et al (2007)[65] determined the implant-abutment interface of alumina and zirconia abutments after dynamic loading. Aluminum oxide, zirconium oxide, and titanium abutments were manufactured from Procera system and were connected to regular platform implants secured in a 30 ° inclined plane. Then subjected to mechanical testing with the load between 20 and 200 N at 1 Hz for about 47.250 cycles. The measurements of micro gaps at the implant-abutment interface from the labial, palatal, mesial and distal surfaces of each specimen were undertaken by SEM prior to and after the experiments. The study resulted that after the dynamic loading ceramic abutments can withstand functional forces like conventional titanium abutments.

Fujiwara C.A et al (2009)[24] determined the interface between implant/abutment of 5 implant systems of As technology, Conexao, Neodent, Sterngold, Implamed and 3i implant innovation and their respective abutments. Interfaces viewed under SEM (Cross sectional analysis) and measurements made at the most external, mid, and the internal point at the implant-abutment interface. The results

obtained in the study revealed that even when using components and implants of the same manufacturer, gaps of 0 to 15.267μm can be found at the implant-abutment interface. According to the measurements obtained, the smallest gaps were found respectively in: a) Type i abutments of Neodent system; b) Type ii abutments of Sterngoldimplamed system; c) Type iii abutments of Conexao system.

Baixe et al (2010)[4] reviewed the microgap between Zirconia abutments and titanium implants of Four systems (Procera Zirconia, Cercon Balance anterior, Zirdesign, and Straumann Cares Ceramic). Microgaps between I-A assemblies of cut sections were analyzed by Scanning electron microscope. The microgap region consisting of first 100μm from the outer surface observed at low magnification and measurements were made on images at the highest magnification. They concluded that the mean gap was larger for flat-to-flat connection systems compared to internal connection system with conical interface.

D Apicella et al (2010)[3] appraised the implant adaptation of stock abutments versus CAD/CAM abutments using radiographic and scanning electron microscopy. There were 72 implants with six equally sized groups (Group1- Implants connected to titanium abutments, Group 2- Implants connected to Zirconia abutments, Group 3- Implants connected to CAD/CAM zirconia abutments, Group 4- Implants connected to CAD/CAM titanium abutments, Group 5- Implants connected to CAD/CAM gold-coated titanium abutments, Group 6- Implants connected to CAD/CAM zirconia abutments). Results determined Aadva and Atlantis CAD/CAM abutments expressed a fit for the Astratech fixture comparing with the stock titanium and zirconia abutments.

Cunha et al (2010)[18] compared the fit accuracy between procera custom abutments and three implant systems. Twenty four zirconia procera abutments were produced using CAD/CAM and compared with 3 implant systems such as Nobel Biocare, Sistema de implantes, Conexao sistema de protesa. Measurements of microgap were measured using scanning electron microscope. They concluded that the association of procera abutment with other implant systems different from its manufacturer demonstrated significant alteration of vertical misfit at implant-abutment interface.

Moraes et al (2010)[47] determined the fit accuracy between procera custom abutments and three implant systems: Noble biocare group, SIN Experimental group, Conexao Experimental group. The Interface between implant and abutment viewed under SEM analysis at 6 measuring sites on each sample. A significant alteration of vertical misfit at implant-abutment interface was evaluated between the procera Zirconia abutment and other implant systems different from its manufacturer.

DE Jesus et al (2011)[61] assessed the misfit alterations of the implant- abutment interface of external and internal connection implant systems when subjected to cyclic loading. Five Groups evaluated were external hexagon implant and UCLA cast-on premachined abutment; internal hexagon implant and premachined abutment; internal octagon implant and prefabricated abutment; external hexagon implant and UCLA cast-on premachined abutment; and external hexagon implant and ceraone abutment. Standard metal crowns were fabricated for each group of implant-abutment assemblies and cemented. The specimens were subjected to five Lakhs cycles at 19.1Hz of frequency and non-axial load of 133N. The author proved that premachined abutments

presented better vertical misfits than premachined cast on abutments for external hex implant connections for both before and after loading analysis. Cyclic loading did not influence the vertical misfits of premachined abutments with internal and external hex connections. However, it increased the vertical misfit of premachined cast-on external hex abutments and premachined octagonal internal connection abutments.

Dittmer et al (2011)[20] did a comparative invitro study of six implant- abutment connection designs and examined regarding load bearing capacities and failure modes. Five implants of Astra Tech, Bego, Camlog, Friadent, Nobel Biocare and Straumann were embedded in stainless steel tubes using polyurethane, for 30 specimens. Specimens were loaded under 30º with respect to implant axis in a universal testing machine using test setup according to ISO 14801. Failure was indicated by load drop of 100 N in force. The study concluded with implant – abutment connection design has a significant influence on load bearing capacity and failure mode of implants; however all implant – abutment connection designs can withstand clinically relevant forces.

Meleo et al (2012)[45] explored the fixture-abutment connection surface and microgap measurements of 3 implant connection systems like Ankylos connection, Staumann connection, Bicon connectionby employing the 3D Micro-tomographic technique. The results depicted a non-devastating approach without exposing the small radio opaque object to any particular chemical treatment at a few micron high resolutions. Overall concluding the geometrical link of the fixture-abutment connection encroaches on the mechanical properties of an implant system.

Gigandet et al (2012)[27]determined the mechanical resistance, rotational misfits and failure modes of three original implant-abutment connections and to evaluate two

connections between non-original abutments connected to one of the original implants. The study wrapped up with the conclusion that the non-original abutments differ in design of the connecting surfaces and material demonstrates higher rotational misfits. Therefore, these differences may result in unexpected failure modes.

Rismanchian et al (2012)[52] evaluated the microgap size and microbial leakage in the connection area of four different abutments to ITI implants. Bacterial leakage were assessed by inoculating bacterial suspension and assessed at different times. The size of microgap of four randomized locations was then measured by scanning electron microscope. They concluded that solid and synocta abutments can significantly decrease the microgap size. However, cast on abutments do not show a significant difference in terms of microgap compared with castable abutments. Micro leakage in the connection area is comparable for these four abutments.

Zanardi et al (2012)[67] evaluated using scanning electron microscopy, the connecting accuracy of interchanged prosthetic abutments for external hexagon implants by measuring the precision of the implant-abutment interface. SIN, Conexao, and Neodent with their respective abutments (milled CoCr collar rotational and non-rotational) were the external hexagon implants and another of an alternative manufacturer (microplant) in a randomly arranged implant-abutment combinations were studied in this study. The degree of interchangeability between the various brands of components defined using the original abutment interface gap with its respective implant is a benchmark dimension in this study. It was concluded that interchanged abutments from the different tested brands did not reproduce the accuracyatThe interface of the original component and its respective implant consistently. The result

suggests that, for the parameters evaluated in this study, the alternative brand abutment is compatible with all three systems.

Baldassarri et al (2012)[6]evaluated the marginal accuracy using scanning electron microscopy, of three implant-ceramic abutment configurations and one implant titanium abutment configuration. Nobel Biocare replace, Biomet3i, Biomet3i Nanotite Tapered certain implants were the implant systems studied. Using CAD-CAM technology, three different custom-made zirconia abutments and custom-made Ti abutments (control) were fabricated. Implants and abutment connection is made and subjected to scanning electron microscopic analysis. It was concluded that, compared to all implant- zirconia abutment configuration, the implant-titanium abutment connection showed significantly better fit. Gap distance measured only at the outer circumference of the Implant Abutment Junctions (IAJ) is the only limitation of this study.

Sola-Ruiz et al (2013)[59]evaluated the vertical misfitwith or without mechanical torque and also with their possible combination between different brands of dental implants and prosthetic abutments. In this study, Five different brands of implant were used: Biofit, Bioner S.A., 3iBiomet, BTI and Nobel Biocare, with their respective prosthetic abutments. Using scanning electron microscopy at 500X, the implant- to – abutment fit/misfit was evaluated at four points (Vestibular, Lingual/Palatal, Mesial, Distal) between abutments and implants of the same brand and different brands with or without mechanical torque. Before applying torque, the vertical misfit (microgaps) of the different combinations tested results varied between 1.6 and 5.6 microns and after applying torque, between 0.9 and 5.9 microns. It may be concluded that vertical fit

values observed in all cases fell within limits of clinical acceptability. No significant results seen. Mechanical torque application improved outcomes. There is compatibility and clinical possibility between implants and abutments of different brand and so of their combination.

Hamilton et al (2013)[32]compared the fit of titanium CAD-CAM abutments using scanning electron microscope with prefabricated abutments on five different implant types (Branemark system, Noble Replace, AstratechOsseoSpeed, Straumann Bone Level, and Straumann Standard Plus). The samples were embedded in epoxy resin, sectioned longitudinally, and polishing of the samples is done. Measurement and values of Microgaps between the implants and abutments at the connecting flanges and internal features were calculated. It was concluded that, compared to the prefabricated abutments, CAD-CAM abutment system appeared to have a comparable fit.

Neves et al (2014)[48]compared the misfits after casting and soldering procedures in external hexagonal implants and their UCLA abutments at implant-abutment interface. Three unit fixed partial implant supported bridge is used for the analysis. The SEM analysis is made. They concluded that, after casting procedure, pre machined abutments containing Ni-Cr-Ti alloy exhibit better mechanical properties. The horizontal misfit's values for most of the abutments before and after the soldering procedures were within acceptable limits. Application of soldering didn't result in significantmisfits, casting procedure resulted in increase of vertical misfits.

Kikuchi et al (2014)[39]evaluated using optical coherence tomography, the marginal fit of implant-abutment interface. OCT can detect smaller gaps and obtain

images in large angulations than X-ray. But the thicker (> 2mm) layer of soft tissue affects the sensitivity of gap detection by OCT. Nevertheless, OCT is a most useful tool to evaluate implant-abutment interface non-destructively as there is no X-ray exposure.

BeriBeri et al (2014)[11] evaluated in vitro leakage at implant- abutment interface using Rhodamine B of osseospeed implants connected to original and compatible abutments. Higher solubility in water and reaction with photo-generated oxyradicals makes Rhodamine B an interesting marker. Titanium design, Natea, Dual, Implant were the compatible abutments used. With the help of spectophotometric analysis, the inner volume of each implant-abutment connections was calculated and leakage was detected for each group at different time intervals. It was concluded that, when compared to the use of abutment and implant from same manufacturer, the use of compatible abutment components with original Astra Tech implants showed significant leakage.

Fernandez et al (2014)[23] computed the micro roughness of the mating surfaces of implant components manufactured with different processes, also enumerated the gap between implant components and to determine whether a correlation exists between micro roughness and microgap. Nine dental implants with a standard external connection, Avinent implant system were paired with three milled, three cast and three sintered compatible cobalt – chromium alloy abutments. The abutment surface was examined by Scanning electron microscope, and the roughness parameter S, was measured using a white – light interferometric microscope at 10 x 100 magnifications. The study reported with milled abutments possess connection geometry with mean

roughness of 29μm, sintered abutments showed a blurred but functional connection with roughness of 115μm, and cast abutments showed with loss of axial symmetry and roughness of 98μm. It concluded with the milled components were smoother than the cast or sintered components and correlation seen between surface roughness and microgap width.

Gill et al (2014)[28] evaluated with the help of cyclic loading, the micro gap size and fatigue behavior of external and internal connections. It was concluded that the internal connections had a smaller micro gap compared to the external ones. The fatigue behavior with the superior results was presented by the external hexagon interface compared to the internal hexagon interfaces. Higher fatigue life of external hexagon interface is due to the size of the resistant action and higher area than the internal, which produces better loaddistribution

Suttin Z et al (2014)[60]studied the seal performance of aftermarket abutments,which was connected to BIOMET 3i T3 with DCD. The aftermarket abutment and screws for the study came from 3 manufacturers (KOMP, Medentika and IPD). Under dynamic loading conditions, the performance of assemblies was assessed. No statistically significant differences in seal strength. A significant difference between each of the after-market components and BIOMET 3i OEM components was found. The average load required to breach the seal was 63%, 60% and 52% lower respectively for the KOMP, Medentika and IPD abutments than the systems assembled with the BIOMET 3iabutments.

Al-Jadaa et al (2015)[1] evaluatedusing a gas enhanced permeation test to assess

implant leakage, the impact of dynamic loading on the implant-abutment interface. Implants such as Astratech, Biomet3i, NobelBiocare were evaluated for leakage. Both static and dynamic conditions between three groups leakage was assessed. It was concluded that compared to dynamic conditions, implants leaking under static conditions had increased potential for bacterial leakage. Best performance was given by Implants with a flat-to-flat interface and internal hexagonal mating surfaces showed with regard to leakage under both static and dynamic conditions.Promising technique for assessing the overall implant system leakageresistance is GEPT.

Bajoghli et al (2016)[5] evaluated the bacterial leakage and microgap along implant-abutment connection in different implant systems. 28 implants in three groups were used 10 zimmer with conical configuration of 8 degrees, 10 dentium with conical connection of 11 degrees, 8 test samples with conical connection in sixteen degrees were used. Microleakage of E.coli was assessed and microgap was measured using scanning electron microscope in four different points. It was concluded that Microleakage exsited in all three groups. Although there was difference in microgaps between three groups, but Microleakage was not statistically significant.

Gehrke et al (2016)[23] evaluated with the help ofconical internal connection (Morse taper), the effects of different torque level at the implant-abutment interface. Different torque level at the implant and the solid abutments were grouped as follows: Group I=25Ncm, Group II=30Ncm, Group III=35Ncm, Group IV=40Ncm. Scanning electron microscopy measures the contact length along the implant-abutment interface. It was concluded that the linear area of contact between the abutment and implant

increases as torque augmented. Increase in the fit (contact) of the implant-abutment interface is due to the higher insertion torque values in a conical internal connection.

Sacrano et al (2016)[53] evaluated the implant-abutment contact surfaces and microgap measurements of different implant connections under 3D x-ray microtomography. A total of 40 internal connection implants were used in this study, 10 were screw retained internal hexagon design, 10 were morse cone taper internal connection and 10 were screw tri-lobed connection. In both the morse cone internal connections, there was no separation of implant-abutment in the conical area, and there was an absolute congruity without any microgaps between abutment and implant. They concluded that different types of implant-abutment joints are responsible for the differences in bacterial penetration.

Alonso- Perez et al (2017)[2] evaluated the marginal accuracy and mechanical behavior of implant- supported crowns restored with original stock abutments and nonoriginal computer aided design/computer assisted manufactured laser sintered abutments. Twenty six implants 3.7mm x 13mm of tapered screw-vent Zimmer were selected grouping into two, firstly, implants connected to original stock abutments (OS) and secondly, implants connected to non-original laser sintered abutments (LS). Out of these samples, 10 were examined to measure the marginal accuracy by scanning electron microscopy and all the samples were used to study the mechanical behavior by undergoing the static loading and dynamic loading after thermocycling with artificial saliva. OS revealed the best marginal accuracy however, LS gap showed a clinical acceptable range of marginal discrepancy. The studies concluded with both abutments are acceptable alternatives to restore implants although; original abutments are much

better fit than the nonoriginals.

Cardozo et al (2017)[16] analyzed the abutment-implant platform gap in internal hex dental implants. A descriptive study was designed to analyze the gap using 20N or 30N torques for the abutment. Three implant units from four different brands were used that fulfilled the study condition of internal hex and standardization. Observations were made and the microgap was measured using scanning electron microscope. Significant differences were found between the gap in abutments installed with either $20N/cm^2$ or $30N/cm^2$, with fewer differences observed in second group. It was concluded that the installation torque of the prosthetic abutment influence the interface microgap between prosthetic connector and implant surface.

MATERIALS AND METHODS

The present *in vitro* study was conducted to comparatively evaluate the microgap at the implant-abutment interface with premachined and customized laser-sintered Co-Cr abutments using scanning electron microscope (SEM).

The following materials, instruments, equipment and methodology were employed:

Materials used for the study:

- Titanium dental implant, standard platform, internal hexagon,3.75mm diameter,10mm length (ADIN Dental Implants., Israel) (Fig. 1)

- Pre-machined titanium abutment, standard platform, internal hexagon (ADIN Dental Implants., Israel) (Fig. 2)

- Cobalt-chromium powder (Kobalt chrome pulvar wirobond c$^+$) (Fig.3)

- Titanium dioxide spray (Easy scan) (Fig. 4)

- Spirit level indicators (Jinhua Hengda tools., China) (Fig. 5)

- Polyvinylsiloxane impression material (Aquasil, Dentsply, Germany) (Fig. 6a, 6b, 6c, 6d)

- Clear autopolymerising acrylic resin (RR Cold Cure., DPI, India) (Fig. 7)

- Aluminium oxide powder, 110μm (Korox, Alpha bond, Australia) (Fig. 8)

- Emery papers (3M India Ltd., Bangalore, India) (Fig. 9)

- Distilled water (Merck & Co., Mumbai INDIA) (Fig. 10)

- Ethyl alcohol 100% (Merck & Co., Mumbai INDIA) (Fig. 11)

Instruments used for the study:

- Teflon holding device (CIPET, Guindy, Chennai) (Fig. 12)

- Hex driver (ADIN Dental Implants., Israel) (Fig. 13)

- Calibrated Torque wrench (ADIN Dental Implants., Israel) (Fig. 14)

- Metal cutting disc and mandrel (Dentorium., New York, U.S.A) (Fig. 15a, 15b)

- Tungsten carbide metal trimming burs (Edenta., Switzerland) (Fig. 15c)

- Rubber polishing point (Fig. 16)

Equipments used for the study:

- Selective Laser Melting machine (SLM) (SLM 125^{HL} Solutions GMbH, Germany) ((Fig. 17)

- Model scanner (Maestro 3D Easy Dental scan, Pontedera (pisa), Italy) (Fig. 18)

- Dental surveyor (Saeshin Precision Ind. Co., Korea) (Fig. 19)

- Sand blasting unit (Delta labs, Chennai, India) (Fig. 20)

- Water jet powered sectioning machine (Germany) (Fig. 21)

- High speed lathe (Demco, California, U.S.A) (Fig. 22)

- Steam cleaner (Confident dental equipment Ltd, India) (Fig. 23)

- Digital Ultrasonic cleaner (Beijing Ultrasonic Co., China) (Fig. 24)

- Dryer (Panasonic corporation made in Thailand) (Fig. 25)

- Scanning electron microscope – (EVO MA 15, CARL ZEISS pvt.ltd.UK) (Fig. 26)

Description of water-jet powered sectioning machine (Fig. 21)

It is a versatile industrial tool capable of cutting a wide variety of materials using high pressure jet of water or a mixture of water with an abrasive substance. The main unit consists of a controller unit, a motion system, a catch tank, a nozzle, an abrasive delivery system, a reverse osmosis water plant and an intensifier pump. The purified water from the RO plant is pressurised by the compressor in the intensifier pump. High pressurised water passes through the control unit, maintaining a pressure of 1800-3800 bar which drives the motion system in different axis. The pressurised water runs along the tube and reaches the cutting unit, thereby concentrating on the point of location to be sectioned and it then mixes with abrasive substance and reaches the nozzle. Depending on the nozzle aperture the sectioning width may vary.

LINE DIAGRAM OF WATERJET MACHINE
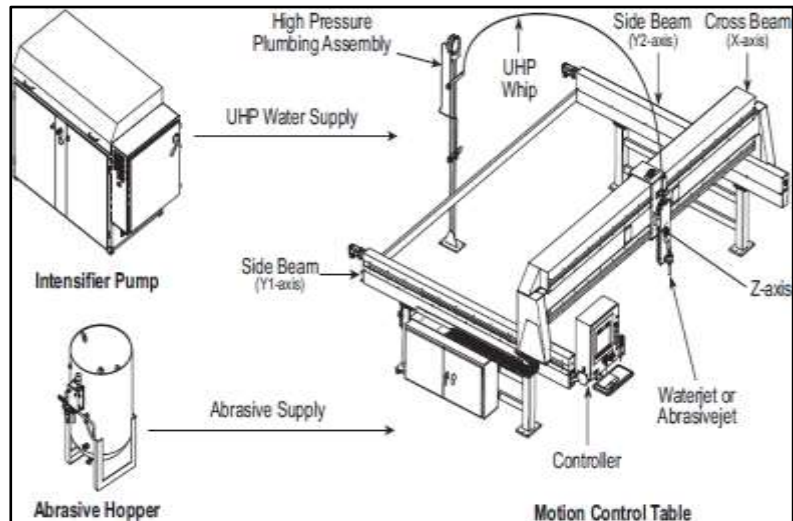
Description of scanning electron microscope (Fig. 26)

Scanning Electron Microscope (SEM) (EVO MA 15) is an analytical electron microscope of choice for users offering the leading imaging and analysis solution in materials Analysis. With a motorised 5 axis stage with large X,Y and Z travels, variable pressure capability as standard and easy to use SmartSEM software, it offers a perfect imaging solution in different fields. It has a working distance of 10 mm and a magnification of 20x to 2, 00000 x. Scanning Electron Microscope uses electrons instead of light to illuminate samples. The electrons from an electron gun are focused into a narrow beam using a series of magnetic lenses. The beam was scans across a sample in a grid pattern and detectors record the resultant image that comes from the sample. Nonconductive samples in the electron microscope will build up

charge on the surface, reducing the image quality. One way to improve image quality is to sputter coat the sample with a conductive material like gold to give the electrons a path to leave the sample. The image on the monitor gets captured using SmartSEM software and was then transferred to the computer.

LINE DIAGRAM OF SCANNING ELECTRON MICROSCOPE
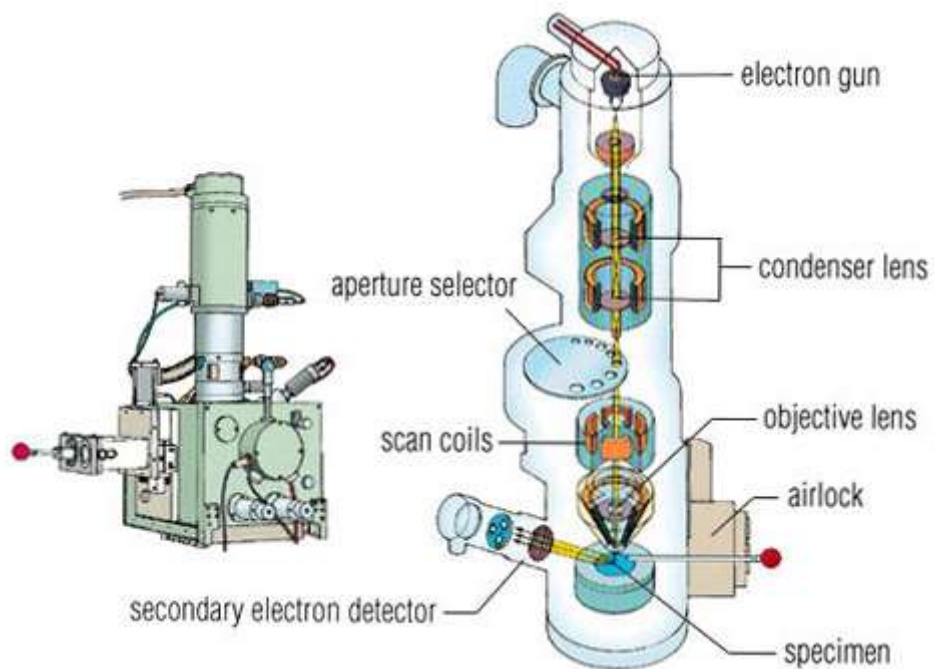
METHODOLOGY

The methodology adopted in the present study is described under the following sections:

    I.   Fabrication of custom-made stainless steel block and receptacle

    II.   Obtaining silicone putty index using stainless steel block and receptacle

    III.   Fabrication of customized laser-sintered Co-Cr abutments

    IV.   Connecting implant abutments to implants and grouping

    V.   Embedding of implant-abutment assembly in the acrylic resin

    VI.   Sectioning of test samples using water jet sectioning machine

    VII.   Preparation of sectioned test samples for SEM analysis

    VIII.   Obtaining SEM images of test samples at the implant-abutment interface

    IX.   Measurement of microgap at the implant-abutment interface on SEM images

    X.   Data tabulation and statistical analysis

I. Fabrication of custom-made stainless steel block and receptacle:

(Fig. 27, 28)

A stainless steel cuboid block of dimensions 27mm x 27mm x18mm (Fig. 27a & 27b) and a stainless steel, perforated metal receptacle of dimensions, 40mmx 50mm x 40mm, (Fig. 28a & 28b) were fabricated. These were used for creating a uniform mold space in the putty index of standardised dimensions.

II. Obtaining silicone putty index using stainless steel block and receptacle: (Fig. 29a-d)

In this study, the stainless steel receptacle was used as a customized impression tray. Addition silicone polyvinylsiloxane impression material of putty consistency (Aquasil, Dentsply, Germany) (Fig. 6a) was hand mixed and placed inside the stainless steel receptacle. Light body consistency polyvinylsiloxane (Aquasil, Dentsply, Germany) (Fig. 6b) was injected using the dispensing gun over the putty material (Fig. 29a). The stainless steel block was then centred and pressed into the impression material (Fig. 29b) such that, the top surface of the block was in level with the top edge of the receptacle. The excess impression material was removed and allowed to set (Fig. 29c). After setting of the impression material, the stainless steel block was removed from the putty index and the mold space area inspected for accuracy and acceptability (Fig. 29d). The putty index obtained was used for the purpose of embedding the implant-abutment assembly in the acrylic resin.

III Fabrication of customized laser-sintered Co-Cr abutments:(Fig. 30-44)

In the present study, ten abutments were customized with Co-Cr alloy powder by the process of laser-sintering. A scan body (Fig. 30) corresponding to the standard platform implant was attached to the internal hexagonal connection of the implant. The scan body was sprayed with Titanium dioxide spray (Easy scan) for the purpose of CAD/CAM scanning (Fig. 31). The implant attached to the scan body (Fig. 32) was positioned on the platform inside the model scanner (Maestro 3D Easy Dental scan, Pontedera (pisa), Italy) (Fig. 18). The scan body was scanned (Fig. 33) to obtain the virtual image of the scan body. Using "exocad" software, the virtual implant was aligned to the image of the scan body to achieve the proper orientation of the implant connection (Fig. 34). A virtual standard platform abutment was then connected to the implant in the software and verified for best fit (Fig. 35). Once the virtual design of the implant abutment (Fig. 36) was ready, these details were extracted and saved in a stereolithographic (STL) format (Fig. 37). The STL data obtained was forwarded to the building chamber (125*125 mm platform) of Selective Laser Melting machine for sintering (SLM 125^{HL} Solutions GMbH, Germany) (Fig. 38), where infrared laser beam was used to fuse the Co-Cr powder to produce a solid object. During sintering, to prevent bending or dislodgement and to obtain the exact shape, size and for the support of the abutment, sprue channel of 40 µm in the platform of the building chamber was created (Fig. 39). Then 20 µm size Co-Cr powder (Kobalt chrome pulvar wirobond c$^+$) (Fig. 3) was

loaded into the canister where a layer of Co-Cr powder was uniformly spread with a powder levelling roller, across the platform. The laser beam scans, heats and fuses the sequential and simultaneous layering of Co-Cr powder during sintering. Laser sintering (Fig. 40) takes place for 31/2 hrs until the abutment was completed to set dimensions. Once the laser sintering was complete, the software was set for "homing" to increase the oxygen content to 16%. Then the lid was opened and the platform bed with the abutments were retrieved (Fig. 41). Further, the abutment sprues were cut (Fig. 42) and the connection area of the abutment was finished with rubber point polishing (Fig. 43). Thus ten customized abutments were fabricated such that it has similar geometry, connection design and dimensions with that of premachined abutments (Fig. 44)

IV. Connecting implant abutments to implants and Grouping: (Fig. 45-46).

Twenty titanium implants of 3.75 mm diameter, 10mm length (ADIN Dental Implants, Israel) with standard platform, internal hexagon connection design (Fig. 1) were used in this study.

In the present study, twenty abutments were used. Of these, ten abutments were premachined (ADIN Dental Implants, Israel) and ten abutments were customized using the laser-sintering technique.

The premachined and customised abutments were randomly selected and each was connected to one randomly selected implant by hand torquing

the abutment screw with the hex driver (ADIN Dental Implants, Israel) (Fig. 45a & 45b).

Based on the type of abutment used, the implant-abutment assemblies were grouped into Group I and Group II. Group I comprised of premachined abutments connected to their respective implants (n=10) (Fig. 46a) and Group II comprised of customized laser-sintered Co-Cr abutments connected to their respective implants (n=10) (Fig. 46b).

V.   Embedding of implant-abutment assembly in the acrylic resin: (Fig. 47 - 57).

In the present study, the implant-abutment assembly was embedded in the putty index into the acrylic resin in the following manner:

Stage I: On the surveying platform of a dental surveyor (Saeshin Precision Ind. Co., Korea) (Fig. 20), the silicon putty index which was previously obtained was stabilized with the mold space facing up. Spirit level indicators (Jinhua Hengda tools, China) (Fig. 5) were used to stabilize the surveying platform parallel to the floor (Fig. 47). The abutment was secured to the surveying mandrel and used as a carrier to orient the implant-abutment assembly in the centre of the putty index (Fig. 48). One implant-abutment assembly was positioned into the putty index at a given time (Fig. 49). This was done to orient and centre the implant into the mold space of the putty index.

The putty index was filled with auto polymerizing clear acrylic resin (Cold Cure, DPI, India) (Fig. 8) up to the crest module of the implant and then allowed to polymerize (Fig. 50a & 50b). This was left undisturbed during setting; the resin block was removed from the index and was numbered (Fig. 51a & 51b). The resin block was secured in the custom-made Teflon holding device (Fig. 13) with the help of a screw (Fig. 52). The hex driver (Adin Dental Implants., Israel) (Fig. 14) was connected to the torque wrench (Adin Dental Implants., Israel) (Fig. 15) and the abutment screw was torqued to 35Ncm as recommended by the manufacturer (Fig. 53a & 53b). The Teflon holding device resists the rotation of the resin block during torquing of the abutment screw. The abutment screw was retorqued after twenty four hours to prevent screw loosening and to ensure proper adaptation between the implant-abutment interfaces (Fig. 54a & 54b).

Stage II:

In the second stage, the abutment over the implant was completely embedded into the auto polymerising resin.

To facilitate retention of the abutment within the resin matrix, the abutment was initially sand blasted using alumina particles of 110 μm grit size (Fig. 9) to produce a uniformly roughened surface (Fig. 55).

The assembly was completely embedded using clear autopolymerising acrylic resin by repositioning the implant-abutment assembly with the mold

space of silicon putty index and allowed it to cure completely overnight (Fig. 56).

The resin block with the implant-abutment assembly was removed from the Teflon holding device and was reseated into the putty index. Clear auto polymerising acrylic resin was filled into the index to embed the implant-abutment assembly to cover the abutment screw access. The resin block was allowed to cure completely overnight. In a similar manner, all the twenty implant-abutment assembly (Group I and Group II) were embedded in the acrylic resin.

The embedded implant-abutment assembly test samples were numbered individually and labelled for group I as GI to GI 10 (Fig. 57a) and for group II as GII to GII 10 (Fig. 57b).

VI. Sectioning of test samples using water jet sectioning machine:

(Fig. 58- 61)

A line was drawn to mark the centre of the implant-abutment assembly on the resin block (Fig. 58). The resin block was stabilized on the sectioning platform of the water jet powered sectioning machine and held securely with the clamp and it was placed on metal beds present in the catch tank (Fig. 59). With the help of the controlling unit the points were marked to locate the desired section of the sample. The controlling unit was used to adjust the pressure. The nozzle aperture tip of 0.76mm was positioned just above the

area to be sectioned. Water mixed with abrasive agents was focused on the marked area of sectioning using the nozzle. The test sample was sectioned under 3500 bar pressure by using water and abrasive (Fig. 60). The sectioning was done vertically along the long axis of implant-abutment assembly using the reference line marked. Similarly, all the twenty test samples were sectioned (Fig. 61a, 61b)

VII. Preparation of sectioned test samples for SEM analysis: (Fig. 62-68)

To aid in proper seating on to the platform of the scanning electron microscope, the base portion of clear acrylic resin of each vertically cross sectioned sample was then further reduced in thickness using an high speed lathe with metal cutting disc to render it flat (Fig. 62). The test samples were subjected to sequential finishing procedure using progressively diminishing grit size (from 400 to 1200) of silicone carbide emery paper (Fig. 63a & 63b) followed by copious rinsing with distilled water and ethyl alcohol to remove clogged debris that would interfere with accurate visualisation of the implant-abutment interface. These were then cleaned using a steam cleaner (Confident dental equipment Ltd, India) (Fig. 24) and followed by ultrasonic bath cleaning (Beijing Ultrasonic Co., China) (Fig. 25) for 10 minutes (Fig. 64 & 65). Finally, all the test specimens were rinsed with ethyl alcohol (Fig. 66) and dried with a hair dryer (Panasonic corporation made in Thailand) (Fig. 26) (Fig. 67) to ensure clean and dry test specimens (Fig. 68a & 68b). The test samples were

then stored in an air-tight container until SEM analysis to avoid further contamination.

VIII. Obtaining SEM images of test samples at the implant-abutment interface: (Fig. 69-71)

The test samples were gold sputtered (K650 sputter coater, Quorum Technologies), prior to SEM procedures to make the samples more electro-conductive, since SEM uses electrons and creates higher magnification and resolution images (Fig. 69)

The implant-abutment interface of each test sample was analysed under Scanning electron microscope (EVO MA 15, CARL ZEISS pvt.Ltd.UK) (Fig. 27) at 10 kV acceleration voltages. Images were obtained at different magnifications such that, the implant-abutment interface area of each test sample could be visualised either under a lower magnification (Fig.70a, 70b) or a specific area could be visualised under suitable higher magnifications in separate images (Fig. 71a, 71b) to aid in accurate measurement of the interface microgap.

IX. Measurement of microgap at the implant-abutment interface on SEM images: (Fig. 72-73)

In the present study, the interface microgap of the implant-abutment assembly of each test sample was measured individually at various points as referred in the schematic diagram (Fig.72). Using an image measuring pixel counting software (Image J, National Institutes for Health) the images of each test

sample were obtained. In this software, the SEM images were installed into the software file. The known distance, pixel, unit of the specific SEM images was transferred to the measuring scale of the software. The microgaps were measured with the linear measuring scale of the software. For each sample, microgap measurement at the implant-abutment interface at the platform and internal connection levels were measured in twelve different points (Fig. 73a & 73b).

X. Data tabulation and statistical analysis

The basic microgap values at the platform level and internal connection level were measured and tabulated using Microsoft Excel 10 (Microsoft, USA) and the mean and standard deviation were calculated. For each test sample, the mean microgap was calculated for a particular point (at platform level and internal connection level) by averaging the microgap measurements obtained on the right and left sides for that point. From each sample mean, the overall mean microgap at that particular point was calculated.

The data were subjected to statistical analysis using SPSS software for Windows 10.0.5 (SPSS Software Corp., Munich, Germany).

ANNEXURE I

METHODOLOGY OVERVIEW

Fabrication of custom made stainless steel block and receptacle

↓

Obtaining silicone putty index using stainless steel block & receptacle

↓

Fabrication of customized laser sintered Co-Cr abutments

↓

Connecting implant abutments to implants and grouping

↓

| Connected standard Ti premachined abutments to implants (n=10) (Group I) | Connected customized laser-sintered abutments to implants (n=10) (Group II) |

↓

Embedding implant-abutment assembly in the acrylic resin

↓

Sectioning of test samples using water jet sectioning machine

↓

Preparation of sectioned test samples for SEM analysis

↓

Obtaining SEM images of test samples at the implant-abutment interface

↓

Measurement of microgap at the implant-abutment interface on SEM images

↓

Data tabulation and statistical analysis

ANNEXURE II

MATERIALS

Fig.1: Titanium dental implant, standard platform, internal hexagon

3.75mm diameter, 10 mm length

Fig.2: Premachined titanium abutment, standard platform, internal

hexagon

Fig.3: Cobalt -chromium powder

Fig.4: Titanium Dioxide spray for CAD/CAM Scanning

Fig.5: Spirit level indicators

Fig. 6a: Putty consistency Polyvinylsiloxane impression material

6b: Light body consistency Polyvinylsiloxane impression material

6c: Dispensing gun

6d: Auto mixing spiral

Fig.7: Clear autopolymerising acrylic resin

Fig.8: Aluminium oxide powder -110µm

Fig.9: Emery papers

Fig.10: Distilled water

Fig.11: Ethyl alcohol (100%)

INSTRUMENTS

Fig.12: Teflon holding device

Fig.13: Hex driver

Fig.14: Calibrated torque wrench
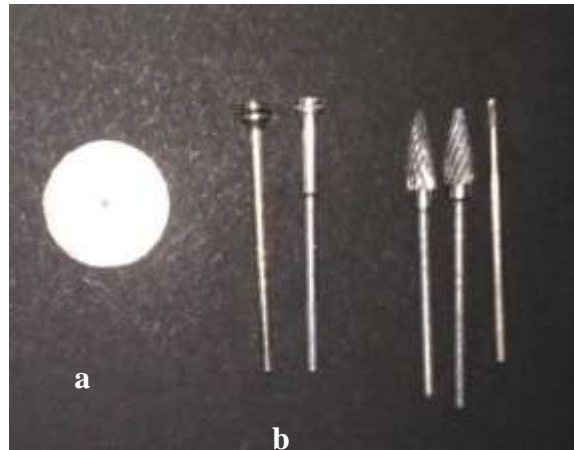
Fig.15a: Metal cutting disc

15b: Disc mandrel

15c: Tungsten carbide burs

Fig.16: Rubber Point Polishing

EQUIPMENTS

Fig 17: Selective laser melting machine

Fig 18: Model Scanner

Fig.19: Dental surveyor

Fig.20: Sand blasting unit
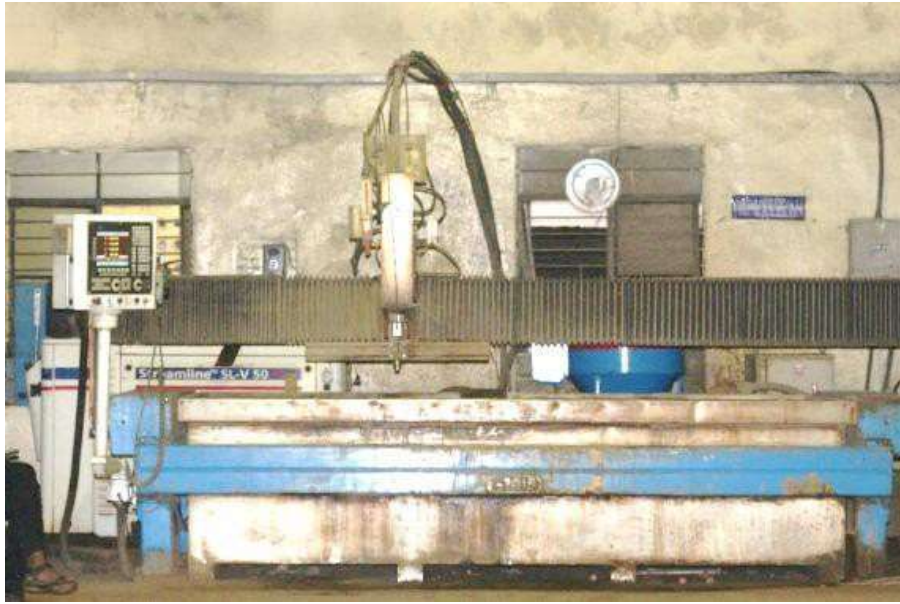
Fig.21: Water jet powered sectioning machine

Fig.22: High speed lathe

Fig.23: Steam cleaner

Fig.24: Digital Ultrasonic cleaner

Fig.25: Dryer

Fig.26: Scanning Electron Microscope

METHODOLOGY

I.   Fabrication of custom-made stainless steel block & receptacle
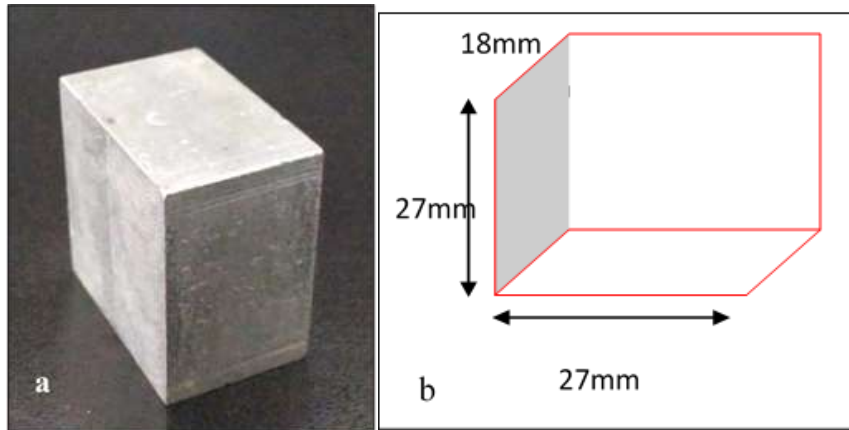
Fig.27a: Custom-made stainless-steel block.

27b: Line diagram of custom-made stainless-steel block
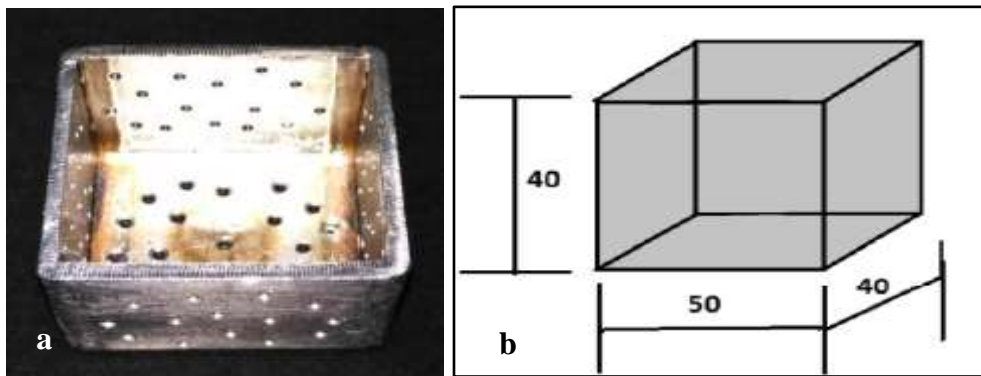
Fig.28a: Custom-made stainless steel perforated metal receptacle

28b: Line diagram of custom-made stainless steel perforated

metal   receptacle

II. Obtaining silicone putty index using stainless steel block & receptacle
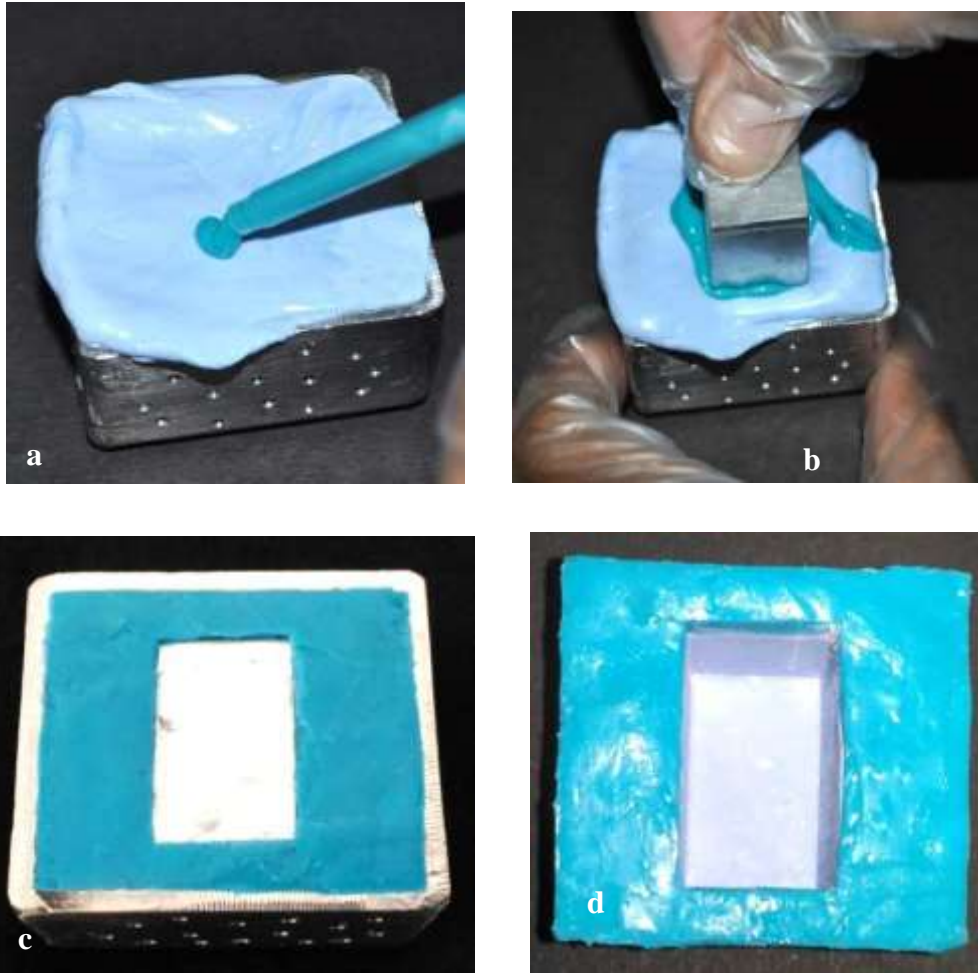
Fig 29a: Filling of custom-made receptacle with polyvinyl siloxane

29b: Making impression of stainless steel block with soft putty

29c: Set impression with stainless steel block

29d: Standardized silicone putty index

III. Fabrication of customized laser- sintered Co-Cr abutments

Fig. 30: Scan body

Fig. 31: Spraying of TiO$_2$ Spray on the scan body

Fig. 32: Attachment of scan body to implant

Fig 33: Scanning of the scan body
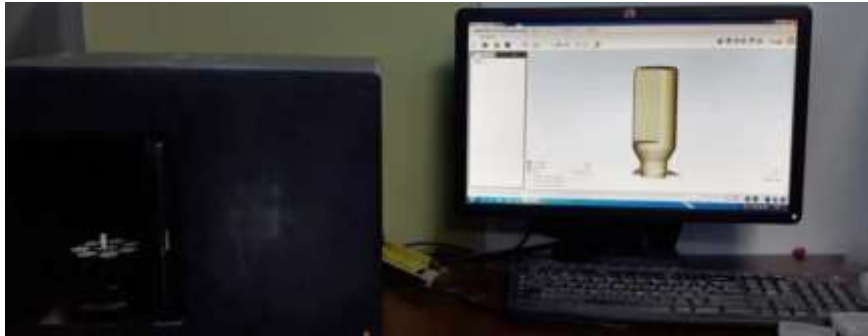
Fig 34: Scanned image in the "exocad" software

Fig 35: Matching of abutment to implant Connection

Fig 36: Virtual design of implant abutment
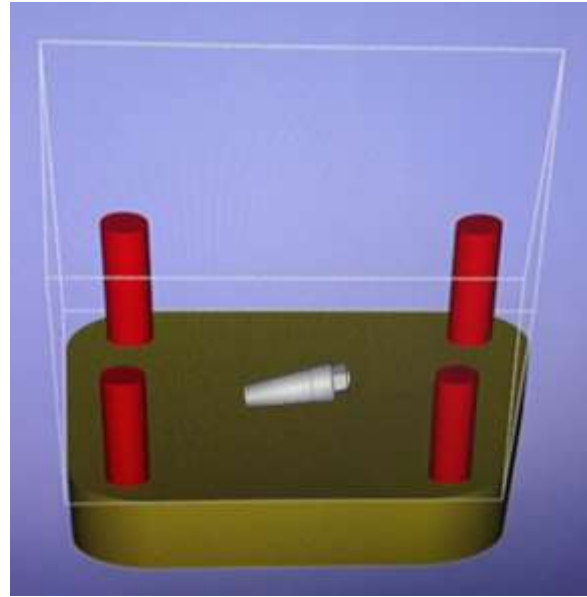
Fig 37: Virtual design of the abutment in STL format

Fig 38: Building chamber in SLM
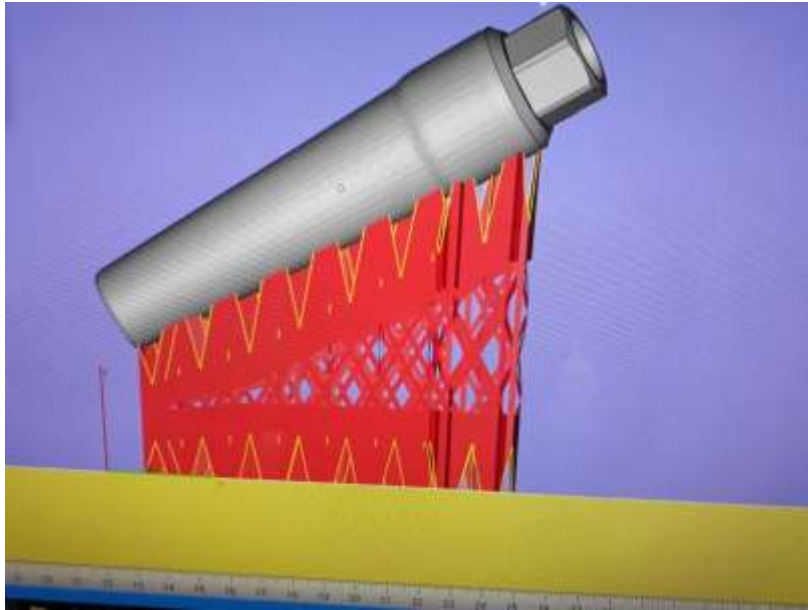
Fig 39: 40μm sprue created in the platform of building chamber

Fig 40: Laser sintering of abutments
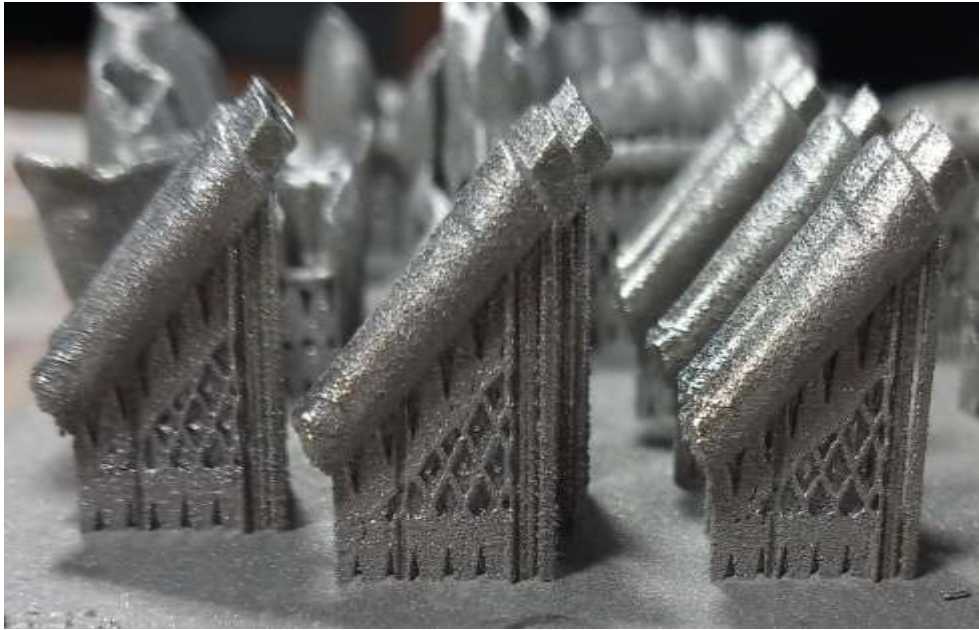
Fig 41: Laser-sintered abutment before sprue detachment

Fig. 42: Laser-sintered abutment after sprue detachment
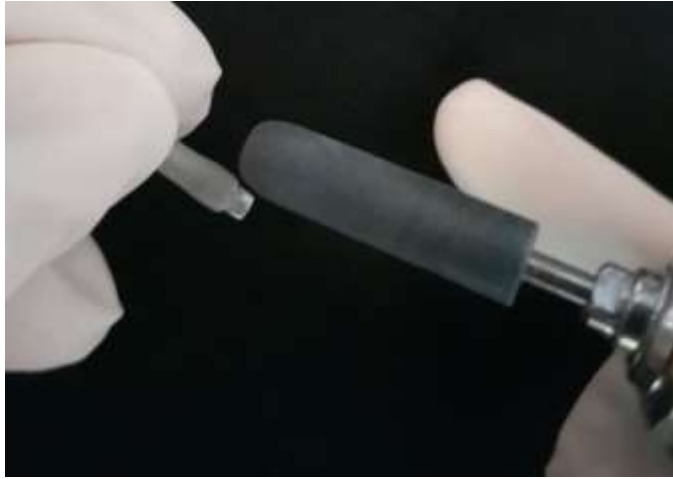
Fig, 43: Rubber point polishing in connection area

Fig 44: Finished customized laser-sintered Co-Cr abutments

IV. Connecting implant-abutments to implants & grouping
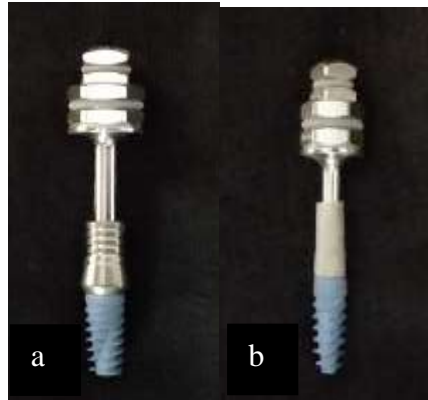
Fig.45a: Single one stage connection with drive (Group I)

Fig.45b: Single one stage connection with drive (Group II)

Fig.46a: Connection of premachined abutments to the implants (Group I)

Fig.46b: Connection of customized laser-sintered abutments to the

implants (Group II)

V. Embedding of implant-abutment assembly in the acrylic resin

Fig.47: Silicone putty index made parallel to the floor using spirit level

indicators

Fig.48: Attaching the connected implant abutment assembly to the

mandrel of surveying arm
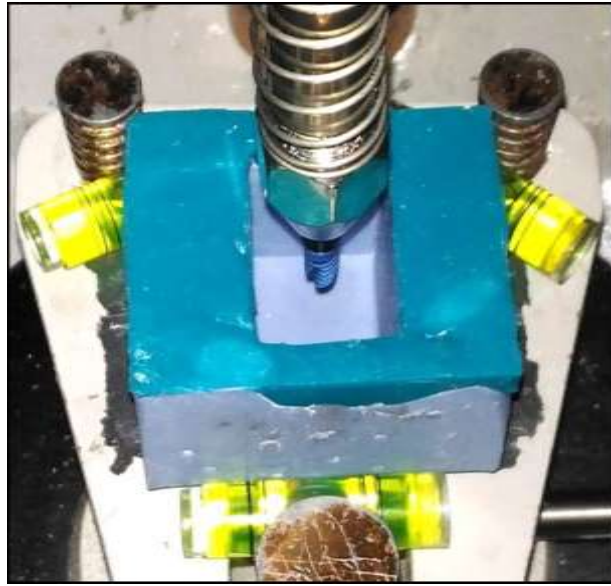
Fig.49: Positioning of implant-abutment assembly in silicone index

Fig.50a: Pouring of clear acrylic resin into silicone putty index
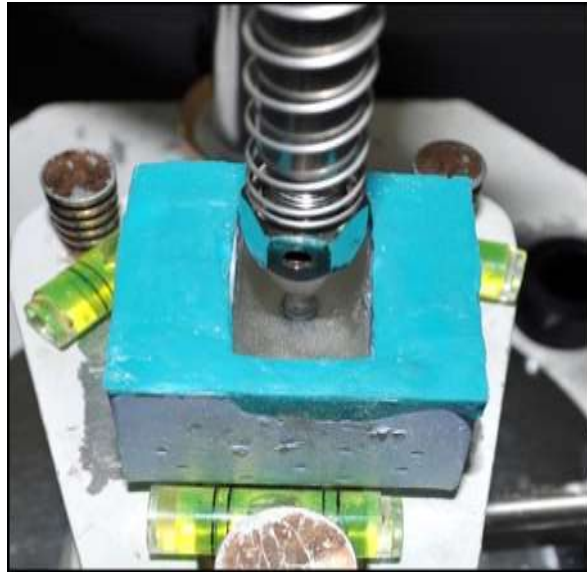
Fig.50b: Implant embedded in acrylic resin

Fig.51a: Secured implant abutment assembly (Group I)

51b: Secured implant abutment assembly (Group II)

Fig.52: Securing the resin block in the Teflon holding device
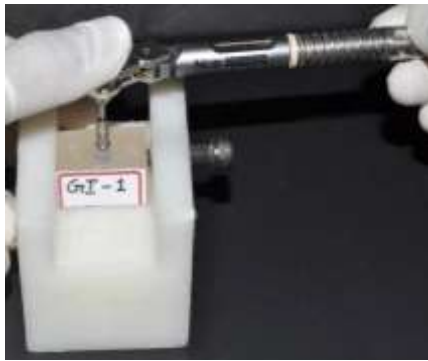
Fig.53a: Torquing of abutment screw (Group I)
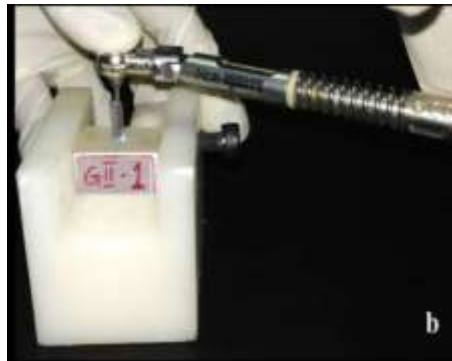
Fig.53b: Torquing of abutment screw (Group II)

Fig.54a: Retorquing of abutment screw after 24 hours (Group I)
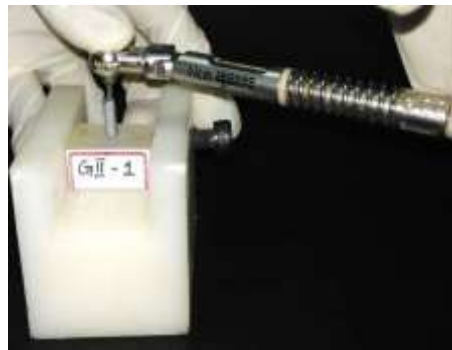
Fig.54b: Retorquing of abutment screw after 24 hour (Group II)
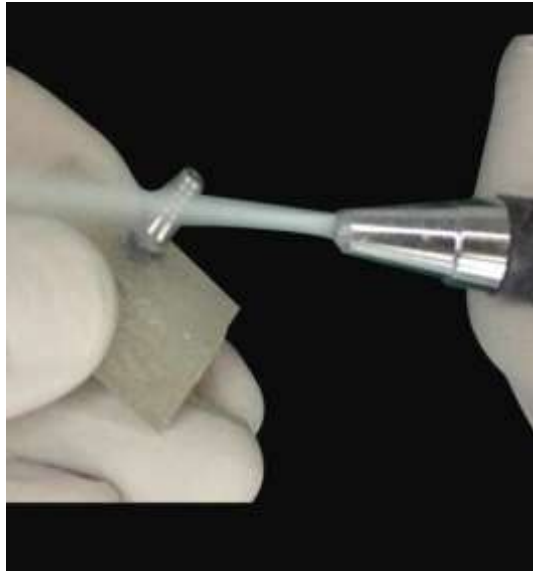
Fig.55: Sand blasting of the abutments
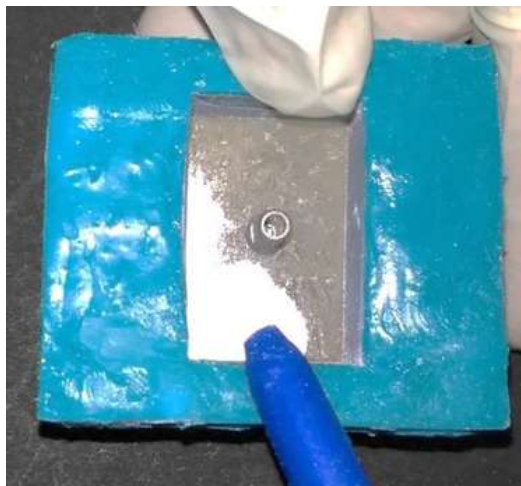
Fig.56: Complete embedding of implant-abutment assembly

Fig.57a: Labelled test samples (Group I)

Fig.57b: Labelled test samples (Group II)

VI.   Sectioning of test samples

Fig.58: Marked reference line on resin block

Fig.59: Resin block secured on sectioning platform of water jet sectioning

equipment

Fig.60: Water jet powered sectioning of test sample
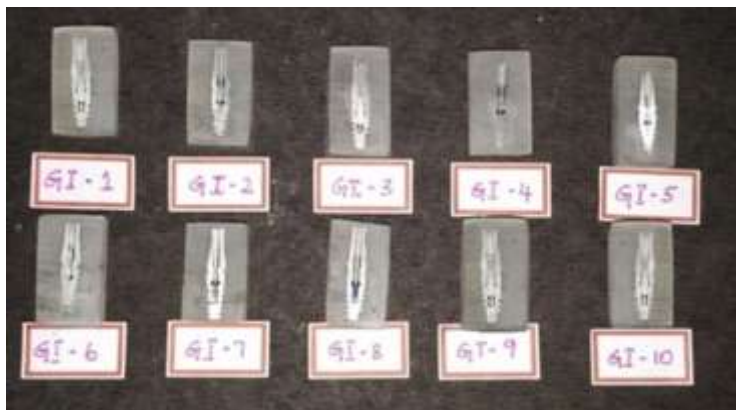
Fig.61a: Sectioned samples of Group I
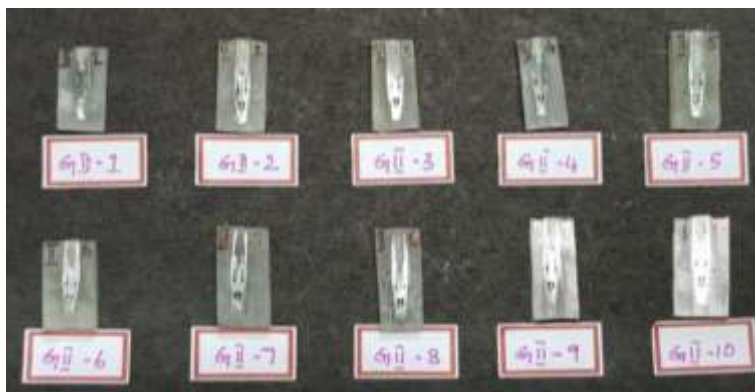
Fig.61b: Sectioned samples of Group II

VII. Preparation of sectioned test samples for SEM analysis
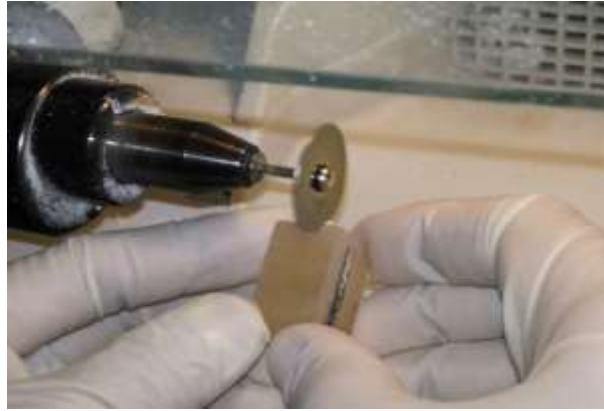
Fig.62: Trimming of excess clear acrylic resin using high speed lathe

Fig.63a: Cleaning and smoothening of sectioned test sample using silicon carbide emery paper (Group I)

63b: Cleaning and smoothening of sectioned test sample using silicon carbide emery paper (Group II)

Fig.64: Steam cleaning of sectioned test sample

Fig.65: Ultrasonic cleaning of sectioned test samples

Fig.66: Sectioned test samples soaked in ethyl alcohol

Fig.67: Drying of test sample using dryer

Fig.68a: Cleaned sectioned test samples (Group I)
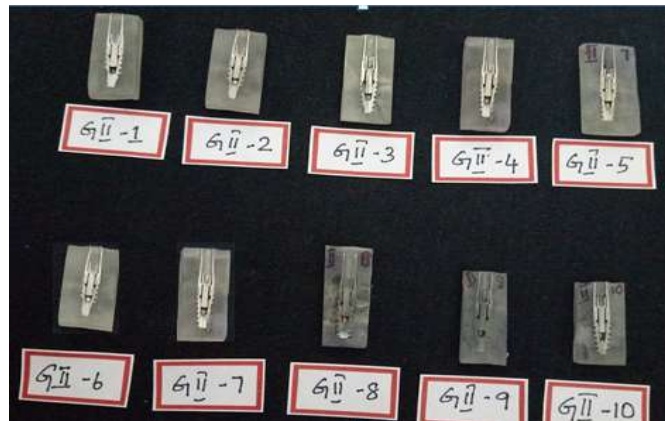
Fig.68b: Cleaned sectioned test samples (Group II)

VIII.   Obtaining SEM images of test samples at the implant-abutment interface

Fig.69: Gold sputtering of test samples
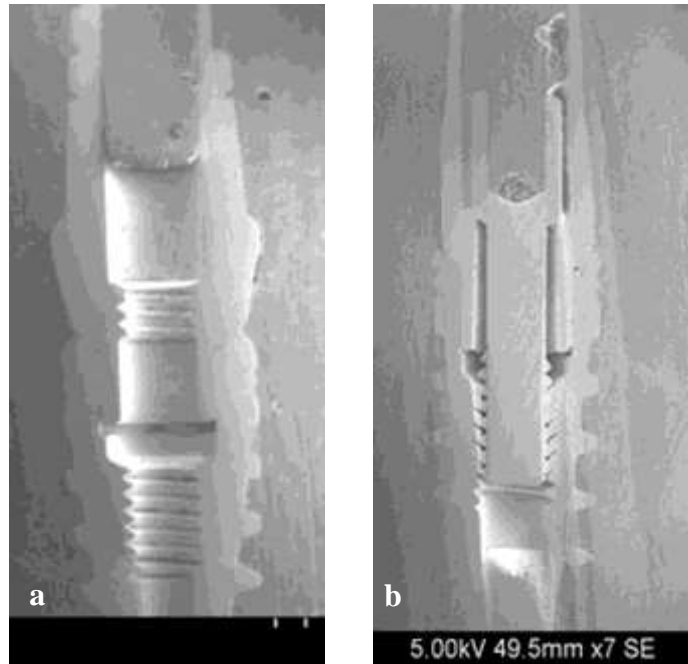
Fig.70a: SEM photomicrograph at lower magnification 7x (Group I)

70b: SEM photomicrograph at lower magnification7x (Group II)
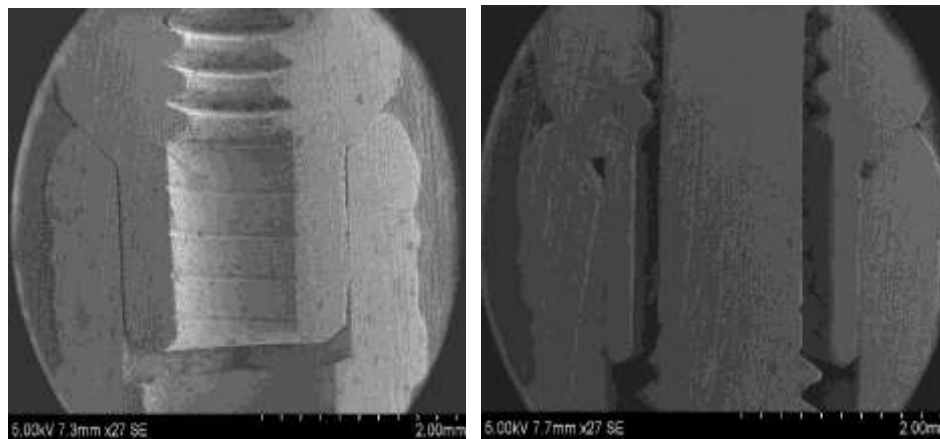
Fig.71a: SEM photomicrograph showing implant-abutment interface at

30x magnification 27x (Group I)

71b: SEM photomicrograph showing implant-abutment interface at 25x

magnification 27x(Group II)

IX.   Measurement of microgap at the implant-abutment interface on SEM images
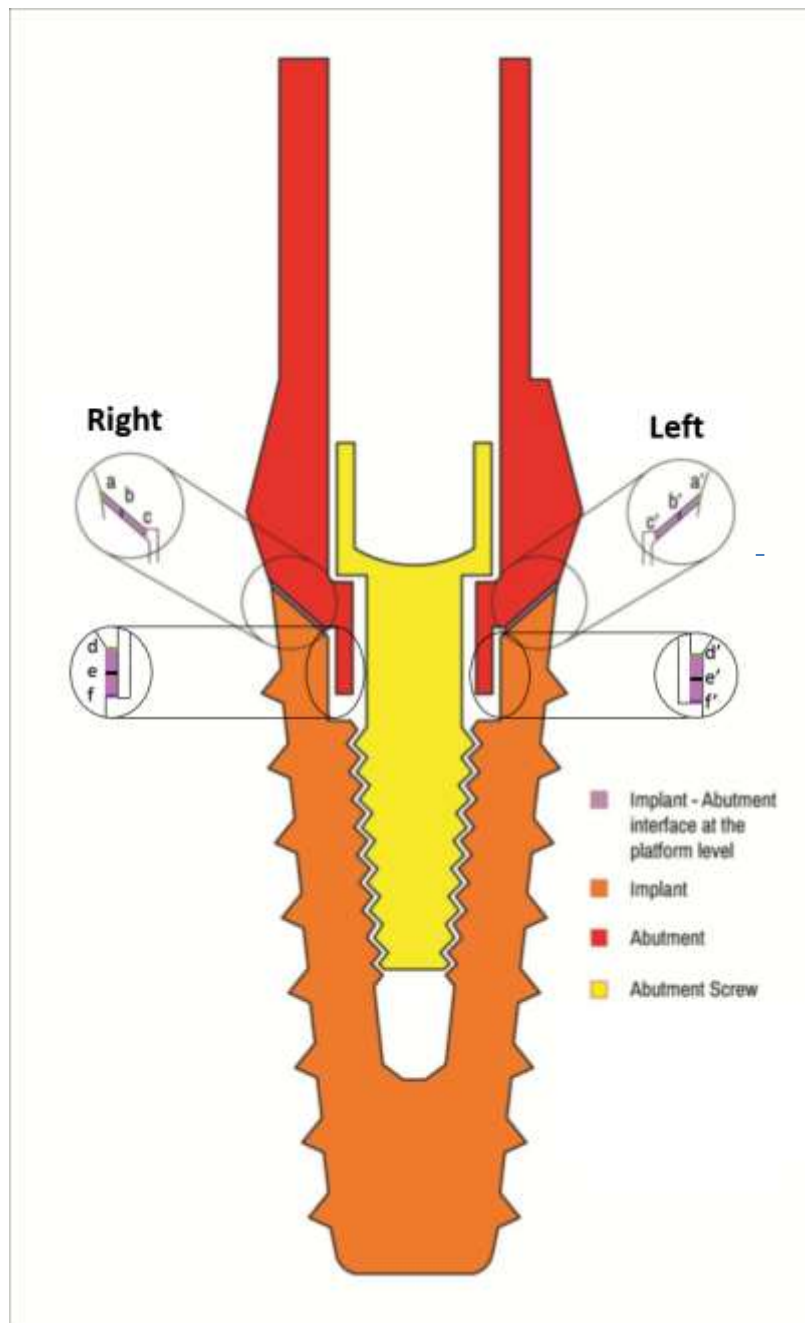
Fig.72: Schematic CAD diagram showing implant-abutment interface with marked reference points.
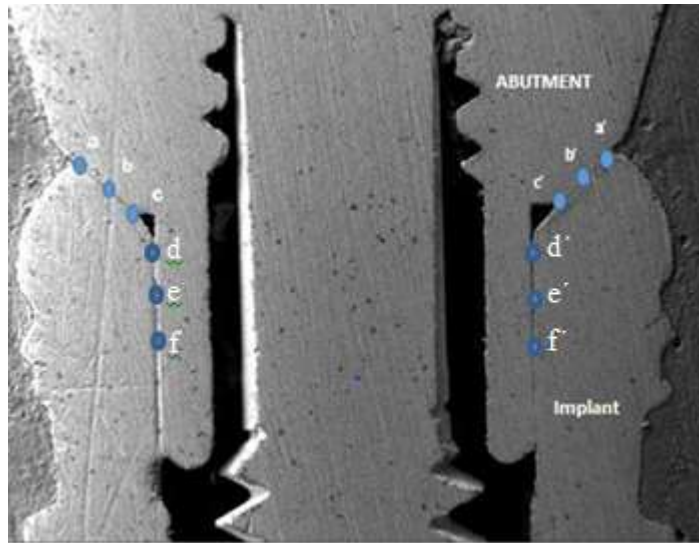
Fig.73a: SEM photomicrograph with marked reference points (Group I)
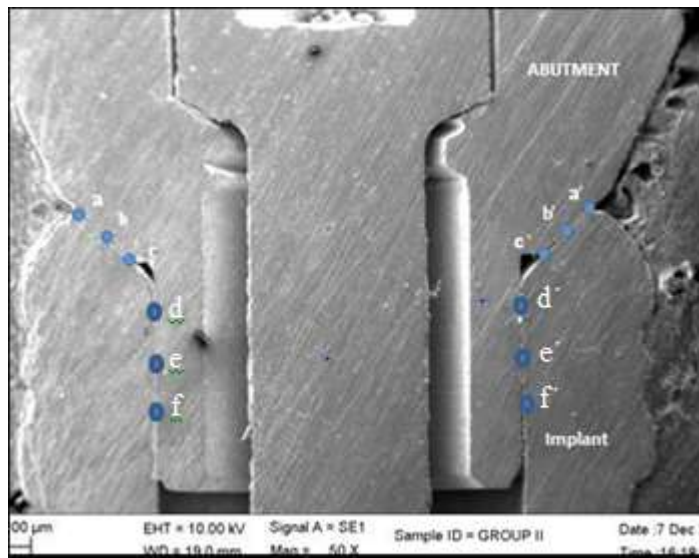
Fig.73b: SEM photomicrograph with marked reference points (Group II)

ANNEXURE III
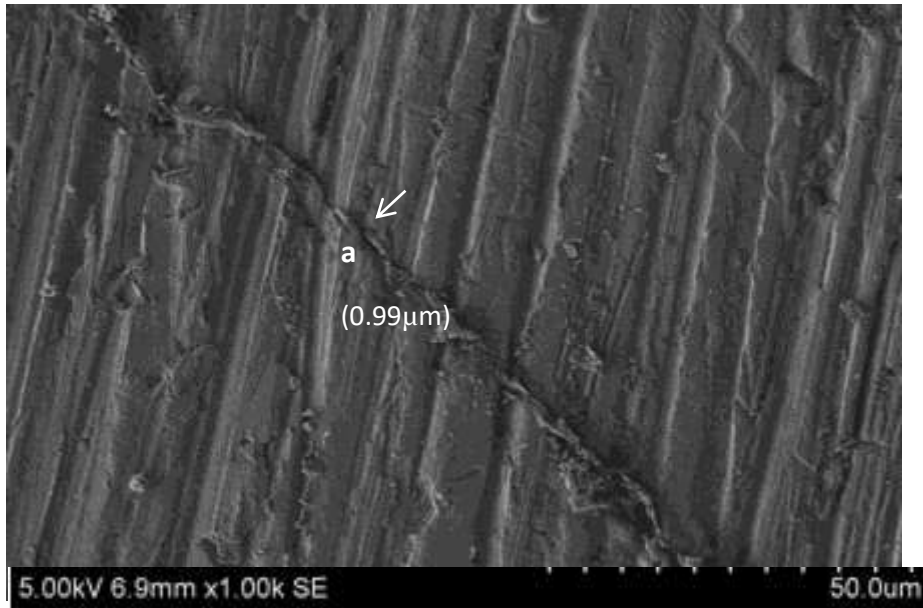
Fig. 74: Measurement of microgap at point a at 1000x (Group I)
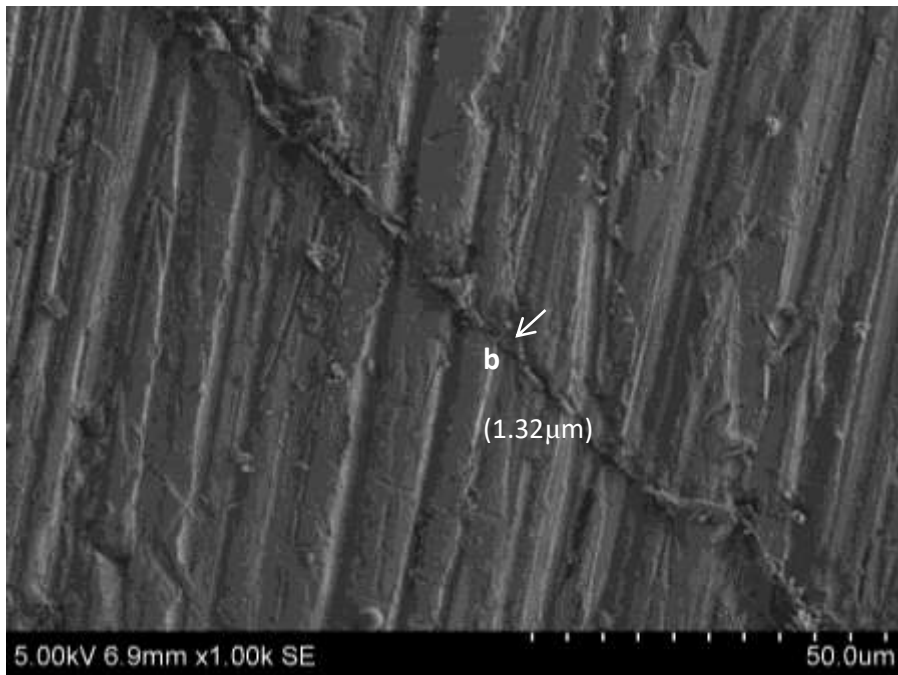
Fig. 75: Measurement of microgap at point b at 1000x (Group I)
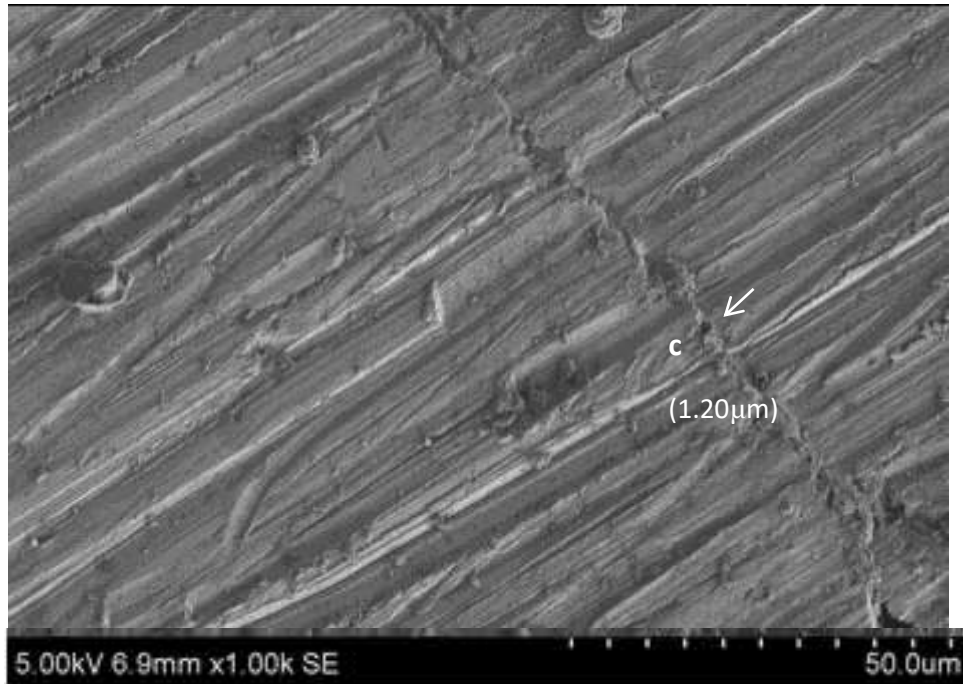
Fig. 76: Measurement of microgap at point c at 1000x (Group I)
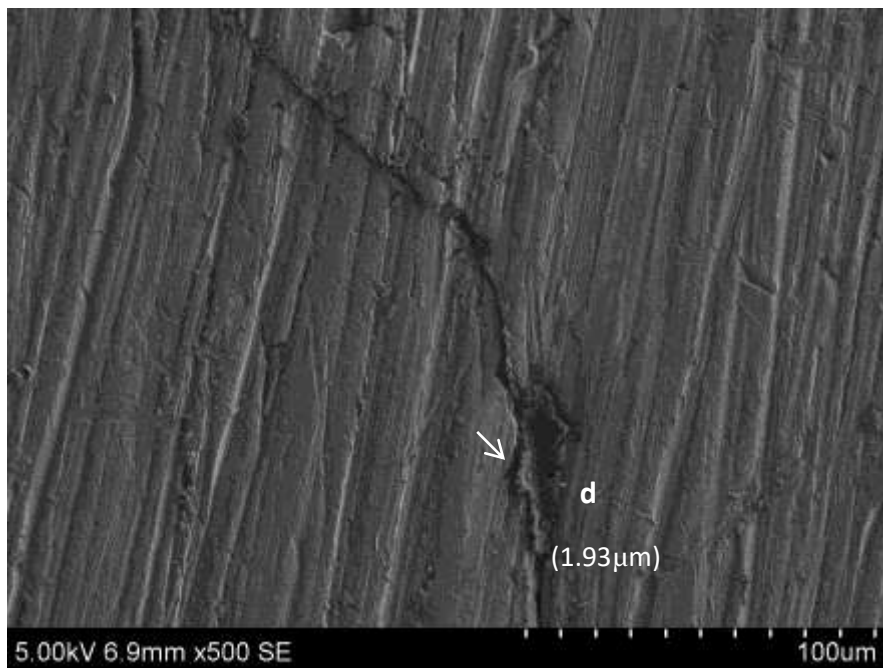
Fig. 77: Measurement of microgap at point d at 500x (Group I)
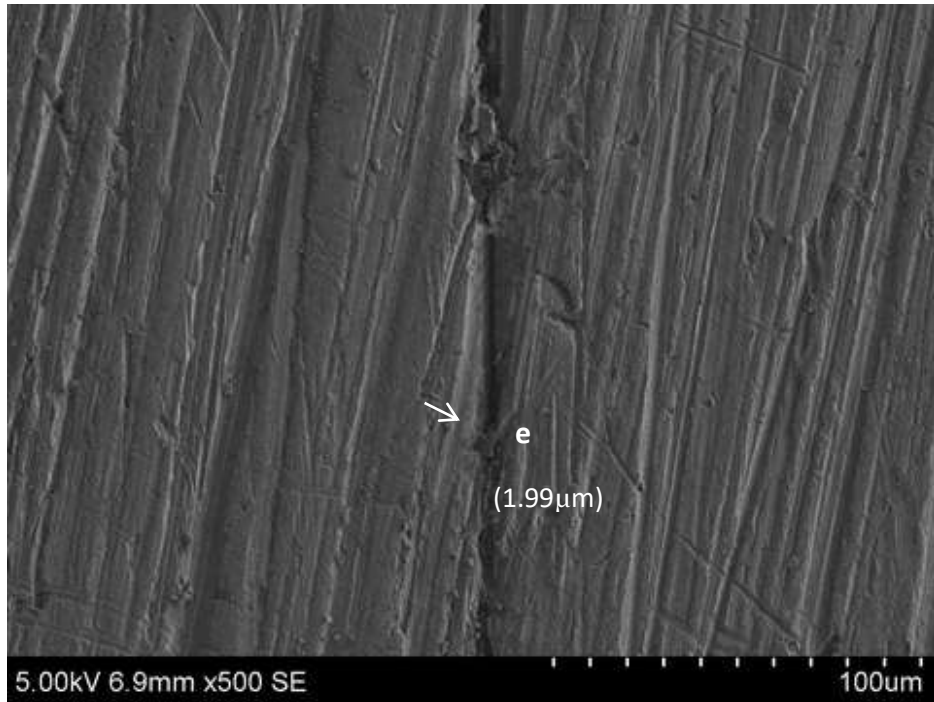
Fig. 78: Measurement of microgap at point e at 500x (Group I)
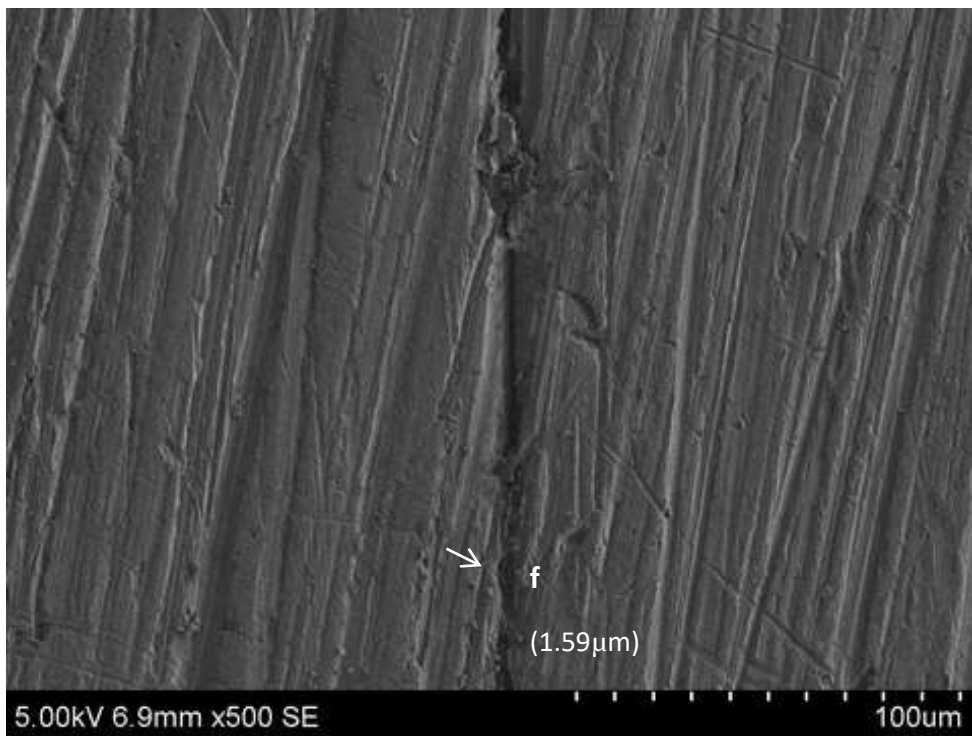
Fig. 79: Measurement of microgap at point f at 500x (Group I)
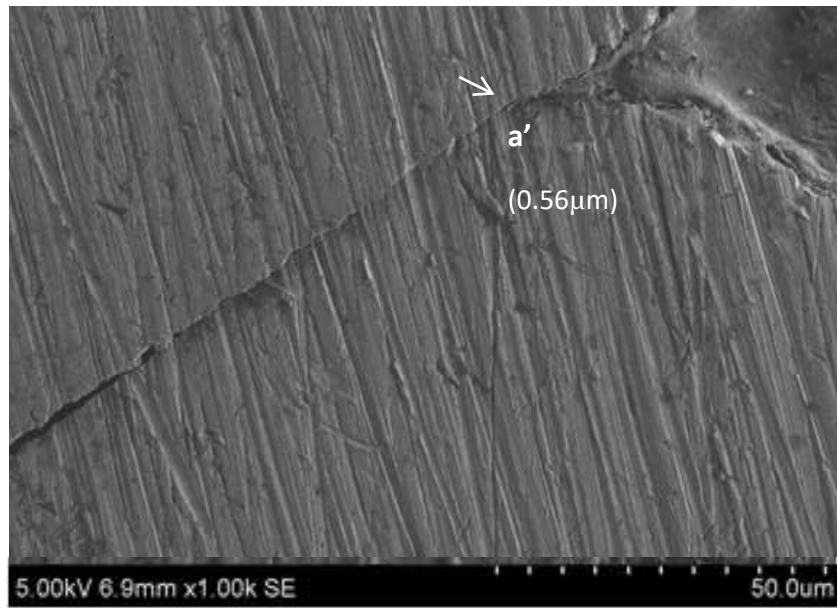
Fig. 80: Measurement of microgap at point a' at 1000x (Group I)
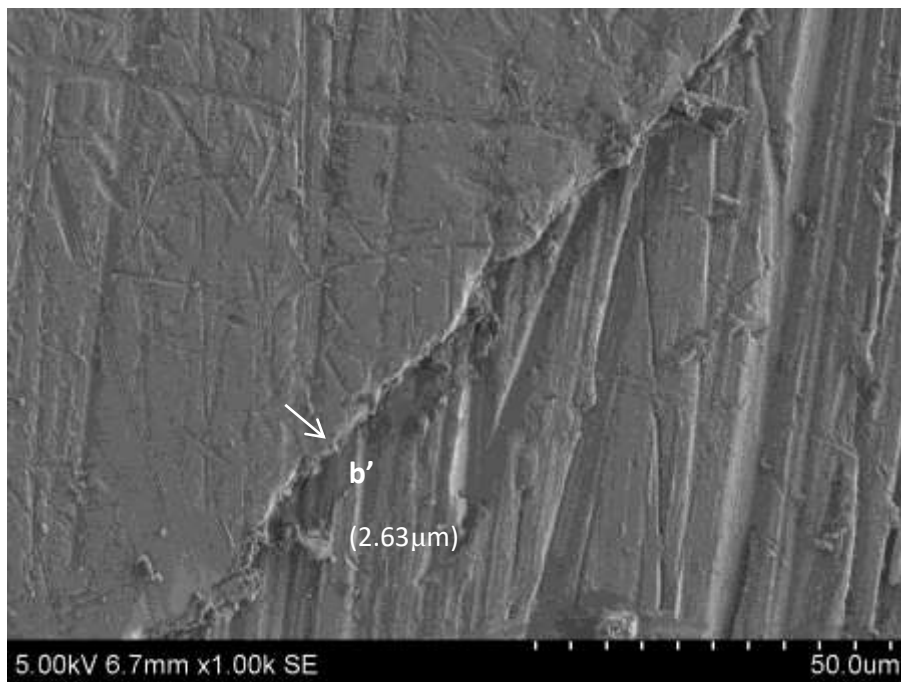
Fig. 81: Measurement of microgap at point b' at 1000x (Group I)
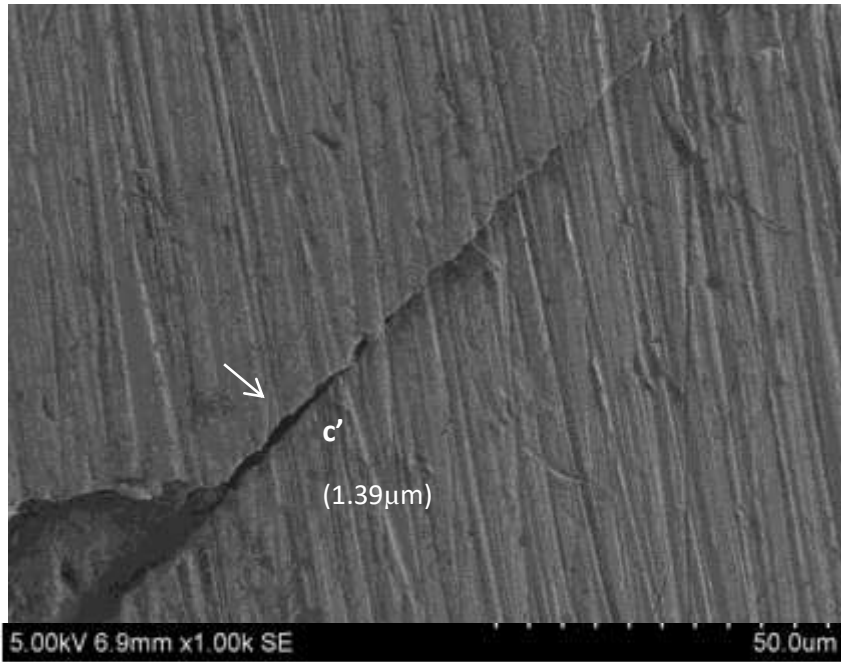
Fig. 82: **Measurement of microgap at point c' at 1000x (Group I)**
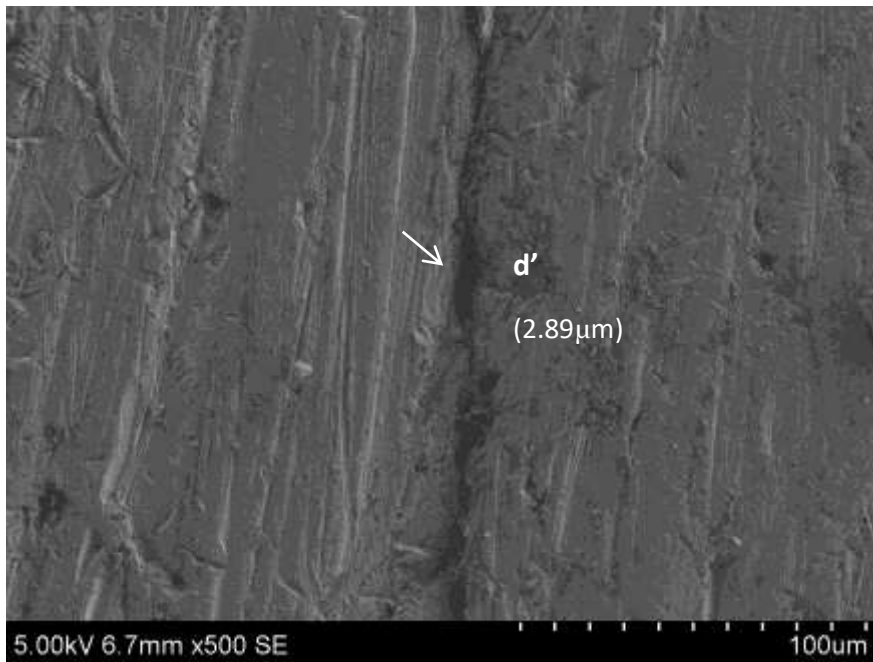
Fig. 83: **Measurement of microgap at point d' at 500x (Group I)**
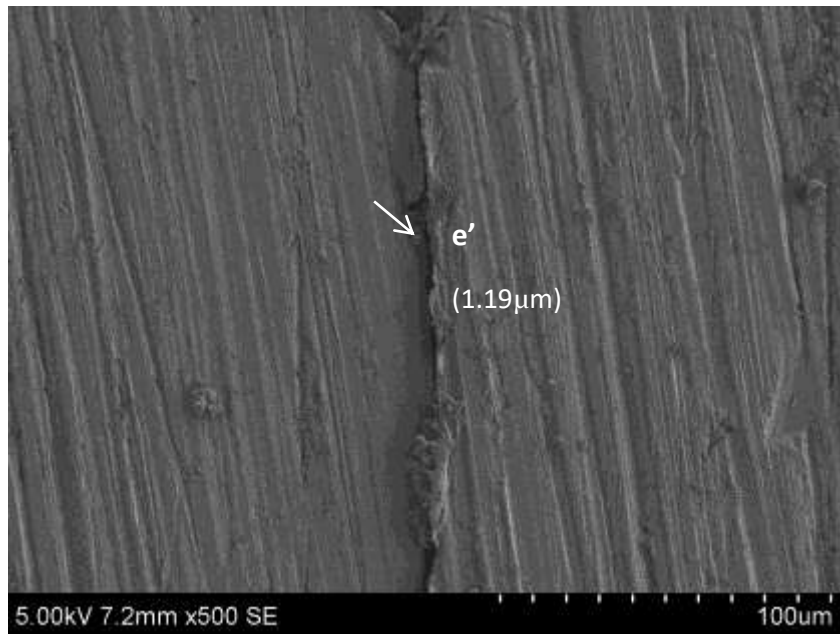
Fig. 84: Measurement of microgap at point e' at 500x (Group I)
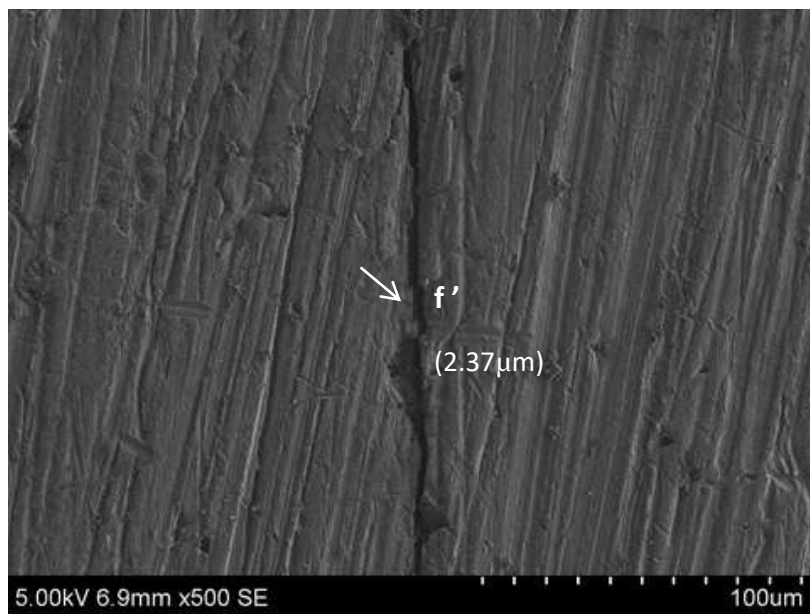
Fig. 85: Measurement of microgap at point f' at 500x (Group I)
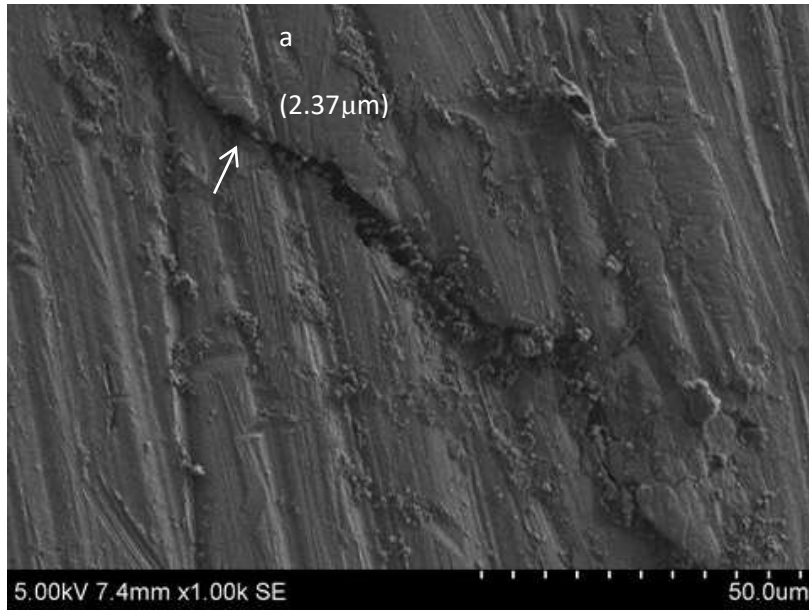
Fig. 86: Measurement of microgap at point a at 1000x (Group II)
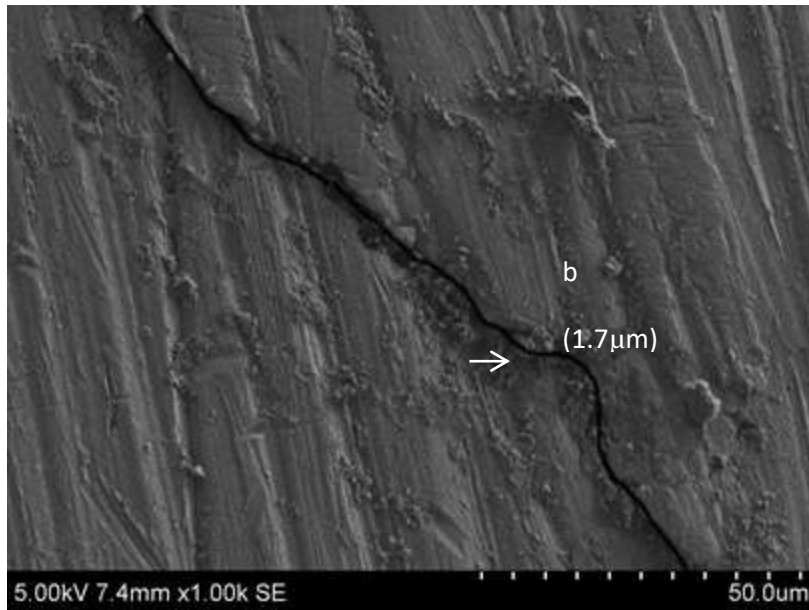
Fig. 87: Measurement of microgap at point b at 1000x (Group II)
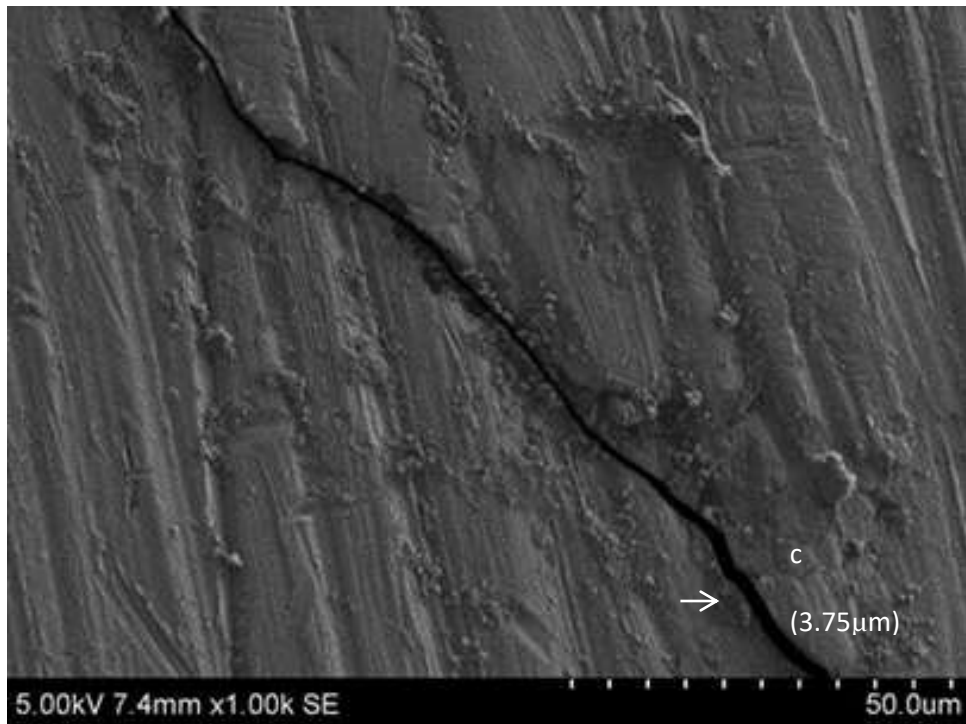
Fig. 88: Measurement of microgap at point c at 1000x (Group II)
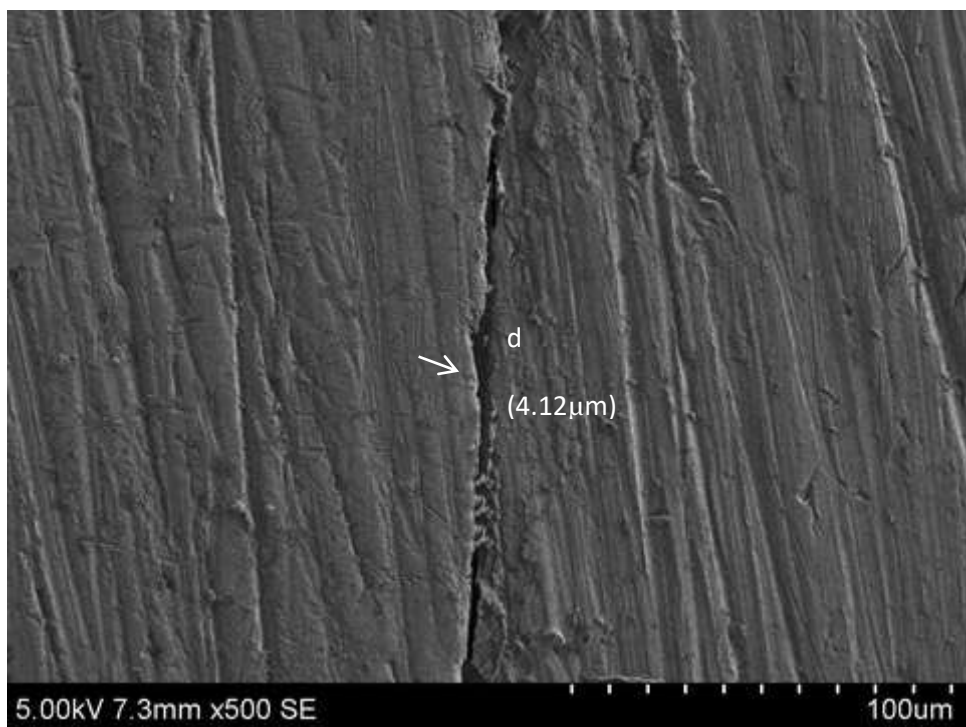
Fig. 89: Measurement of microgap at point d at 500x (Group II)
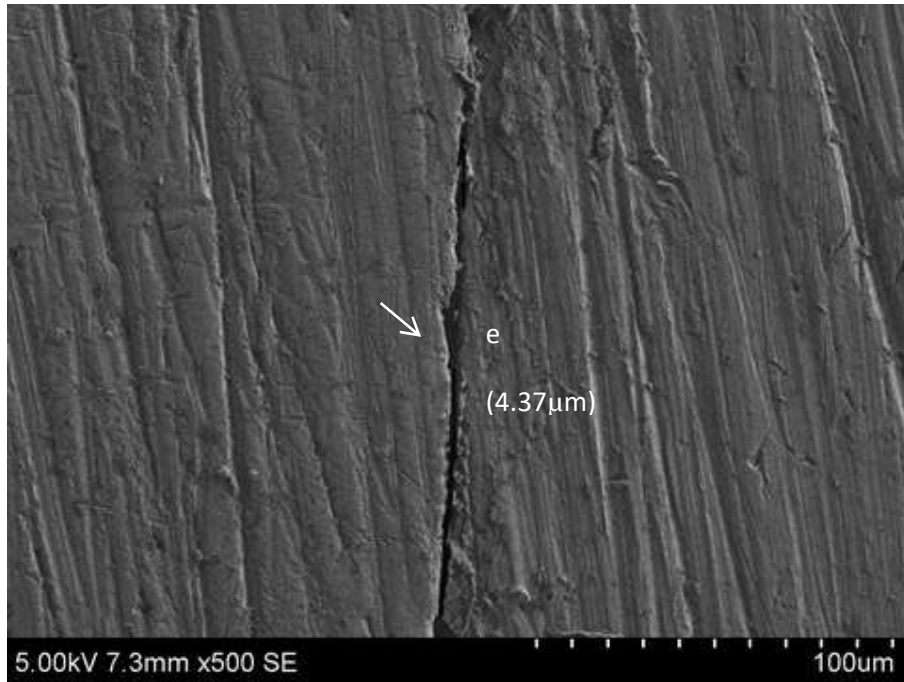
Fig. 90: Measurement of microgap at point e at 500x (Group II)
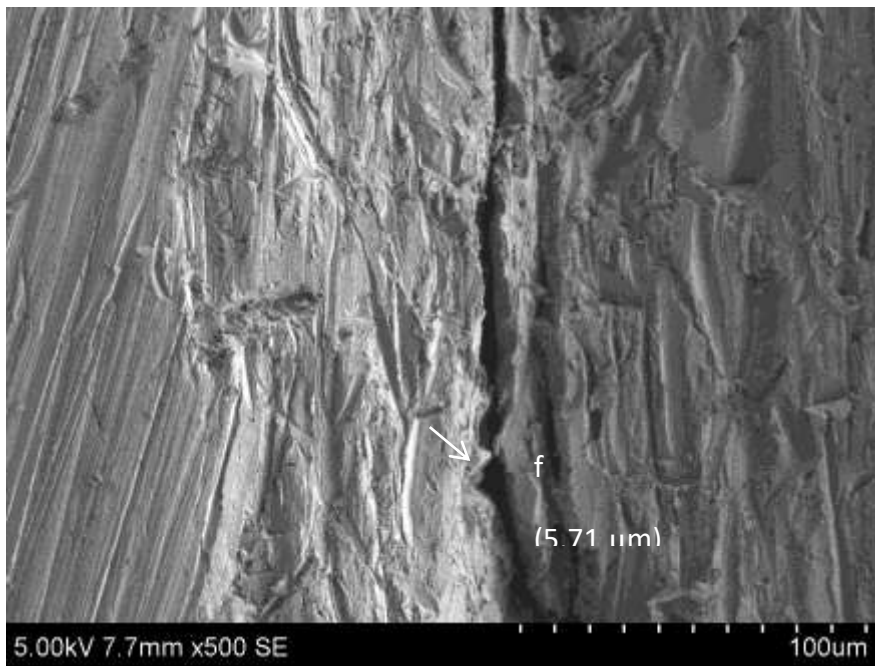
Fig. 91: Measurement of microgap at point f at 500x (Group II)
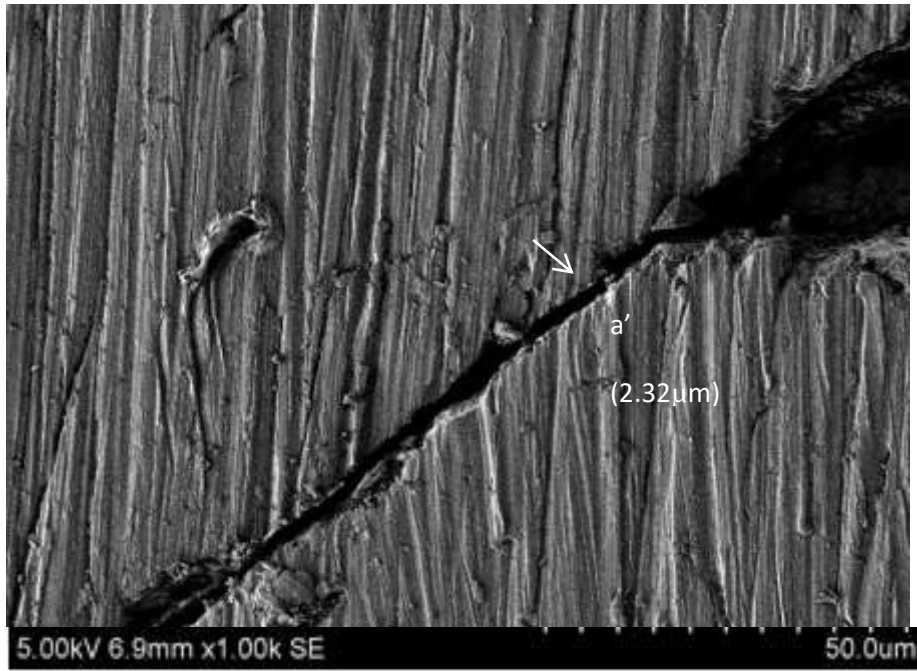
Fig. 92: Measurement of microgap at point a' at 1000x (Group II)
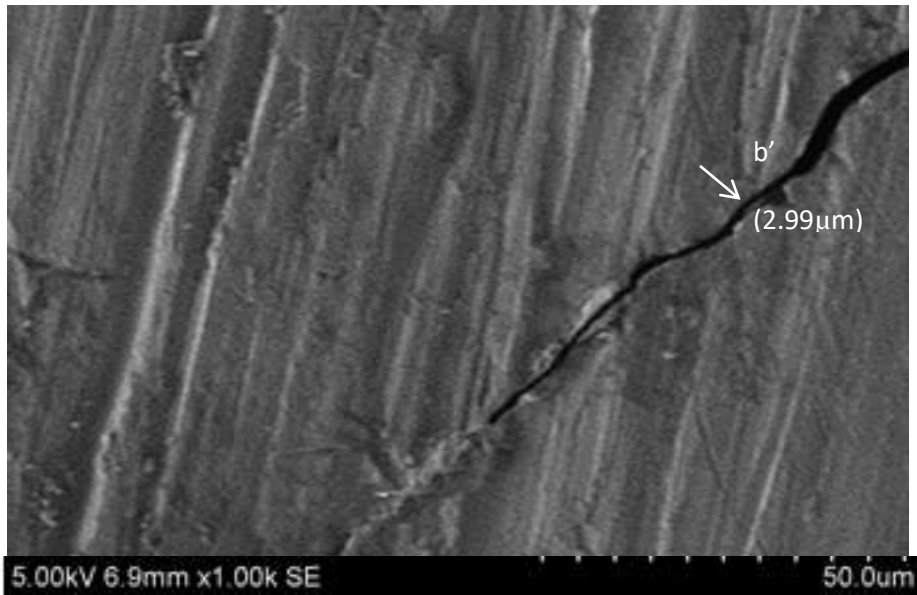
Fig. 93: Measurement of microgap at point b' at 1000x (Group II)
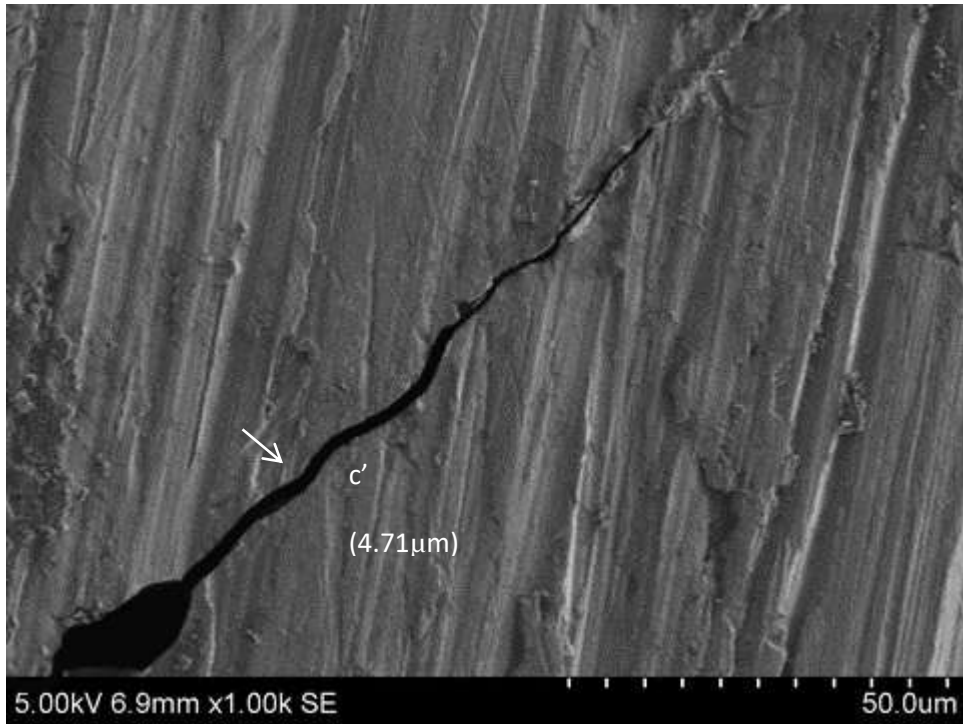
Fig. 94: Measurement of microgap at point c' at 1000x (Group II)
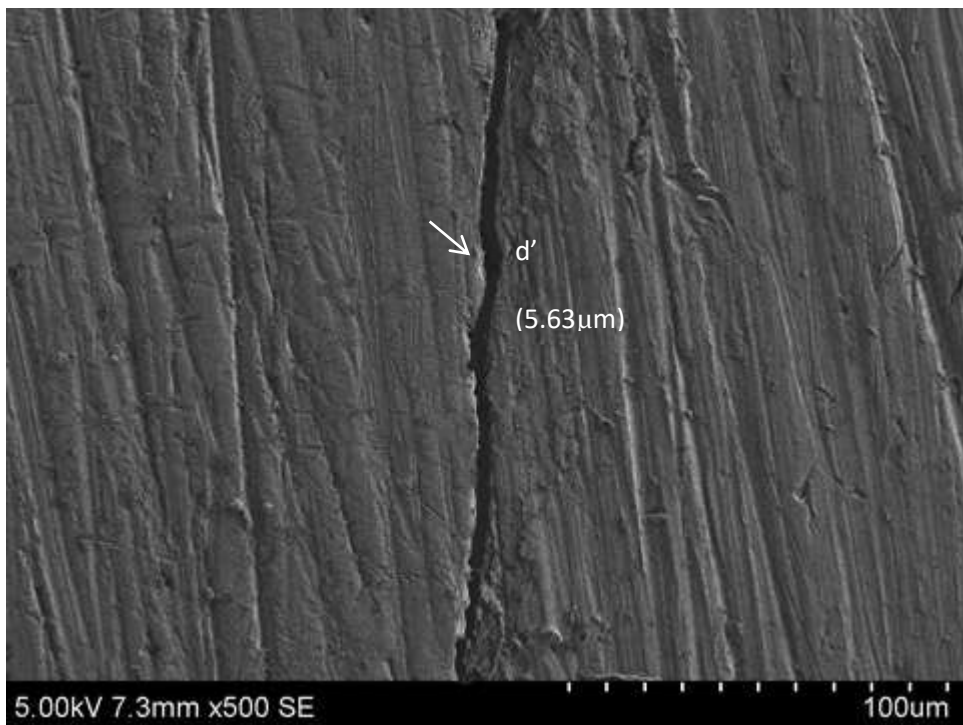
Fig. 95: Measurement of microgap at point d' at 500x (Group II)
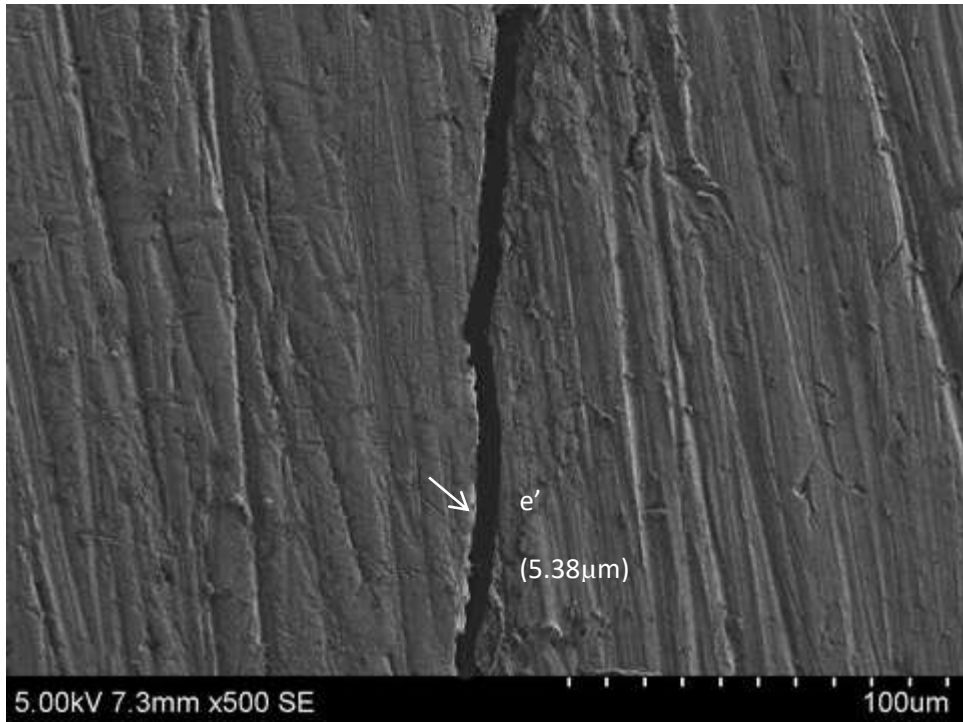
Fig. 96: Measurement of microgap at point e' at 500x (Group II)
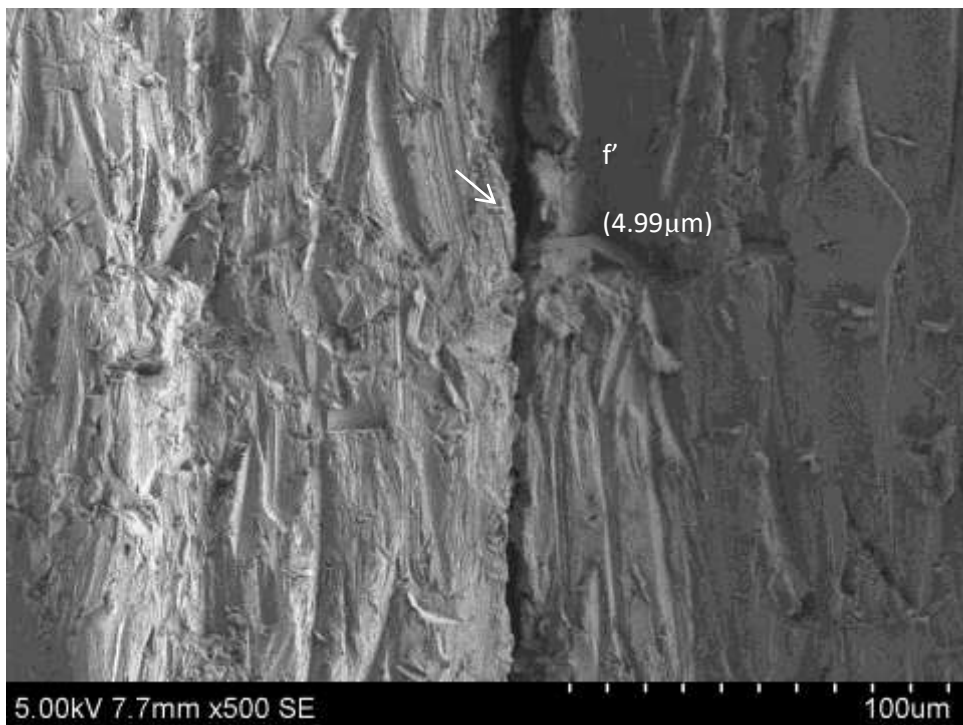
Fig. 97: Measurement of microgap at point f' at 500x (Group II)

RESULTS

The present *in vitro* study was conducted to comparatively evaluate the microgap at the implant-abutment interface with premachined and customized laser-sintered Co-Cr abutments.

Ten Ti premachined abutments (Group I) and ten customized laser-sintered Co-Cr abutments (Group II) were connected to the Ti implants and embedded in clear autopolymerising acrylic resin. These were vertically sectioned using a water jet powered sectioning machine. Scanning electron microscopic images of all the samples were obtained. The microgap at the implant-abutment interface was measured at the right and left sides for each sample of both test groups. In each sample, twelve points at the implant-abutment interface at platform level and internal connection level, six each on the right and on the left sides were selected for measurement at platform level and at internal connection level.

Representative scanning electron microscopic images showing the microgap at the implant-abutment interface at the platform level and internal connection of both test groups and measurements at the respective points were made. The representative photomicrographic images are presented in Annexure III. The mean microgap at the implant-abutment interface at the six points [A, B, C, D, E, F] was calculated by averaging the values obtained from left and right sides obtained from each sample. These were considered as the basic data and the respective means derived and are represented in Tables I – XVIII; Graphs I – XVIII (Annexure IV). The data were subjected to statistical analysis using non parametric Mann- Whitney U test.

38

Table 1: Basic and mean microgap at the implant-abutment interface of Ti implants and Ti premachined abutments at point IA (Right side: a; Left side: a'), at the platform level for Group I

Sample No.	Microgap (μm)		Sample Mean IA (μm)
	Point a (μm) (right side)	Point a′ (μm) (left side)	
1	0.99	1.65	1.32
2	0.120	0.56	0.34
3	3.65	1.450	2.55
4	0.00	0.845	0.4225
5	0.00	0.627	0.3135
6	1.07	0.280	0.675
7	0.89	0.00	0.445
8	0.44	0.82	0.63
9	0.56	0.712	0.636
10	0.63	0.20	0.415
Group Mean(μm)/ S.D = 0.774/0.688			

Inference:

For the point (IA) of Group I test samples, the maximum microgap value was 3.65μm (Sample no. 3; right side) and the minimum microgap value was 0.000μm (Sample no 4, 5 and 7 on both left and right sides respectively). The group mean microgap value at IA was 0.774 μm.

Table II: Basic and mean microgap at the implant-abutment interface of Ti implants and Ti premachined abutments at point IB (Right side: b; Left side: b'), at the platform level for Group I

Sample No.	Microgap (µm)		Sample Mean IB (µm)
	Point b (µm) (right side)	Point b′(µm) (left side)	
1	1.32	2.63	1.975
2	2.02	0.00	1.01
3	2.390	2.02	2.205
4	0.418	0.857	0.6375
5	0.140	0.198	0.169
6	1.01	0.627	0.8185
7	0.98	1.27	1.125
8	0.56	0.85	0.705
9	0.360	0.280	0.32
10	0.81	0.60	0.705
Group Mean(µm)/S.D= 0.967/0.658			

Inference:

For the point (IB) of Group I test samples, the maximum microgap value was 2.63µm (Sample no. 1; left side) and the minimum microgap value was 0.000µm (Sample no.2; left side). The group mean microgap value at IB was 0.967 µm.

Table III: Basic and mean microgap at the implant-abutment interface of Ti implants and Ti premachined abutments at point IC (Right side: c; Left side: c'), at the platform level for Group I

Sample No.	Microgap (µm)		Sample Mean IC (µm)
	Point c(µm) (right side)	Point c′(µm) (left side)	
1	1.20	1.39	1.295
2	4.83	5.32	5.075
3	2.390	1.520	1.955
4	2.65	5.09	3.87
5	2.31	1.40	1.855
6	2.11	0.581	1.3455
7	1.77	0.84	1.305
8	1.210	0.72	0.965
9	1.17	0.990	1.08
10	3.09	0.98	2.035
Group Mean(µm)/S.D= 2.078/1.343			

Inference:

For point (IC) of Group I test samples, the maximum microgap value was found to be 5.32µm (Sample no. 2; left side) and the minimum microgap value was found to be 0.581 µm (Sample no. 6; left side). The group mean microgap value at IC was 2.078 µm.

Table IV: Basic and mean microgap at the implant-abutment interface of Ti implants and Ti premachined abutments at point ID (Right side: d; Left side: d') at the internal connection level for Group I.

Sample No.	Microgap (µm)		Sample Mean ID (µm)
	Point d (µm) (right side)	Point d′ (µm) (left side)	
1	1.93	2.89	2.41
2	1.59	2.78	2.185
3	1.98	2.02	2.00
4	2.78	1.72	2.25
5	2.34	2.45	2.395
6	3.02	2.59	2.805
7	1.43	2.39	1.91
8	3.28	2.99	3.135
9	2.42	2.03	2.225
10	1.64	1.99	1.815
Group Mean(µm)/ S.D = 2.313/0.4044			

Inference:

For the point (ID) at internal connection level of Group I test samples, the maximum microgap value was found to be 3.28µm (Sample no. 8; right side) and the minimum microgap value was found to be 1.43 µm (Sample no. 7; right side). The group mean microgap value at ID was 2.313µm.

Table V: Basic and mean microgap at the implant-abutment interface of Ti implants and Ti premachined abutments at point IE (Right side: e; Left side: e') at the internal connection level Group I.

Sample No.	Microgap (µm)		Sample Mean IE (µm)
	Point e (µm) (right side)	Point e′(µm) (left side)	
1	1.99	1.19	1.59
2	1.98	1.64	1.81
3	0.794	0.79	0.792
4	2.82	1.98	2.4
5	1.19	1.32	1.255
6	2.63	2.41	2.52
7	1.64	2.02	1.83
8	2.45	2.76	2.605
9	2.39	2.38	2.385
10	2.02	2.15	2.085
Group Mean(µm)/S.D= 1.927/0.5912			

Inference:

For the point (IE) at internal connection level of Group I test samples, the maximum microgap value was found to be 2.82µm (Sample no. 4; right side) and the minimum microgap value was found to be 0.794 µm (Sample no. 3; on both right side and left sides). The group mean microgap value at IE was 1.927µm.

Table VI: Basic and mean microgap at the implant-abutment interface of Ti implants and Ti premachined abutments at point IF (Right side: f; Left side: f') at the internal connection level for Group I.

Sample No.	Microgap (µm)		Sample Mean IF (µm)
	Point f(µm) (right side)	Point f′(µm) (left side)	
1	1.59	2.37	1.98
2	1.98	1.72	1.85
3	1.19	1.99	1.59
4	1.99	2.32	2.155
5	2.38	2.78	2.58
6	3.16	3.99	3.575
7	1.59	1.89	1.74
8	2.51	2.33	2.42
9	2.32	2.12	2.22
10	1.59	1.98	1.785
Group Mean(µm)/S.D = 2.189/0.5784			

Inference:

For the point (IF) at internal connection level of Group I test samples, the maximum microgap value was found to be 3.99µm (Sample no. 6; left side) and the minimum microgap value was found to be 1.19 µm (Sample no. 3; right side). The group mean microgap value at IF was 2.189µm.

Table VII: Basic and mean microgap at the implant-abutment interface of Ti implants and customized laser-sintered Co-Cr abutments at point IIA (Right side: a; Left side: a') at the platform level for Group II

Sample No.	Microgap (µm)		Sample Mean IIA (µm)
	Point a (µm) (right side)	Point a'(µm) (left side)	
1	1.42	2.32	1.87
2	2.43	2.25	2.34
3	2.04	1.86	1.95
4	1.06	1.60	1.33
5	1.84	1.28	1.56
6	1.87	1.95	1.91
7	1.99	1.83	1.91
8	1.16	1.00	1.08
9	2.83	2.67	2.75
10	2.32	2.05	2.1855
Group Mean(µm)/S.D = 1.888/0.484			

Inference:

For the point (IIA) of Group II test samples, the maximum microgap value was 2.83µm (Sample no. 9; right side) and the minimum microgap value was 1.00µm (Sample no. 8; left side). The group mean microgap value at IIA was 1.888µm.

Table VIII: Basic and mean microgap at the implant-abutment interface of Ti implants and customized laser-sintered Co-Cr abutments at point IIB (Right side: b; Left side: b') at the platform level for Group II

Sample No.	Microgap (μm)		Sample Mean IIB (μm)
	Point b (μm) (right side)	Point b' (μm) (left side)	
1	1.74	2.99	2.365
2	3.41	2.80	3.105
3	1.51	1.86	1.685
4	0.51	0.99	0.75
5	2.54	0.98	1.76
6	1.33	2.25	1.79
7	0.00	1.83	0.915
8	1.40	0.84	1.12
9	2.390	3.24	2.815
10	3.29	2.41	2.85
Group Mean(μm)/S.D = 1.915/0.842			

Inference:

For the point (IIB) of Group II test samples, the maximum microgap value was 3.41μm (Sample no. 2; right side) and the minimum microgap value was 0.00μm (Sample no. 7; right side). The group mean microgap value at IIB was 1.915μm.

Table IX: Basic and mean microgap at the implant-abutment interface of Ti implants and customized laser-sintered Co-Cr abutments at point IIC (Right side: c; Left side: c'), at the platform level for Group II

Sample No.	Microgap (µm)		Sample Mean IIC (µm)
	Point c (µm) (right side)	Point c′ (µm) (left side)	
1	3.75	4.71	4.23
2	3.99	3.690	3.84
3	2.39	2.14	2.265
4	1.39	1.61	1.5
5	3.14	2.04	2.59
6	1.87	2.38	2.125
7	0.72	1.71	1.215
8	1.12	0.84	0.98
9	6.21	3.22	4.715
10	3.36	2.590	2.975
Group Mean(µm)/S.D = 2.643/1.285			

Inference:

For the point (IIC) of Group II test samples, the maximum microgap value was 6.21µm (Sample no. 9; right side) and the minimum microgap value was 0.72µm (Sample no.7; right side). The group mean microgap value at IIC was 2.643µm.

Table X: Basic and mean microgap at the implant-abutment interface of Ti implants and customized laser-sintered Co-Cr abutments at point IID (Right side: d; Left side: d'), at the internal connection level for Group II

Sample No.	Microgap (µm)		Sample Mean IID (µm)
	Point d (µm) (right side)	Point d' (µm) (left side)	
1	4.12	5.63	4.875
2	3.16	10.28	6.72
3	6.08	9.32	7.7
4	5.95	8.66	7.305
5	6.11	7.21	6.66
6	5.38	4.71	5.045
7	6.33	7.87	7.1
8	4.32	3.58	3.95
9	6.36	6.03	6.195
10	5.17	4.71	4.94
Group Mean(µm)/S.D = 6.049/1.259			

Inference:

For the point (IID) at internal connection level of Group II test samples, the maximum microgap value was 10.28µm (Sample no. 2; left side) and the minimum microgap value was 3.16µm (Sample no.2; right side). The group mean microgap value at IID was 6.049µm.

Table XI: Basic and mean microgap at the implant-abutment interface of Ti implants and customized laser-sintered Co-Cr abutments at point IIE (Right side: e; Left side: e'), at the internal connection level for Group II

Sample No.	Microgap (µm)		Sample Mean IIE (µm)
	Point e (µm) (right side)	Point e' (µm) (left side)	
1	4.37	5.38	4.875
2	2.77	6.99	4.88
3	4.02	5.69	4.855
4	4.99	5.98	5.485
5	5.32	6.89	6.105
6	8.11	11.32	9.715
7	5.44	9.52	7.48
8	4.01	5.79	4.9
9	5.02	5.17	5.095
10	6.72	8.71	7.715
Group Mean(µm)/S.D = 6.110/1.664			

Inference:

For the point (IIE) at internal connection level of Group II test samples, the maximum microgap value was 11.32µm (Sample no. 6; left side) and the minimum microgap value was 2.77µm (Sample no.2; right side). The group mean microgap value at IIE was 6.110µm.

Table XII: Basic and mean microgap at the implant-abutment interface of Ti implants and customized laser-sintered Co-Cr abutments at point IIF (Right side: f; Left side: f'), at the internal connection level for Group II

Sample No.	Microgap (µm)		Sample Mean IIF (µm)
	Point f (µm) (right side)	Point f′ (µm) (left side)	
1	5.71	4.99	5.35
2	3.58	7.51	5.545
3	4.43	7.43	5.93
4	5.21	6.07	5.64
5	4.82	7.33	6.075
6	7.89	6.14	7.015
7	8.99	5.72	7.355
8	3.99	6.08	5.035
9	4.80	7.21	6.005
10	5.60	6.78	6.19
Group Mean(µm)/S.D = 6.014/0.715			

Inference:

For the point (IIF) at internal connection level of Group II test samples, the maximum microgap value was 8.99µm (Sample no. 7; right side) and the minimum microgap value was 3.58µm (Sample no.2; right side). The group mean microgap value at IIF was 6.014µm.

Table XIII: Comparative evaluation of mean microgap at the implant-abutment interface at point A at the platform level for Group I & Group II (IA vs. IIA)

GROUP	No. of Samples	Mean(μm)	Standard Deviation(S.D)	p value
IA	10	0.774	0.688	0.000*
IIA	10	1.888	0.484	

p value < 0.05; Significant

Inference:

On statistical analysis using Non parametric Mann-Whitney U test to compare the mean microgap values at the point A, of Group I and Group II test samples (IA & IIA respectively), it was found that the mean microgap value for Group I test samples was lesser than that of Group II test samples and this was found to be statistically significant (P value < 0.05).

Table XIV: Comparative evaluation of mean microgap at the implant-abutment interface at point B at the platform level for Group I & Group II (IB vs. IIB)

GROUP	No. of Samples	Mean(μm)	Standard Deviation(S.D)	p value
IB	10	0.967	0.658	0.002[*]
IIB	10	1.915	0.842	

p value < 0.05; Significant

Inference:

On statistical analysis using Non parametric Mann-Whitney U to compare the mean microgap values at the point B, of the Group I and Group II test samples (IB & IIB respectively), it was found that the mean microgap value at the midpoint of Group I test samples was lesser than that of Group II test samples and this was found to be statistically significant ($p < 0.05$).

Table XV: Comparative evaluation of mean microgap at the implant-abutment interface at point C at the platform level for Group I & Group II (IC vs. IIC)

GROUP	No. of Samples	Mean(μm)	Standard Deviation(S.D)	p value
IC	10	2.078	1.343	0.110
IIC	10	2.643	1.285	

p value > 0.05; Non significant

Inference:

On statistical analysis using Non parametric Mann-Whitney U to compare the mean microgap values at the point C, of the Group I and Group II test samples (IC & IIC respectively), it was found that the mean microgap value at the most internal point of Group I test samples was lesser than that of Group II test samples and this was found to be statistically insignificant (P value > 0.05).

Table XVI: Comparative evaluation of mean microgap at the implant-abutment interface at point D at the internal connection level for Group I & Group II (ID vs. IID)

GROUP	No. of Samples	Mean(μm)	Standard Deviation(S.D)	p value
ID	10	2.313	0.404	0.00[*]
IID	10	6.049	1.259	

p value < 0.05 Significant

Inference:

On statistical analysis using Non parametric Mann-Whitney U to compare the mean microgap values at the point D, at internal connection level of the Group I and Group II test samples (ID & IID respectively), it was found that the mean microgap value at the point of Group ID test samples was lesser than that of Group II test samples and this was found to be statistically significant (p value < 0.05).

Table XVII: Comparative evaluation of mean microgap at the implant-abutment interface at point E at the internal connection level for Group I & Group II (IE vs. IIE)

GROUP	No. of Samples	Mean(µm)	Standard Deviation(S.D)	p value
IE	10	1.927	0.591	0.00^*
IIE	10	6.110	1.664	

p value < 0.05 Significant

Inference:

On statistical analysis using Non parametric Mann-Whitney U to compare the mean microgap values at the point E, at internal connection level of the Group I and Group II test samples (IE & IIE respectively), it was found that the mean microgap value at the point of Group IE test samples was lesser than that of Group II test samples and this was found to be statistically significant (P value < 0.05).

Table XVIII: Comparative evaluation of mean microgap at the implant-abutment interface at point F at the internal connection level for Group I & Group II (IF vs. IIF)

GROUP	No. of Samples	Mean(µm)	Standard Deviation(S.D)	p value
IF	10	2.189	0.578	0.00*
IIF	10	6.014	0.715	

p value < 0.05 Significant

Inference:

On statistical analysis using Non parametric Mann-Whitney U to compare the mean microgap values at the point F, at internal connection level of the Group I and Group II test samples (IF & IIF respectively), it was found that the mean microgap value at the point of Group IF test samples was lesser than that of Group II test samples and this was found to be statistically significant (p value < 0.05).

Graph 1: Basic and mean microgap at the implant-abutment interface of Ti implants and Ti premachined abutments at point IA, at the platform level for Group I
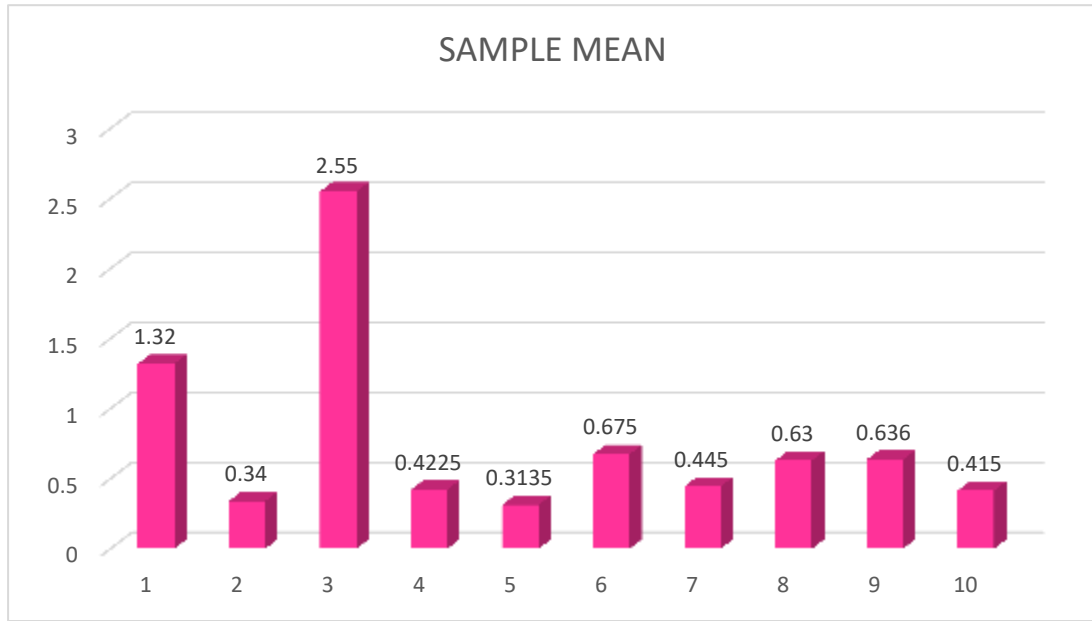
Graph II: Basic and mean microgap at the implant-abutment interface of Ti implants and Ti premachined abutments at point IB, at the platform level for Group I
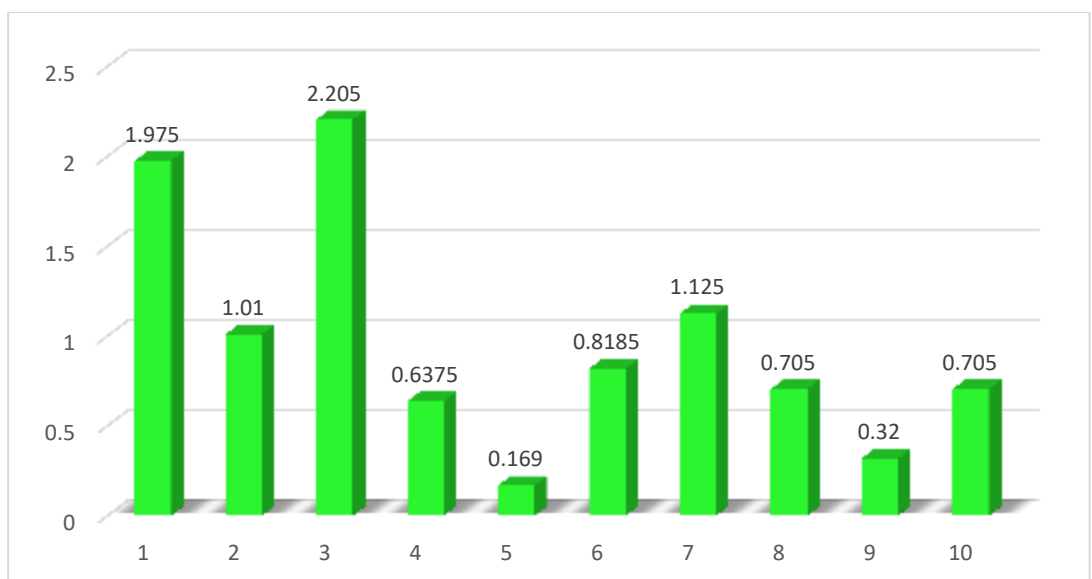
Graph III: Basic and mean microgap at the implant-abutment interface of Ti implants and Ti premachined abutments at point IC, at the platform level for Group I
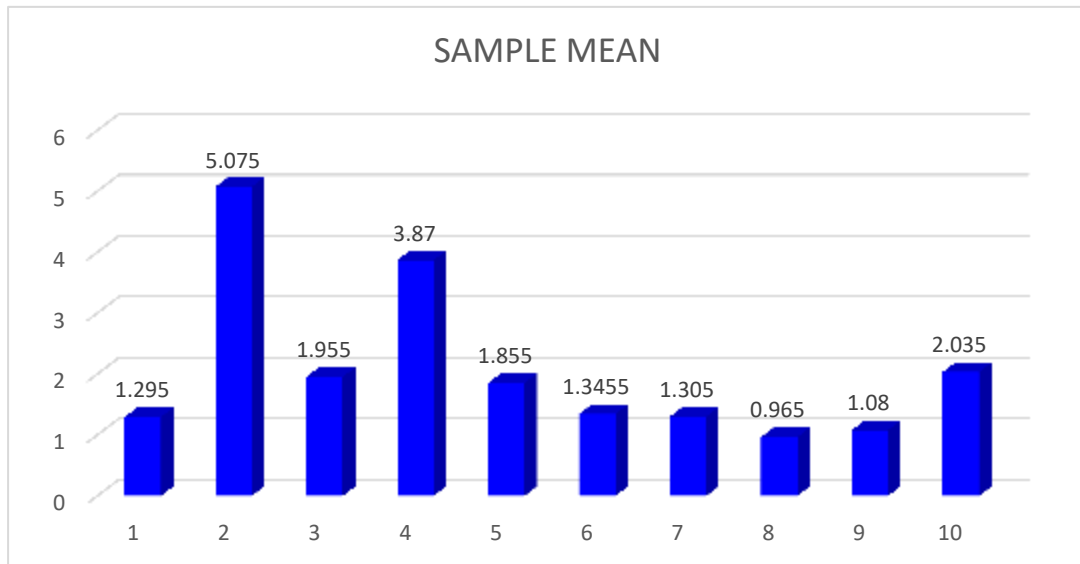
Graph IV: Basic and mean microgap at the implant-abutment interface of Ti implants and Ti premachined abutments at point ID, at the internal connection level for Group I
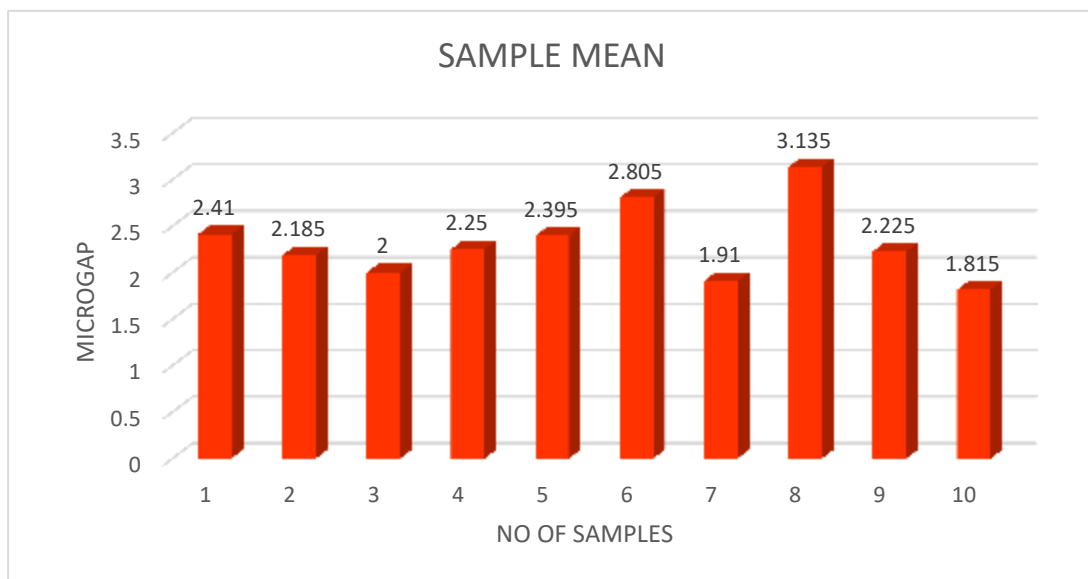
Graph V: Basic and mean microgap at the implant-abutment interface of Ti implants and Ti premachined abutments at point IE, at the internal connection level for Group I
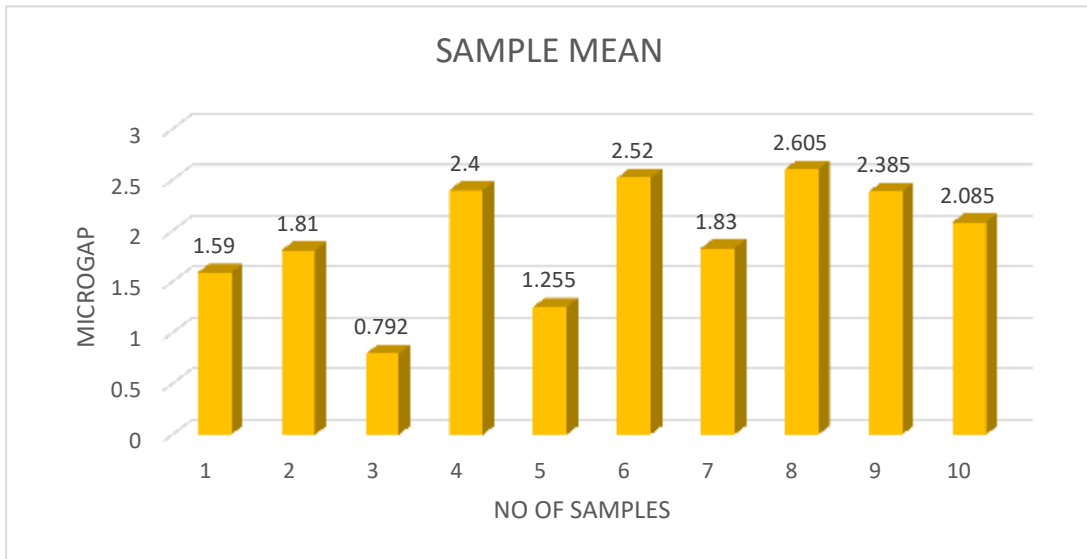
Graph VI: Basic and mean microgap at the implant-abutment interface of Ti implants and Ti premachined abutments at point IF, at the internal connection level for Group I
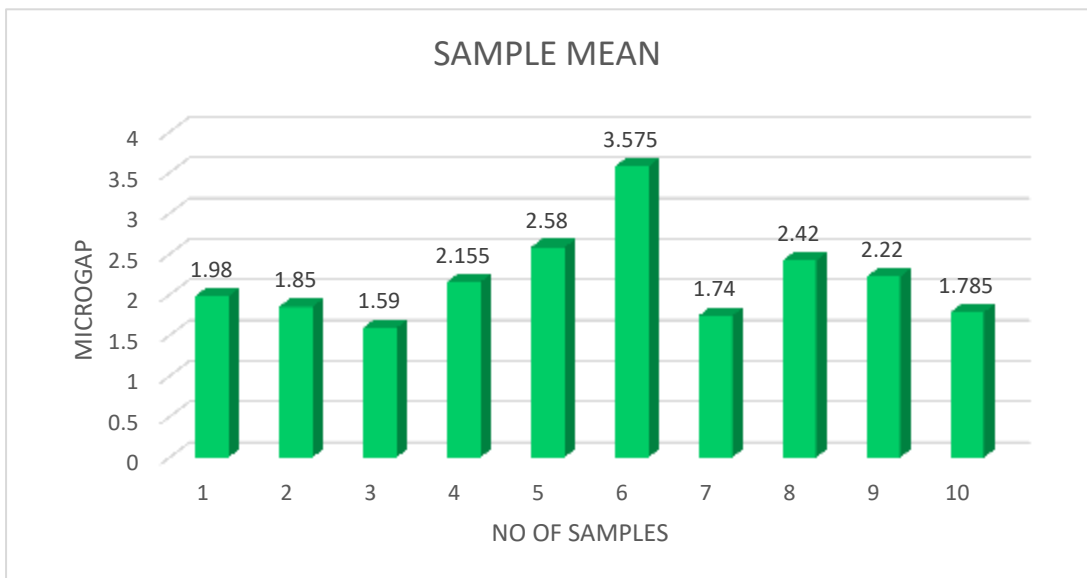
Graph VII: Basic and mean microgap at the implant-abutment interface of Ti implants and customized laser-sintered Co-Cr abutments at the point IIA, at the platform level for Group II

SAMPLE MEAN
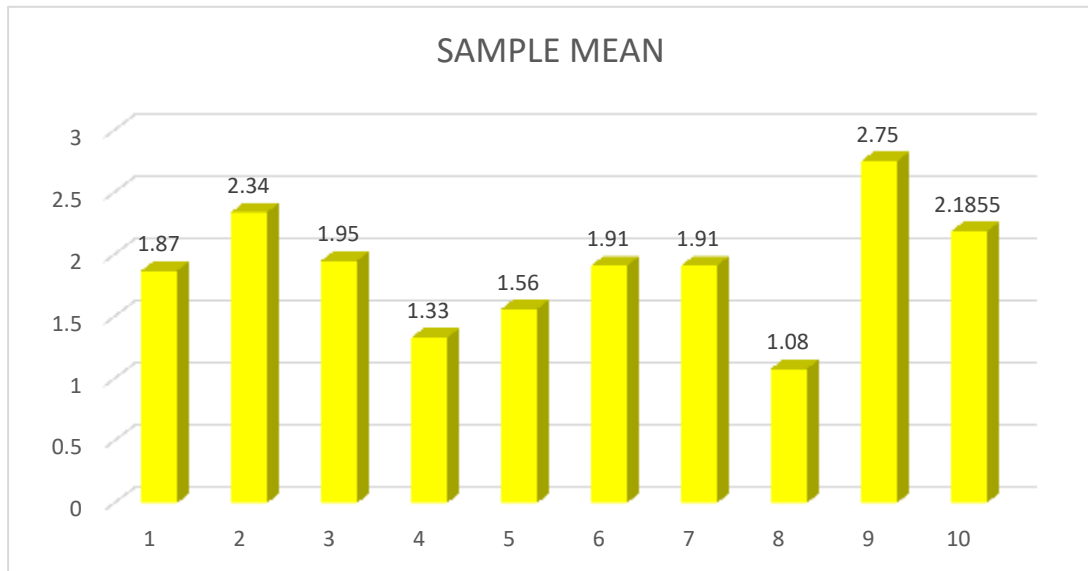
Graph VIII: Basic and mean microgap at the implant-abutment interface of Ti implants and customized laser-sintered Co-Cr abutments at the point IIB, at the platform level for Group II
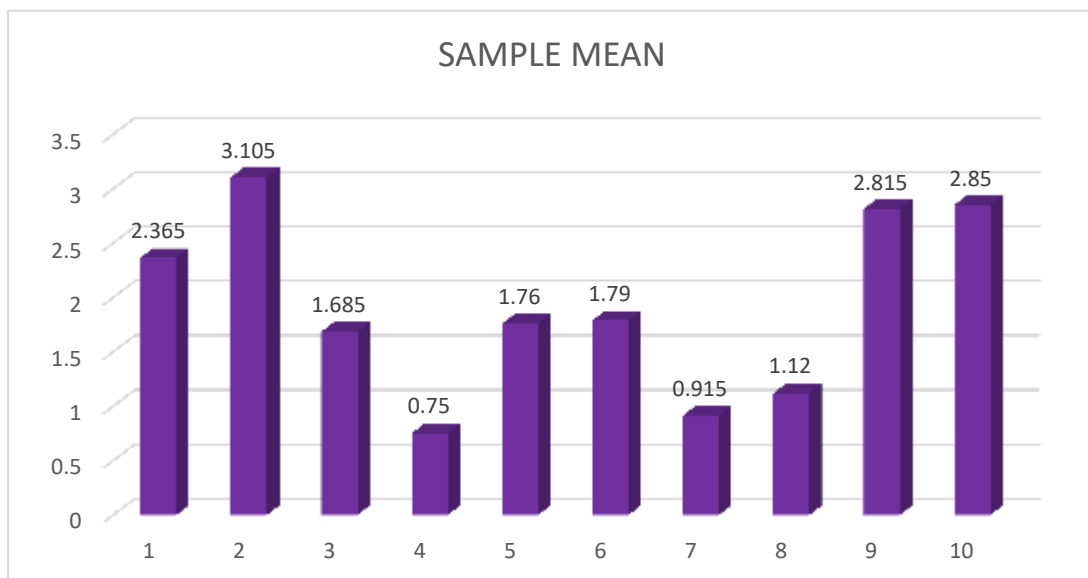
SAMPLE MEAN

Graph IX: Basic and mean microgap at the implant-abutment interface of Ti implants and customized laser-sintered Co-Cr abutments at point IIC, at the platform level for Group II

SAMPLE MEAN

Sample	Value
1	4.23
2	3.84
3	2.265
4	1.5
5	2.59
6	2.125
7	1.215
8	0.98
9	4.715
10	2.975

Graph X: Basic and mean microgap at the implant-abutment interface of Ti implants and customized laser-sintered Co-Cr abutments at point IID, at the internal connection level for Group II

SAMPLE MEAN

MICROGAP

Sample	Value
1	4.875
2	6.72
3	7.7
4	7.305
5	6.66
6	5.045
7	7.1
8	3.95
9	6.195
10	4.94

NO OF SAMPLES
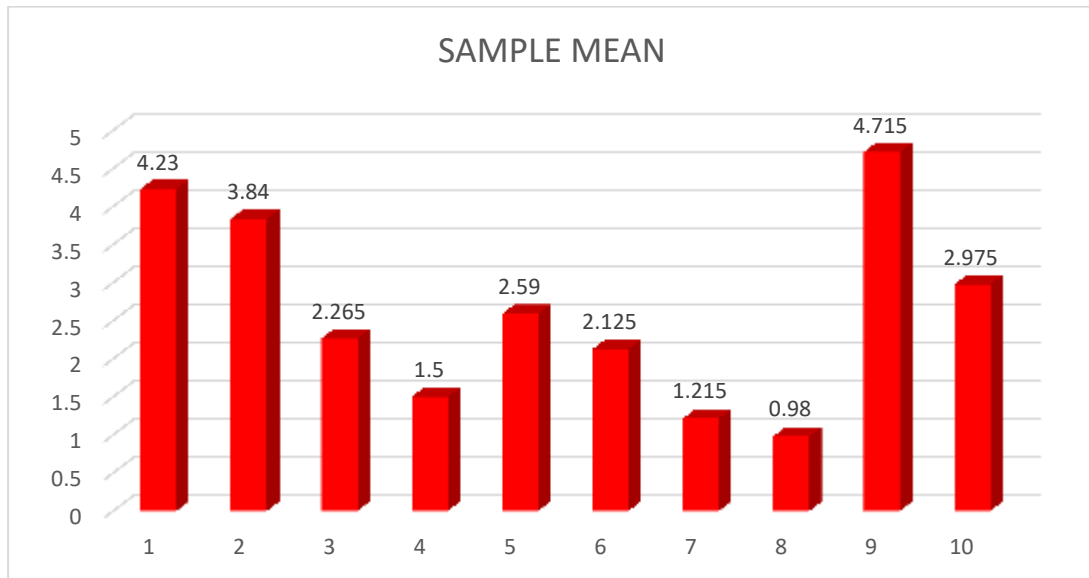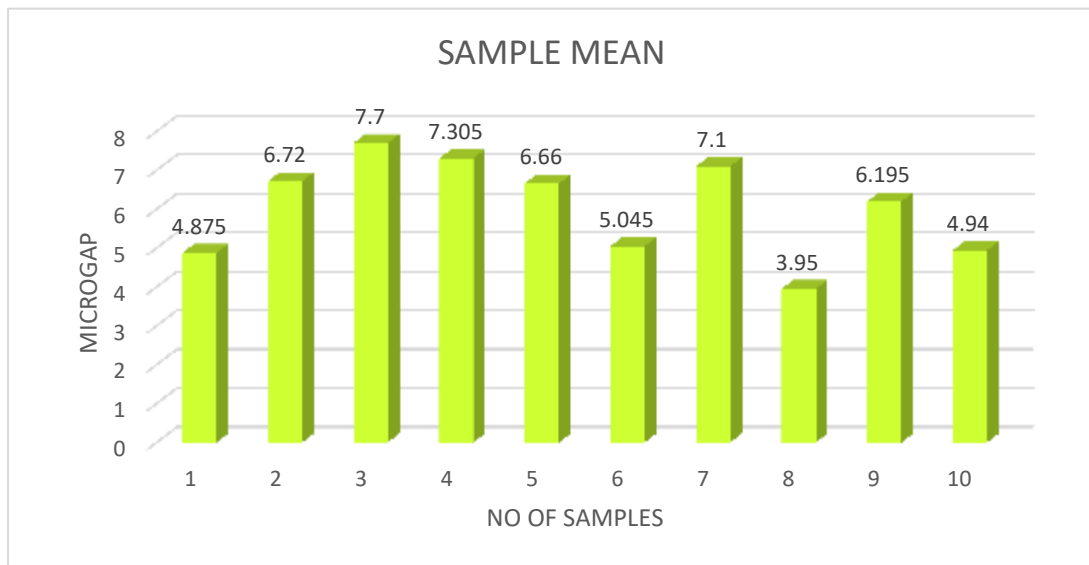
Graph XI: Basic and mean microgap at the implant-abutment interface of Ti implants and customized laser-sintered Co-Cr abutments at point IIE, at internal connection level for Group II
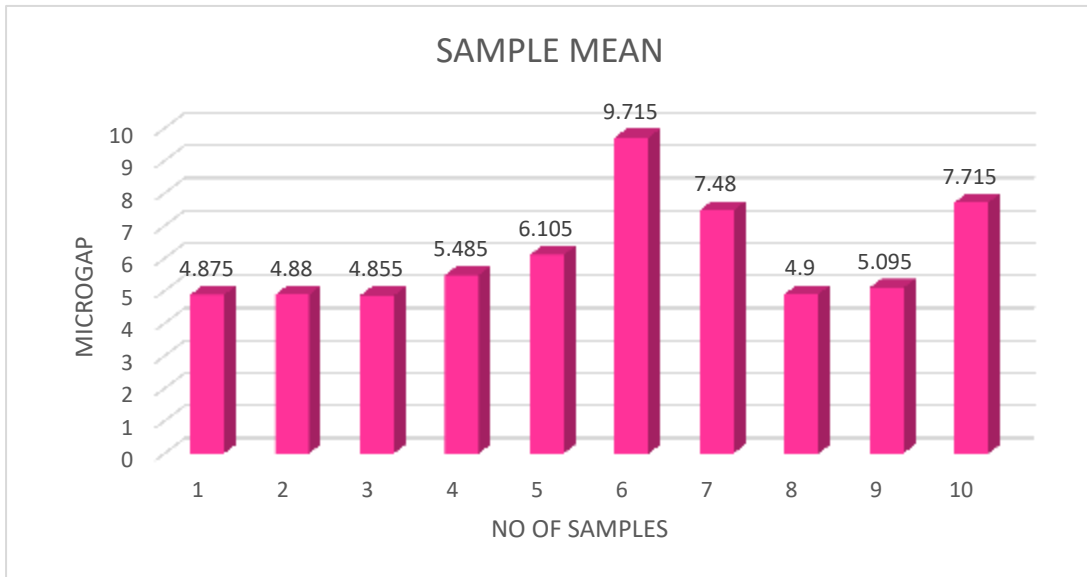
Graph XII: Basic and mean microgap at the implant-abutment interface of Ti implants and customized laser-sintered Co-Cr abutments at the point IIF, at the internal connection level for Group II
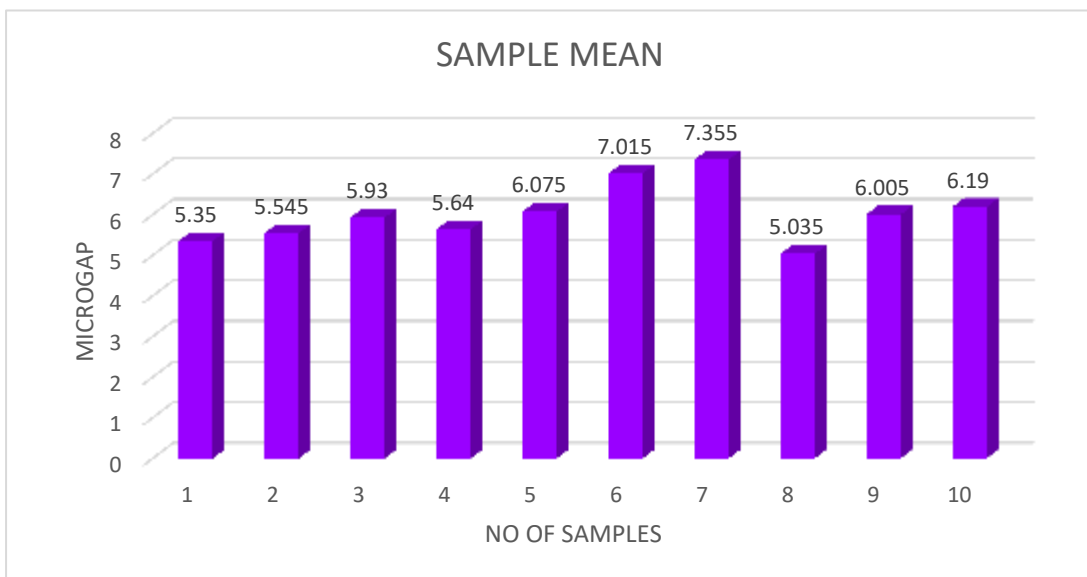
Graph XIII: Comparative evaluation of mean microgap at the implant-abutment interface at point A at platform level for Group I & Group II (IA vs. IIA)
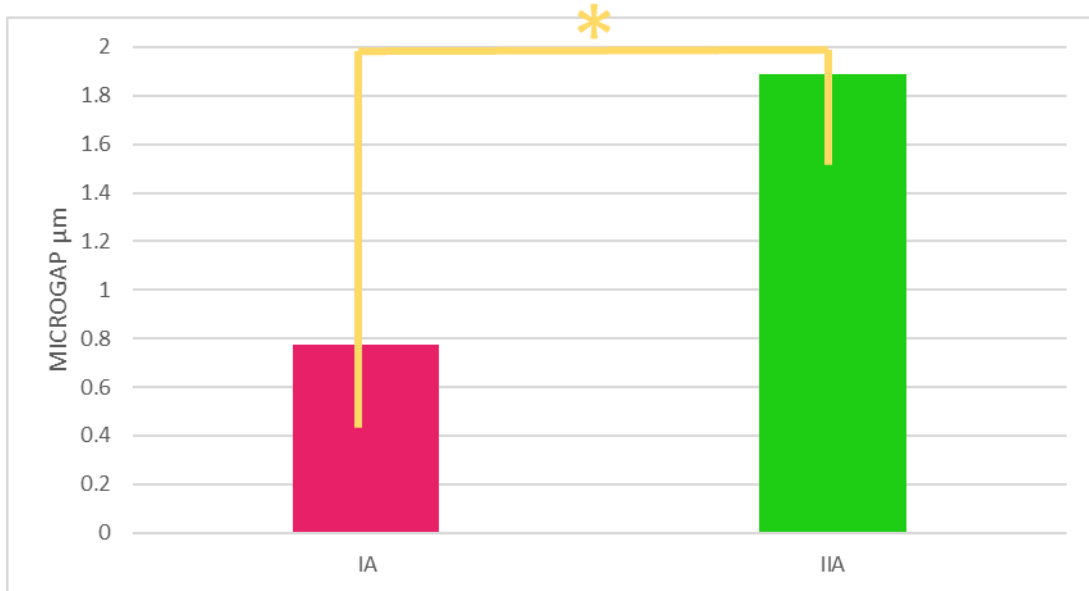
* = (p< 0.05)

Graph XIV: Comparative evaluation of mean microgap at the implant- abutment interface at point B at platform level for Group I & Group II (IB vs. IIB)
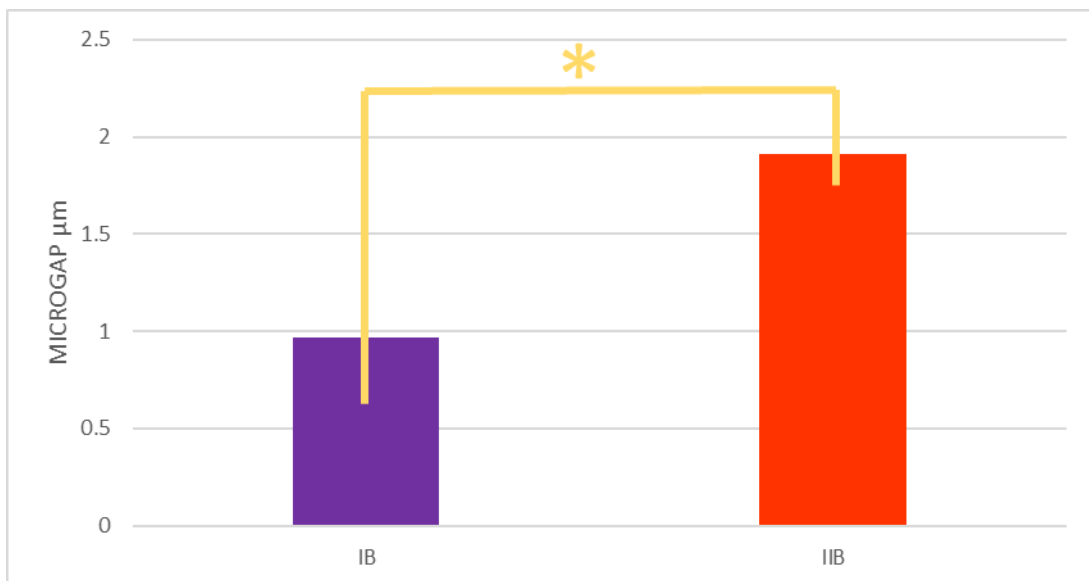
* = (p< 0.05)

Graph XV: Comparative evaluation of mean microgap at the implant-abutment interface at point C at platform level for Group I & Group II (IC vs. IIC)
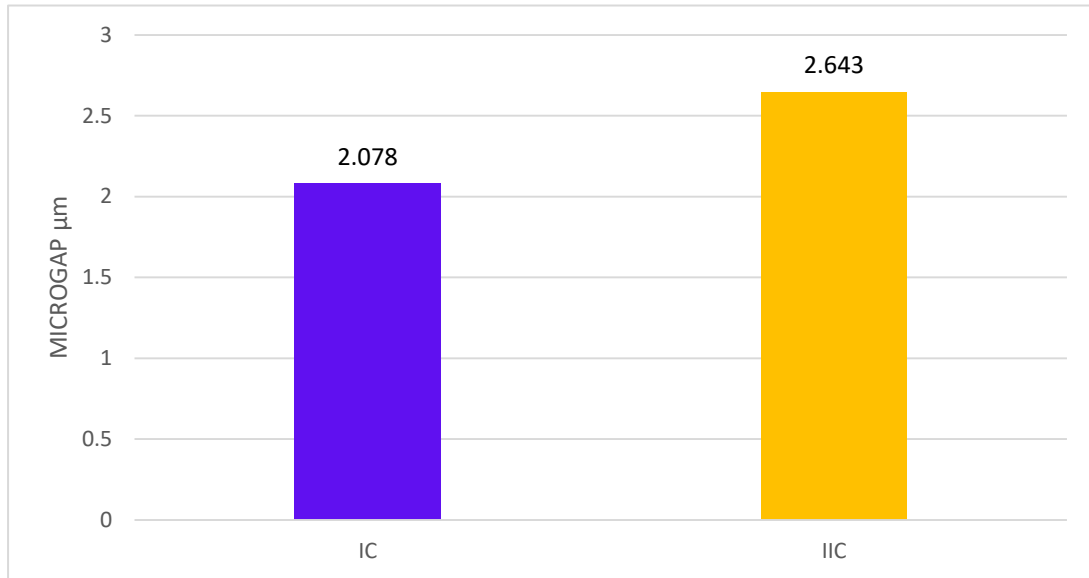
Graph XVI: Comparative evaluation of mean microgap at the implant-abutment interface at point D at internal connection level for Group I & Group II (ID vs. IID)
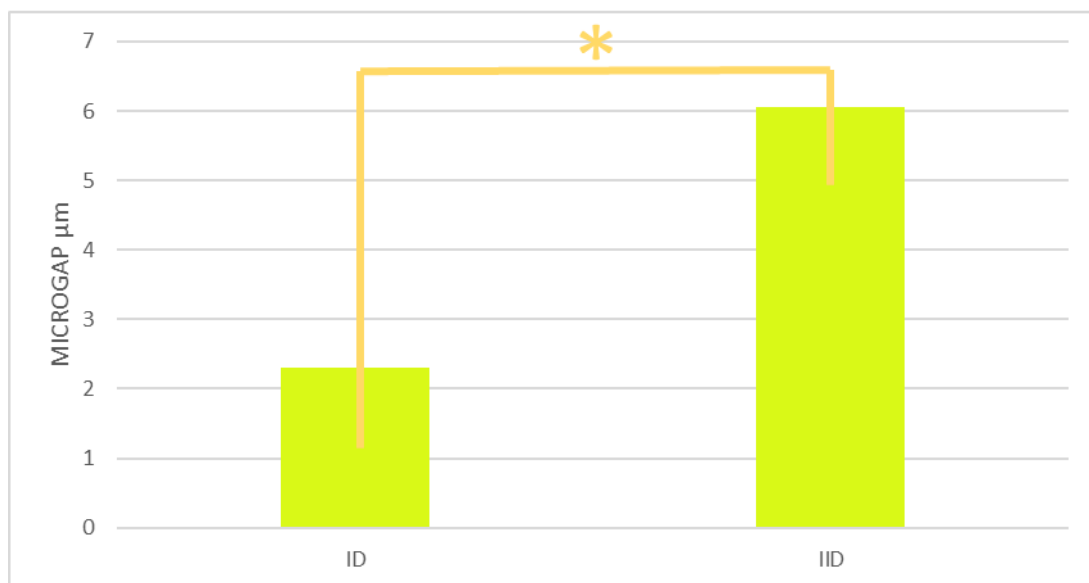
$*$ = (p< 0.05)

Graph XVII: Comparative evaluation of mean microgap at the implant-abutment interface at point E at internal connection level for Group I & Group II (IE vs. IIE)
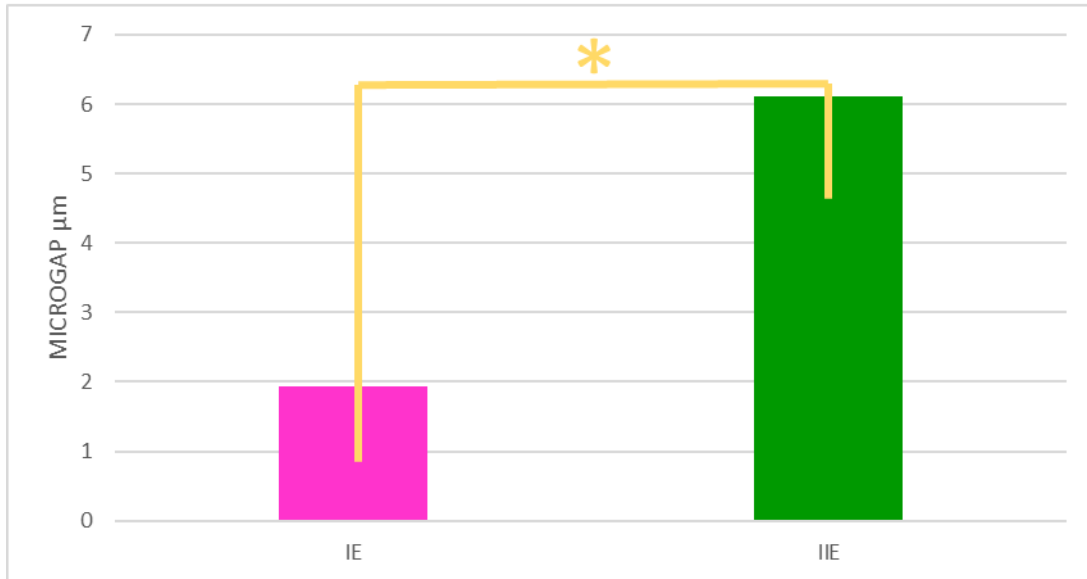
* = (p< 0.05)

Graph XVIII: Comparative evaluation of mean microgap at the implant-abutment interface at point F at internal connection level for Group I & Group II (IF vs. IIF)
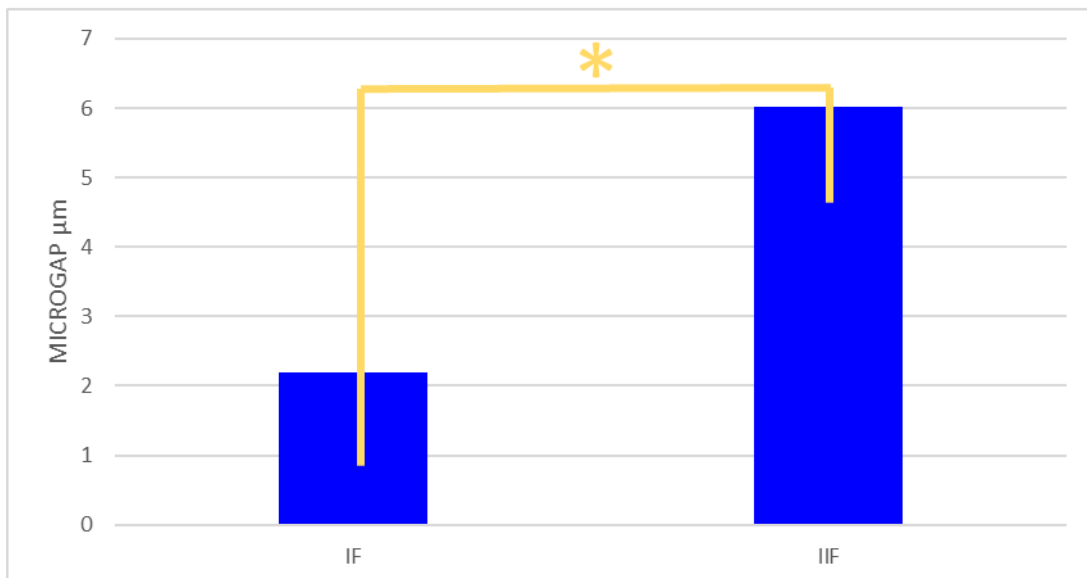
* = (p< 0.05)

DISCUSSION

In recent years, Osseointegrated dental implants have become increasingly important in the field of oral rehabilitation of partial or completely edentulous patients and a successful implant therapy demands a balance between biological and mechanical factors that influence the effectiveness of oral implants[22, 23, 25, 26]

Implant system consist of two components, the implant that is placed during the first surgical phase, and the abutment is later screwed onto the implant to support the prosthetic restorations [10, 11, 28, 44, ,46,56]. The mating surfaces of the implant and its abutment form the implant-abutment interface and are considered to be a crucial aspect in the implant design. The design of the fixture-abutment interface may have an impact on the amount of microbial leakage between the two parts [1,26, 32, 55]. Several issues have been reported by many authors with abutment misfit and microgaps, including screw loosening,[6,23,29,32,36,55,] microleakage,[14,23,33,36,34,58] abrasion and wear of components,[27] potential for bone loss,[27, 31] and :the micro-pump effect".[27]

Although many studies have shown the importance of implant-abutment fit is available, no standardised, agreed-upon method for measurement of interface gap has been established.[12,13,15,36] Various methods of measuring the interface gap have been reported which include, direct view or measurement of the interface at the margin, cross-sectional measurement

after sectioning, the impression technique, radiographic appearance, micro-leakage, degree of rotational freedom and the use of an explorer with a visual examination.[4,6,36,39,44] Many authors recommended that have recommended conducting comprehensive such analysis on sectioned implant-abutment assemblies to enable a more and extensive observation of the adaptation along the implant-abutment interface. The cross-sectional sectioned view allows greater accuracy in reproducibility of reference points than the circumferential view[32]

Premachined abutments, including those that underwent overcasting and porcelain building have a better fit than castable abutments.[15,16] Various studies have reported lower micro-gap and misfit values for pre-machined abutments than with cast- on abutments.[7,15,48] Implant manufacturers, design and produce implants and abutments such that, there is an intimate fit between the components at the implant-abutment interface. The objective is that the implant-abutment assembly should achieve physically tight connection. These are termed as premachined components,. However, in certain situations, customized abutments are indicated. Implant abutments can be customized by casting, milling and laser-sintering procedures. Surface irregularities due to customization process can enhance the microgap at the implant-abutment interface.[23] The control of roughness on the mating surfaces at the implant-customized abutment interface could reduce afore mentioned complications by controlling the microgap.[23]

Precision of fit between the implant components play a major role in microgap and micro leakage. Imperfect fit between implant and abutment leading to micro movements of the implant components during function and allow the initiation of pumping effect,[32] causing bacteria to move through the implant-abutment interface. A number of studies evaluated implant-abutment interface using premachined abutments and the microgaps ranges from 0 to 150µm.[3,4,25,28,29,45] Discrepancies greater than 10 microns are reported to result in bacterial colonization and inadequate screw mechanics, which may lead to failures.[59] Currently, studies comparing the implant-abutment interface of internal hexagon connection designs while using premachined versus laser-sintered abutments by measuring at the interface in vertically sectioned test samples are sparse.

The aim of the present *in vitro* study was to comparatively evaluate the microgap at the implant-abutment interface with premachined and customized laser-sintered Co-Cr abutments using scanning electron microscopy (SEM). The null hypothesis of the present study was that there would be no significant difference in microgap at the implant-abutment interface with either premachined or customized abutments.

All the steps discussed in the methodology for test sample preparation were performed by a single operator to avoid operator-based errors. Titanium dental implants of the same dimensions with the internal hexagon design were employed for standardization of the implant fixtures. To avoid mechanical

complications related to external hex implants various internal connections have been developed.[28] Even though various internal connection designs like internal octagon, cone screw, cone hex, spline, are available the internal hexagon implant has been a wide choice in restorative dentistry to transfer stresses of the abutment screws and the crestal bone as it distributes the lateral loading deep within the implant leading to better implant-abutment joint stability and strength.[12] Hence, in the present study implants with internal hex connection design were selected.

In single-tooth implant prosthesis, the interface and its connecting screw are exposed to rigorous load applications, the load distribution effect is absent leading to more bending moments due to non-axial loading, screw loosening, abutment screw fracture and implant fracture.[19,62] Studies on fit at the interface in single-implant situations comparing premachined and customized abutments are few. Hence, the implant-abutment interface was assessed on unsplinted single implants in the present study.

There are number of studies pertaining to the comparison of premachined abutments vs premachined abutments[3,4,6,17,25,28,29,39,59] and cast on abutments.[37] However studies on customized abutments are sparse. The microgap of implant-abutment connections could be reduced with smoother mating surfaces.[23]

Several techniques and materials are available to custom fabricate prosthetic structures. High precision in manufacturing results in lower degrees of abutment rotation and smaller gaps at the interface, and therefore

less bacterial colonization, tissue alteration, and tension on retaining screws.[2,23] The main abutment manufacturing techniques are milling, casting and laser-sintering. The control of roughness on the mating surfaces of implant components before their use could reduce screw loosening as well as the microgap between implant components.[23] The use of stock milled abutments is limited due to standard shape of piece. However, the connection of premachined abutment to implant known as friction fit, provides a perfect assembly between the components.[2] Laser-sintering enables direct fabrication of prototypes for development of prostheses.[2] Hence in this study, customized laser-sintered Co-Cr abutments were used. During fabrication, the connection area of the abutment was not touched but polished to ensure standardization and to prevent manufacturer's errors.

In the present study, the microgap was measured along the implant-abutment interface at the platform level and internal connection level after sectioning of embedded implant abutment assemblies. Embedding of implant-abutment assembly done in clear acrylic autopolymerising resin, since it allows easy visualization of implant and its angulation during embedding and sectioning procedures.

The embedding procedure of the assemblies was accomplished in two stages to permit torquing and retorquing of the abutment screws effectively.[8,38]

In the present study, 35Ncm torque was given using mechanical torque wrench during these procedures in line with manufacturer's

61

recommendations. Retorquing of implant-abutment assembly was done after 24 hours to ensure proper adaptation between implant components and maintenance of preload as recommended by the manufacturer. Gehrke et al[25] reported significant reductions in interface gaps with increase in tightening torque from 25 to 40 Ncm.

Sandblasting of abutment surfaces was done for the mechanical retention within the resin during sectioning procedures. Complete embedding of the implant-abutment involves, complete closure of the abutment screw channel with the autopolymerising resin to prevent loosening of screw threads.

In number of studies, sectioning of the implant-abutment assemblies were carried out by diamond disc in a metallographic cutter,[25] grinder polishing unit[35, 38] with copious water irrigation to avoid clogging of metal debris in the interface region. However, these procedures are technique-sensitive and may result in unevenly cut surface. To avoid this, in the present study, vertical sectioning of test samples was done using water jet sectioning machine. The direction and precise location of sectioning tip can be pre-programmed in the controlling unit to aid in even sectioning of samples. And the size of sectioning tip nozzle can be selected accordingly. Here in this study. 0.76 mm diameter nozzle size was selected to achieve exact sectioned samples. Moreover, with the pressure in the range of 1800-3800 bars along with the abrasive sand particles, clogging of metal debris that can hinder the precise location and measurement of implant- abutment interface gap can be minimized. The other cleaning and polishing procedures followed in this

study were done to obtain well-delineated implant-abutment images during SEM.[3,5,24,25,35,38]

The measurement and analysis of microgap at the implant-abutment interface can be done by scanning electron microscopy (SEM),[17,24,32,35,47,52,59,63] 3D micro-tomographic technique,[45,53] optical microscopy (O.M.),[17,21,28] scanning laser microscopy (SLM),[63] optical coherence tomography[39] and radiography.[33,41] Of these scanning electron microscopy is efficient method for analysis of the implant-abutment interface and was adopted for obtaining the microgap measurements in this study. The wide range of magnifications possible was well-suited to observe the interface adequately. The measurements were marked on the reference points at the implant-abutment interface at the platform[24] and internal connection level. Pixel-counting software was then used to measure the implant-abutment microgap.[32]

The results of the present study showed the following: the microgap at the most point A at the implant-abutment interface at platform level of Group I samples (Table I, Graph I) showed a variation in measurement from 0 µm to 3.65µm, with the mean microgap (IA) of 0.774µm. The microgap at point B at the implant-abutment interface at platform level of Group I samples (Table II, Graph II) showed a variation in measurement from 0µm to 2.63µm, with the mean microgap (IB) of 0.967µm. The microgap at the point C at the implant-abutment interface at platform level of Group I samples (Table III, Graph III) showed a variation in measurement from 0.581µm to 5.32µm, with

the mean microgap (IC) of 2.078μm. The microgap at the point D at the implant-abutment interface at internal connection level of Group I samples (Table IV, Graph IV) showed a variation in measurement from 1.43μm to 3.28μm, with the mean microgap (ID) of 2.313μm. The microgap at the point E at the implant-abutment interface at internal connection level of Group I samples (Table V, Graph V) showed a variation in measurement from 0.794μm to 2.82μm, with the mean microgap (IE) of 1.927μm. The microgap at the point F at the implant-abutment interface at internal connection level of Group I samples (Table VI, Graph VI) showed a variation in measurement from 1.19μm to 3.99μm, with the mean microgap (IF) of 2.189μm.

In Group II samples (Table VII, Graph VII), the microgap at point A there was a variation in measurement from 1.00 to 2.830μm with the mean microgap (IIA) of 1.888μm. The microgap at point B (Table VIII, Graph VIII), there was a variation in measurement from 0.00 to 3.41μm with the mean microgap (IIB) of 1.915μm. The microgap at point C (Table IX, Graph IX), there was a variation in measurement from 0.72 to 6.21μm with the mean microgap (IIC) of 2.643μm. The microgap at point D (Table X, Graph X), there was a variation in measurement from 3.16 to 10.28μm with the mean microgap (IID) of 6.049μm. The microgap at point E (Table XI, Graph XI), there was a variation in measurement from 2.77 to 11.32μm with the mean microgap (IIB) of 6.110μm.

Non parametric Mann-Whitney U test showed that the point C at platform level (Table XV, Graph XV) at the implant-abutment interface did

not show statistically significant differences (P > 0.05) in the microgap between premachined and customized laser-sintered Co-Cr abutments. Statistically significant differences were found at point A (Table XIII, Graph XIII), point B (Table XIV, Graph XIV), point D (Table XVI, Graph XVI), point E (Table XVII, Graph XVII), and point F (Table XVIII, Graph XVIII) at the implant-abutment interface between premachined and customized laser-sintered Co-Cr abutments (P < 0.05).

The ideal vertical misfit would be no microgap[36,61] However, previous literature on microgap assessment at the implant-abutment interface have ranged from 0 to 135µm4,5,6,13,16,17,19,23,24,25,32,36,40,59,60,61,64,65, Among these studies, higher interface gaps have been observed in studies involving castable or milled abutments, with mean microgap ranging from 1 to 135µm[23]. Tsuge et al[63] observed very low microgap values for premachined internal and external connection implants, ranging from 2.3µm to5.6µm, corroborating that even premachined abutments can present microgap at the implant-interface interface.[61]

Fujiwara et al[24] studied interface gaps in sectioned samples of castable external hex implants ranging from 0µm to 15.267µm while using implants and components of the same manufacturer when observed at the most external, middle and most internal points at the platform level of sectioned specimens. The present study also measured the interface gaps at the above mentioned reference points at the interface for internal hex connections using

either premachined or customized laser-sintered Co-Cr abutments after sectioning. The findings of this study reveal much lesser interface gaps in all the areas observed with premachined abutments compared to customized laser-sintered Co-Cr abutments. These differences can be attributed to the differences in process of fabrication, polishing procedures.

The average dimension of a microbe is less than 2µm and hence bacterial adhesion and colonization can be assumed in all implant-abutment interface configurations.[6] Thus lesser the microgap, lower is the risk of colonization and peri-implant inflammation. Moreover, interface gaps < 10 µm have been considered as acceptable with negligible or reduced biological and/or mechanical complications.[59] Though the mean microgap values obtained from both premachined and customized laser-sintered Co-Cr abutments were within the clinically acceptable range, the null hypothesis of this study is rejected.

Studies per se evaluating customized laser-sintered Co-Cr abutments are very few.[2,23] Fernandes et al[23] reported that microgap inaccuracies compounded by the multiple fabrication process that compromise the implant-abutment interface fitting.

The results of the present study indicate that the manufacturing technique is also a variable that influences the presence of microgap, probably due to different surface roughness produced by the manufacturing method. The results of the present study were measured on the cobalt-chromium samples which are presumably related to the manufacturing

process, in turn, affect the connection misfit and the surface roughness, thereby affecting the microgap. The CAD design of the abutment obtained was not from the manufacturer but from the third party implant library may influence the microgap.

The present study had some limitations. Parameters such as mechanical behavior, microbial leakage, cyclic loading and fatigue testing may affect the interface differently and were not part of the present study design. Further, the moist oral environment may also impact these parameters differently than the dry testing conditions employed in the present study. One limitation with evaluating sectioned test samples is that these cannot be used to monitor changes in test conditions where measurements are required before and after testing. Also, the test groups can be expanded to include other customized abutments such as milled and cast-on and/or connection designs. Future studies incorporating the above along with a larger sample size simulating *in vivo* conditions are recommended to add merit to the findings obtained with the present study.

CONCLUSION

The following conclusions were drawn based on the results obtained in the present *in vitro* study which was conducted to comparatively evaluate the microgap at the implant-abutment interface with premachined and customized laser-sintered Co-Cr abutments.

1. The mean microgap at the implant-abutment interface of Ti implants and Ti premachined abutments at point A, at the platform level **(Group I, Point IA)** was found to be **0.774μm**.

2. The mean microgap at the implant-abutment interface of Ti implants and Ti premachined abutments at point B, at the platform level **(Group I, Point IB)** was found to be **0.967μm**.

3. The mean microgap at the implant-abutment interface of Ti implants and Ti premachined abutments at point C, at the platform level **(Group I, Point IC)** was found to be **2.078μm**.

4. The mean microgap at the implant-abutment interface of Ti implants and customized laser-sintered Co-Cr abutments at point D, at the internal connection level **(Group I, Point ID)** was found to be **2.313μm**.

5. The mean microgap at the implant-abutment interface of Ti implants and customized laser-sintered Co-Cr abutments at point E, at the itnternal connection level **(Group I, Point IE)** was found to be **1.927μm**.

6. The mean microgap at the implant-abutment interface of Ti implants and customized laser-sintered Co-Cr abutments at point F, at the internal connection level **(Group I, Point IF)** was found to be **2.189µm**.

7. The mean microgap at the implant-abutment interface of Ti implants and customized laser-sintered Co-Cr abutments at point A, at the platform level **(Group II, Point IIA)** was found to be **1.888µm**.

8. The mean microgap at the implant-abutment interface of Ti implants and customized laser-sintered Co-Cr abutments at point B, at the platform level **(Group II, Point IIB)** was found to be **1.915µm.**

9. The mean microgap at the implant-abutment interface of Ti implants and customized laser-sintered Co-Cr abutments at point C, at the platform level **(Group II, Point IIC)** was found to be **2.643µm**.

10. The mean microgap at the implant-abutment interface of Ti implants and customized laser-sintered Co-Cr abutments at point D, at the internal connection level **(Group II, Point IID)** was found to be **6.049µm**.

11. The mean microgap at the implant-abutment interface of Ti implants and customized laser-sintered Co-Cr abutments at point E, at the internal connection level **(Group II, Point IIE)** was found to be **6.110µm.**

12. The mean microgap at the implant-abutment interface of Ti implants and customized laser-sintered Co-Cr abutments at point F, at the internal connection level **(Group II, Point IIF)** was found to be **6.014µm**

13. On comparison between the mean microgap at the implant-abutment interface at point A, at the platform level between Ti implants and premachined abutments **(IA: 0.774µm),** with that of Ti implants and customized laser-sintered Co-Cr abutments **(IIA: 1.888µm)**, it was found that the microgap for premachined abutments at point A, was lesser than

that of customized laser-sintered abutments. This difference was statistically significant (P < 0.05).

14. On comparison between the mean microgap at the implant-abutment interface at point B, at the platform level between Ti implants and premachined abutments **(IB: 0.967µm),** with that of Ti implants and customized laser-sintered Co-Cr abutments **(IIB: 1.915µm),** it was found that the microgap for premachined abutments at point B, was lesser than that of customized laser-sintered Co-Cr abutments. This difference was found to be statistically significant (P < 0.05).

15. On comparison between the mean microgap at the implant-abutment interface at point C, at the platform level between Ti implants and premachined abutments **(IC: 2.078µm),** with that of Ti implants and customized laser-sintered Co-Cr abutments **(IIC: 2.643µm),** it was found that the microgap for premachined abutments at point C, was lesser than that of customized laser-sintered Co-Cr abutments. This difference was found to be statistically insignificant (P > 0.05).

16. On comparison between the mean microgap at the implant-abutment interface at point D, at the internal connection level between Ti implants and premachined abutments **(ID: 2.313µm),** with that of Ti implants and customized laser-sintered Co-Cr abutments **(IID: 6.049µm),** it was found that the microgap for premachined abutments at point D was lesser than that of customized laser-sintered abutments. This difference was found to be statistically significant (P < 0.05).

17. On comparison between the mean microgap at the implant-abutment interface at point E, at the internal connection level between Ti implants and premachined abutments **(IE: 1.927µm),** with that of Ti implants and customized laser-sintered Co-Cr abutments **(IIE: 6.110µm),** it was found that the microgap for premachined abutments at point E, was lesser than

that of customized laser-sintered abutments. This difference was found to be statistically significant ($P < 0.05$).

18. On comparison between the mean microgap at the implant-abutment interface at point F, at the internal connection level between Ti implants and premachined abutments **(IF: 2.189μm),** with that of Ti implants and customized laser-sintered Co-Cr abutments **(IIF: 6.014μm),** it was found that the microgap for premachined abutments at point F, was lesser than that of customized laser-sintered abutments. This difference was found to be statistically significant ($P < 0.05$).

SUMMARY

The present *in vitro* study was conducted to comparatively evaluate the microgap at the implant-abutment interface with premachined and customized laser-sintered Co-Cr abutments

Twenty titanium implants of internal hexagon connection design were selected and randomly divided into two groups of 10 each. The first group of 10 implants was connected to their respective premachined standard Ti abutments. The second group of 10 implants was connected to customized laser-sintered Co-Cr abutments. The implant-abutment assemblies were torque tightened to 35 Ncm and embedded individually using clear autopolymerising acrylic resin to obtain resin blocks. The embedded specimens were subjected to sectioning using water jet powered sectioning machine followed by sequential finishing and cleaning process to obtain a smooth uniform flat surface and to remove the clogged debris.

Scanning electron microscopic images of the implant- abutment interface at the platform level and internal connection level were obtained individually for each sample. Using pixel counting software, the microgap at the implant-abutment interface at the platform level and internal connection level was measured at 6 different points on both right and the left sides for each test sample of both test groups. The reference points were marked and designated as Points a, b, c on right side and as Points a′, b′, and c′ on left side of implant-abutment interface at the platform level. The reference points were marked and designated as Points d, e, f on right side and as Points d′, e′, and f′ on left side of implant-abutment interface at the internal connection level.

Mean microgap for each point (A, B, C, D, E, F) of both test groups was obtained. The data was tabulated and analyzed using non parametric Mann-Whitney U test.

The mean microgap at the points A, B and C at the implant-premachined abutment interface at platform level of Group I was found to be 0.774µm, 0.967µm and 2.078µm respectively. The mean microgap at points A, B and C at the implant-customized laser-sintered abutment interface at platform level of Group II was found to be 1.888µm, 1.915µm and 2.643µm respectively. The mean microgap at points D, E and F at the implant-premachined abutment interface at internal connection level of Group I was found to be 2.313µm, 1.927µm and 2.189µm respectively. The mean microgap at points D, E, and F at the implant-customized laser-sintered abutment interface at internal connection level of Group II was found to be 6.049µm, 6.110µm and 6.014µm respectively. On statistical comparison, the differences in the microgap measurements for both test groups at the platform level and internal connection level were statistically significant except at the point C where it showed significantly lesser values of microgap for the premachined abutments.

In this *in vitro* study, all the mean values of microgap obtained at the six reference points of the premachined abutments were found to be less than that of customized laser-sintered Co-Cr abutments with statistically significant difference. Thus, the null hypothesis of this study is not validated, because the present study had revealed that there was a statistically significant difference in the microgap at implant-abutment interface between the premachined abutments and customized laser-sintered abutments, but, the microgap values are within the clinically acceptable range.

BIBLIOGRAPHY

1. **Al-Jadaa A, Attin T, Peltomäki T, Heumann C, Schmidlin PR.** Impact of dynamic loading on the implant-abutment interface using a gas enhanced permeation test *In Vitro.* Open Dent J, 2015;9:112-119.

2. **Alonso-Perez R, Bartolome JF, Ferreiroa A, Salido MP, Pradies G.** Evaluation of the mechanical behavior an marginal accuracy of stock and laser-sintered implant abutments. Int J Prosthodont 2017;30:136-138.

3. **Apicella D, Veltri M, Chieffi N, Polimeni A, Giovannetti A, Ferrari M.** Implant adaptation of stock abutments versus CAD/CAM abutments: a radiographic and scanning electron microscopy study. Annall dl Stomatologia 2010:1(3-4):9-13.

4. **Baixe S, Fauxpoint G, Arntz Y, Etienne O.** Microgap between zirconia abutments and titanium implants. Int J Oral Maxillofac Implants 2010;25:455-460.

5. **Bajoghli F, Amjadi M, Akouchekian M, Narimani T.** Bacterial leakage and microgap along implant-abutment connection in three different implant systems. Int J of Adv Biotec and research 2016;7:4

6. **Baldassarri M, Hjerppe J, Romeo D.** Marginal accuracy of three implant-ceramic abutment configurations. Int J Oral Maxillofac Implants 2012;27:537-543.

7. **Barbosa SGA, Simamoto Junior PC, Fernandes Neto AJ, Mattos MGC, Neves FD.** Prosthetic laboratory influence on the vertical misfit at the implant/ ucla abutment interface. Braz DentJ 2007;18(2):139-43.

8. **Barbosa GAS, Bernardes SR, das Neves FD, Fernandes Neto AJ, de Mattos Mda G, Ribeiro RF.** Relation between implant/abutment vertical misfit and torque loss of abutment screws. Braz Dent J 2008;14(4):358-63.

9. **Baumgarten H, Suttin Z, Schmidlin PR, Portes SS**. Dental implant system seal integrity and the quest for sustainable aesthetics. J Implant Recons Dent 2014;5(2):01-08.

10. **Berberi A, Tehini G, Rifai K, Eddine FBN, Badran B, Akl H**. In vitro evaluation of leakage of implant- abutment connection of three implant systems having the same prosthetic interface using Rhoamine B. International journal of dentistry 11 may 2014

11. **Berberi A, Tehini G, Rifai K, Eddine FBN, Badran B, Akl H**. Leakage evaluation of original and compatible implant-abutment connections: *In vitro* study using Rhodamine B. J Dent Biomechanics 2014;5:01-07.

12. **Binon PP**. Implants and components: Entering the new millennium. Int J Oral Maxillofac Implants 2000;15(1):77-95.

13. **Binon PP**. Evaluation of machining accuracy and consistency of selected implants, standard abutments and laboratory analogs. Int J Prosthodont 1995;8(2):162-78.

14. **Broggini N, McManus LM, Hermann JS, Medina RU, Oates TW, Schenk RK, Buser D, Mellonig JT, Cochran DL.** Persistent acute inflammation at the implant-abutment interface. J Dent Res 2003;82(3):232-37.

15. **Byme D, Houston F, Cleary R, Claffey N.** The fit of cast and premachined implant abutments. J Prosthet Dent 1998;80:184-92.

16. **Cardozo R, Olate S, Navarro P, Araya J, Gonzalez O.** Analysis of the abutment-implant platform gap in internal hex dental implants. Biomed Res 2017;28 (8): 3336-3339.

17. **Coelho AL, Suzuki M, Dibart S, Da Silva N, Coelho PG.** Cross-sectional analysis of the implant-abutment interface. J Oral Rehab 2007;34:508-16.

18. **Cunha TMA, Araújo RPC, Rocha PVB, Amoedo RMP.** Comparison of fit accuracy between procera custom abutments and three implant systems. Clin Implant Dent Rel Res 2012;14(6):890-95.

19. **Dellow AG.** Scanning electron microscopy evaluation of the interfacial fit of interchanged components of four dental implant systems. Int J Prosthodont 1997;10:216-221.

20. **Dittmer S, Kohorst P, Jendras M, Borchers L, Stiesch M.** Effect of implant-abutment connection design on load bearing capacity and failure mode of implants. Journal of prosthodontics 2011; 20: 510-516

21. **Faria KO, Silveira-Junior CD, da Silva-Neto JP, Mattos MGC, da Silva MR, Neves FD.** Comparison of methods to evaluate implant-abutment interface. Braz J Oral Sci 2013;12(1):37-40.

22. **Faria R, May LG, de Vasconcellos DK, Volpato CAM, Bottino MA.** Evaluation of the bacterial leakage along the implant-abutment interface. J Dent Implants 2011;1(2):51-57.

23. **Fernández M, Delgado L, Molmeneu M, Garcia D, Rodriguez D.** Analysis of the misfit of dental implant-supported prosthesis made with

three manufacturing processes. J Prosthet Dent 2014;111:116-23.

24. **Fujiwara CA, Filho OM, Oliveira NTC, Queiroz TP, Abla MS, Pardini LC.** Assessment of the interface between implant and abutments of five systems by scanning electronic microscopy. J Osseointe 2009;2(1):60-93.

25. **Gehrke SA, Shibli JA, Aramburu Junior JS, de Val JEMS, Calvo-Girardo JL, Dedavid BA.** Effects of different torque levels on the implant-abutment interface in a conical connection. Braz Oral Res 2016;30(1):e-40.

26. **Gherlone EF, Capparé P, Pasciuta R, Grusovin MG, Mancini N, Burioni R.** Evaluation of resistance against bacterial microleakage of a new conical implant-abutment connection versus conventional connections: an in vitro study. New Microbiologica 2016;39:49-56.

27. **Gigandet M, Bigolin G, Faoro F, Bürgin W, Bragger U.** Implants with original and non-original abutment connections. Clin Implant Dent Rel Res 2012;01-10.

28. **Gil FJ, Herrero-Climent M, Lázaro P, Rios JV.** Implant-abutment connections: influence of the design on the microgap and their fatigue and fracture behaviour of dental implants. J Mater Sci: Mater: Med 2014.

29. **Goodacre Charles J, Kan JYK, Runcharassaeng K.** Clinical complications with implants and implant prostheses. J Prosthet Dent 2003;90(2):121-32.

30. **Gross M, Abramovich I, Weiss EI.** Microleakage at the abutment-implant interface of osseointegrated implants: A comparative study. Int J Oral Maxillofac Implants 1999;14:94-100.

31. **Guimaraes MP, Nishioka RS, Bottino MA.** Analysis of

implant/abutment marginal fitting. PGR – Pois –Grad Fac Pdontol Sao Jose dos Campos. 2001;4(2):12-19.

32. **Hamiliton A, Judge RB, Palamara JE, Evans C.** Evaluation of the fit of CAD/CAM abutments. Int J Prosthodont. 2013;26(4):370-380.

33. **Harder S. Dimaczek B, Acil Y, Terheyden H, Freitag-Wolf S, Kern S**. Molecular leakage at implant-abutment connection- in vitro investigation of tightness of internal conical implant-abutment connections against endotoxin penetration. Clin Oral Invest. 2009.

34. **Jaarda MJ, Razzoog ME, Gratton DG.** Geometric comparison of five interchangeable implant prosthetic retaining screws. J Prosthet Dent. 1995;74:373-9.

35. **Jeong YT, Chung CH, Lee HT**. Screw joint stability according to abutment screw materials. J Korean Acad Prosthodont. 2001;39(3):297-305.

36. **Kano SC, Binon PP, Curtis DA.** A classification system to measure the implant-abutment microgap. Int J Oral Maxillofac Implants. 2007;22:879-885.

37. **Kano SC, Binon PP, Bonfante G, Curtis DA.** The effect of casting procedures on rotational misfit in castable abutments. Int J Oral Maxillofac Implants. 2007;22:575-579.

38. **Kim JS, Kim HJ, Chung CH, Baek DH.** Fit of fixture/abutment/ screw interfaces of internal connection implant system. J Korean Acad Prosthodont. 2005; 43(3): 338-51

39. **Kikuchi K, Akiba N, Sadr A, Sumi Y, Tagami J, Minakuchi S.** Evaluation of the marginal fit at implant-abutment interface by optical

coherence tomography. J Biomedical Optics. 2014;19(5):001-007.

40. **Kim JW, Heo YR, Kim HJ, Chung CH.** A comparative study on the fit and screw joint stability of ready-made abutment and CAD/CAM custom-made abutment. J Korean Acad Prosthodont. 2013;51(4):276-283.

41. **Lang LA, Sierraalta M, Hoffensperger M, Wang RF.** Evaluation of the precision of fit between the procera custom abutment and various implant systems. Oral Maxillofac Implants. 2003;18:652-658.

42. **Lakha, Kheur M, Kheur S, Sandhu R.** Bacterial colonization at implant-abutment interface: a systematic review. J Dent Specialities. 2015;3(2):176-179.

43. **Lewis MB, Klineberg I.** Prosthodontic considerations designed to optimize outcomes for single-tooth implants- A review of the literature. Aust Dent J. 2011;56:181-192.

44. **Lorenzoni FC, Coelho PG, Bonfante G, Carvalho RM, Silva NRFA, Suzuki M, Silva TL, Bonfante EA.** Sealing Capability and SEM observation of the implant-abutment interface. Int J Dent. 2011; 01-06

45. **Meleo D, Baggi L, Girolamo MD, Carlo FD, Pecci R, Bedini R.** Fixture-abutment connection surface and microgap measurements by 3D micro-tomographic technique analysis. Ann Ist Super Sanita. 2012;48(1):53-58.

46. **Mobilio N, Fasiol A, Franceschetti G, Catapona S.** Marginal vertical fit along the implant-abutment interface: A microscope qualitative analysis. Dent J 2016;4:31.

47. **Moraes LMC, Rosserri PHO, Rossetti LMN, do vale Pedreira APR,**

Valle AL, Bonachela WC. Marginal fit at cylinder-abutment interface before and after overcasting procedure. J Appl Oral Sci. 2015;13(4):366-71.

48. **Neves FD, Elias GA, Silva-Neto JP, Dantas LC, Mota AS, Neto AJF.** Comparison of implant-abutment interface misfits after casting and soldering procedures. J Oral Implantology. 2014;11(2):129-35.

49. **Ormaechea MB, Millstein P, Hirayama H.** Tube angulation effect on radiographic analysis of the implant-abutment interface. Int J Oral Maxillofac Implant. 1999;14(1):77-85.

50. **Polido WD.** Original versus interchangeable abutments: Is it worth the saving. Dent Pres Implantol. 2014;8(3):6-7.

51. **Quek HC, Tan KB, Nicholls JI**. Load fatigue performance of four implant-abutment interface designs: effect of torque level and implant system. Int J Oral Maxillofac Implants. 2008;23:253-262.

52. **Rismanchian M, Hatami M, Badrian H, Khalighinejad N, Goroohi H**. Evaluation of microgap size and microbial leakage in the connection area of four abutments with Straumann (ITI) Implant. J Oral Implantology. 2012;28(6):677-685.

53. **Scarano A, Valbonetti L, Degidi M, Pecci R, Piattelli A.** Implant-abutment contact surfaces and microgap measurements of different implant connections under 3D x-ray microtomography. Implant Dent 2016; 25: 656-662.

54. **Shah RK, Aras AM, Chitre V.** Implant-abutment selection: A literature review. Int J Oral Implantol Clin Res 2014; 5 (2): 43-49.

55. **Shenava A.** Failure mode of implant abutment connections an

overview. J Dent Med Sci. 2013;11(3):32-35.

56. **Shetty M, Prasad K, Shetty NHG, Jaiman R.** Implant abutment connection: Biomechanical perspectives. Nitte Uni J Health Sci. 2014;4(2):47-53.

57. **Shin HM, Huh JB, Jeon YC, Chang BM, Jeong CM**. Influence of the implant- abutment connection design and diameter on the screw joint stability. J Adv Prosthodont. 2014;6:126-132.

58. **Sipahi C, Piskin B, Ayyildiz S, Uyar A.** Comparison of saliva leakage amounts into internal implant cavities in three different internal implant-abutment interface configurations. Cumhuriyet Dent J. 2015;18(2):156-68.

59. **Sola-Ruiz MF, Otaolaurruchi ES, Vicente GS, Cossio IG, Borras VA**. Accuracy combining different brands of implants and abutments. Med Oral Patol Oral Cir Bucal. 2013;18(2):332-36.

60. **Suttin Z, Towse R, Cruz J.** A novel method for assessing implant-abutment connection seal robustness. Poster presentation (P188:Academy of Osseointegration, 27th Annual Meeting, March 2012; Phoenix, Arizona, USA.

61. **Tavarez RRJ, Bonachela WC, Xible AA.** Effect of cyclic load on vertical misfit of prefabricated and cast implant single abutment. J App Oral Sci. 2011;19(1):16-21.

62. **Theoharidou A, Petridis HP, Tzannas K, Garefis P.** Abutment screw loosening in single-implant restorations: A systematic review. Int J Oral Maxillofac Implants. 2008;23:681-690.

63. **Tsuge T, Hagiwara Y, Matsumura H.** Marginal fit and microgaps of

implant-abutment interface with internal anti-rotation configuration. Dent Mater J. 2008;27(1):29-34.

64. **Vidigal Jr GM, Novaes Jr AB, Chevitarese O, Avillez RR, Groisman M.** Evaluation of the implant-abutment connection interface using scanning electron microscopy. Braz Dent J. 1995;6(1):17-23.

65. **Yüzügüllü B, Avci M.** The implant-abutment interface of alumina and zirconia abutments. Clin Implant Dent Rel Res. 2008;01-09.

66. **Zaghloul HH, Younis JF.** Marginal fit of implant-supported all ceramic zirconia frameworks. J Oral Implantology. 2013;29(4):417- 24

67. **Zanardi PR, Costa B, Stegun RC, Sesma N, Mori M, Lagana DC.** Connecting accuracy of interchanged prosthetic abutments of different dental implants using scanning electron microscopy. Braz Dent J. 2012;23(5):502-07.

ANNEXURE V

PLAGIARISM REPORT
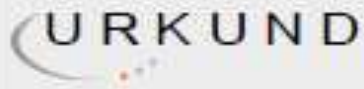
URKUND

Urkund Analysis Result

Analysed Document:	plagarism jan23.docx (D34976077)
Submitted:	1/24/2018 10:21:00 AM
Submitted By:	ashwinisukanyagunasekar@gmail.com
Significance:	2 %

Sources included in the report:

PLAGIARISM 01.doc (D34330025)

Instances where selected sources appear:

13